Search for a charged Higgs boson in pp collisions at root s=8 TeV

Khatchatryan, V.

2015-11

Khatchatryan , V , Eerola , P , Pekkanen , J , Voutilainen , M , Härkönen , J , Karimäki , V , Kinnunen , R , Lampén , T , Lassila-Perini , K , Laurila , S , Lehti , S , Lindén , T , Luukka , P , Mäenpää , T , Peltola , T , Tuominen , E , Tuominiemi , J , Tuovinen , E , Wendland , L , Talvitie , J , Tuuva , T & The CMS Collaboration 2015 , ' Search for a charged Higgs boson in pp collisions at root s=8 TeV ' , Journal of High Energy Physics , no. 11 , 018 . https://doi.org/10.1007/JHEP11(201

http://hdl.handle.net/10138/159443
https://doi.org/10.1007/JHEP11(2015)018

Published for SISSA by Springer

Received: *August 31, 2015*
Accepted: *September 29, 2015*
Published: *November 4, 2015*

Search for a charged Higgs boson in pp collisions at $\sqrt{s} = 8$ TeV

The CMS collaboration

E-mail: cms-publication-committee-chair@cern.ch

Abstract: A search for a charged Higgs boson is performed with a data sample corresponding to an integrated luminosity of $19.7 \pm 0.5\,\text{fb}^{-1}$ collected with the CMS detector in proton-proton collisions at $\sqrt{s} = 8$,TeV. The charged Higgs boson is searched for in top quark decays for $m_{\text{H}^\pm} < m_\text{t} - m_\text{b}$, and in the direct production $\text{pp} \to \text{t(b)H}^\pm$ for $m_{\text{H}^\pm} > m_\text{t} - m_\text{b}$. The $\text{H}^\pm \to \tau^\pm\nu_\tau$ and $\text{H}^\pm \to \text{tb}$ decay modes in the final states τ_h+jets, $\mu\tau_\text{h}$, ℓ+jets, and $\ell\ell'$ (ℓ =e, μ) are considered in the search. No signal is observed and 95% confidence level upper limits are set on the charged Higgs boson production. A model-independent upper limit on the product branching fraction $\mathcal{B}(\text{t} \to \text{H}^\pm\text{b})\,\mathcal{B}(\text{H}^\pm \to \tau^\pm\nu_\tau) =$ 1.2–0.15% is obtained in the mass range $m_{\text{H}^\pm} = 80$–$160\,\text{GeV}$, while the upper limit on the cross section times branching fraction $\sigma(\text{pp} \to \text{t(b)H}^\pm)\,\mathcal{B}(\text{H}^\pm \to \tau^\pm\nu_\tau) = 0.38$–$0.025\,\text{pb}$ is set in the mass range $m_{\text{H}^+} = 180$–$600\,\text{GeV}$. Here, $\sigma(\text{pp} \to \text{t(b)H}^\pm)$ stands for the cross section sum $\sigma(\text{pp} \to \bar{\text{t}}\text{(b)H}^+) + \sigma(\text{pp} \to \text{t}(\bar{\text{b}})\text{H}^-)$. Assuming $\mathcal{B}(\text{H}^\pm \to \text{tb}) = 1$, an upper limit on $\sigma(\text{pp} \to \text{t(b)H}^\pm)$ of 2.0–0.13 pb is set for $m_{\text{H}^\pm} = 180$–$600\,\text{GeV}$. The combination of all considered decay modes and final states is used to set exclusion limits in the $m_{\text{H}^\pm}$–$\tan\beta$ parameter space in different MSSM benchmark scenarios.

Keywords: Hadron-Hadron Scattering, Higgs physics, Supersymmetry

ArXiv ePrint: 1508.07774

doi:10.1007/JHEP11(2015)018

JHEP11(2015)018

Contents

JHEP11(2015)018

JHEP11(2015)018

1 Introduction

In 2012, a neutral boson with a mass of approximately 125 GeV was discovered by the CMS and ATLAS experiments [1–3] at the CERN LHC. The properties of the new boson are consistent with those predicted for the standard model (SM) Higgs boson [4–9]. Models with an extended Higgs sector are constrained by the measured mass, CP quantum numbers, and production rates of the new boson. The discovery of another scalar boson, neutral or charged, would represent unambiguous evidence for the presence of physics beyond the SM.

Charged Higgs bosons are predicted in models including at least two Higgs doublets. The simplest of such models are the two-Higgs-doublet models (2HDM) [10]. Two Higgs doublets result in five physical Higgs bosons: light and heavy CP-even Higgs bosons h and H, a CP-odd Higgs boson A, plus two charged Higgs bosons $H^\pm$. Throughout this paper, charge conjugate states are implied, the cross section $\sigma(pp \to \bar{t}(b)H^+)$ denotes the sum $\sigma(pp \to \bar{t}(b)H^+) + \sigma(pp \to t(\bar{b})H^-)$, and the branching fractions $\mathcal{B}(H^+ \to X)$ stand for $\mathcal{B}(H^\pm \to X)$. The minimal supersymmetric SM (MSSM) [11–18] used as a benchmark in this paper is a special case of a Type-II 2HDM scenario. In such a scenario, the couplings of the charged Higgs boson to up-type quarks is proportional to $\cot\beta$ while the charged Higgs boson couplings to the down-type quarks and charged leptons are proportional to $\tan\beta$, where $\tan\beta$ is defined as the ratio of the vacuum expectation values of the two Higgs boson doublet fields.

If the mass of the charged Higgs boson is smaller than the mass difference between the top and the bottom quarks, $m_{H^+} < m_t - m_b$, the top quark can decay via $t \to H^+b$. In this case, the charged Higgs boson is produced most frequently via $t\bar{t}$ production. In the MSSM scenarios considered, it preferentially decays to a τ lepton and the corresponding neutrino, $H^+ \to \tau^+\nu_\tau$, for $\tan\beta > 5$ [19]. A representative diagram for the production and decay mode for a low-mass charged Higgs boson is shown in figure 1 (left). Compared to the SM prediction, the presence of the $H^+ \to \tau^+\nu_\tau$ decay modes would alter the τ yield in the decays of $t\bar{t}$ pairs.

The Large Electron-Positron (LEP) collider experiments determined a model-independent lower limit of 78.6 GeV on the H^+ mass [20–23] at a 95% confidence level (CL). The most sensitive 95% CL upper limits on $\mathcal{B}(t \to H^+b)$ have been determined by the ATLAS and CMS experiments and are described in the following. For the $H^+ \to \tau^+\nu_\tau$ decay

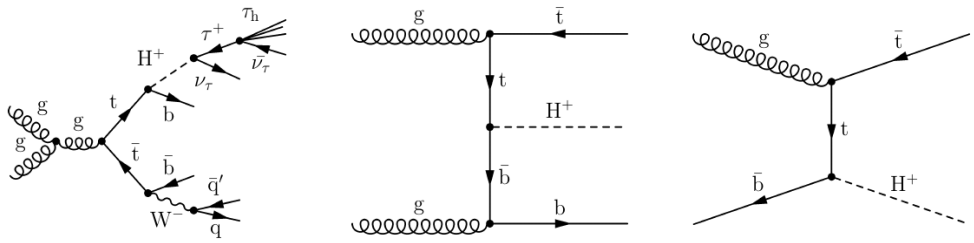

Figure 1. Left: a representative diagram for the production mode of the light charged Higgs boson through $t\bar{t}$ production with a subsequent decay to the τ_h+jets final state. Middle and right: representative diagrams for the direct production of the charged Higgs boson in the four-flavour scheme and five-flavour scheme, respectively.

mode with the hadronic decay of the τ lepton (τ_h) and hadronic W boson decays (τ_h+jets) final state, 95% CL upper limits of 1.3–0.2% have been set on $\mathcal{B}(t \to H^+b)\,\mathcal{B}(H^+ \to \tau^+\nu_\tau)$ for $m_{H^+} = 80$–$160\,\text{GeV}$ by the ATLAS experiment using data at $\sqrt{s} = 8\,\text{TeV}$ [24]. For the $\ell\tau_h$ (ℓ=e, μ) final states 95% CL upper limits of 3–9% have been set by the ATLAS and CMS experiments on $\mathcal{B}(t \to H^+b)$ in the $H^+ \to \tau^+\nu_\tau$ decay mode for $m_{H^+} = 80$–$160\,\text{GeV}$ assuming $\mathcal{B}(H^+ \to \tau^+\nu_\tau) = 1$ and using data at $\sqrt{s} = 7\,\text{TeV}$ [25, 26]. The $H^+ \to c\bar{s}$ decay mode, whose branching fraction dominates for $\tan\beta < 5$, has been studied by the ATLAS experiment, with 95% CL upper limits of 5–1% set on $\mathcal{B}(t \to H^+b)$ for $m_{H^+} = 90$–$160\,\text{GeV}$, under the assumption $\mathcal{B}(H^+ \to c\bar{s}) = 1$ and using data at $\sqrt{s} = 7\,\text{TeV}$ [27].

If the charged Higgs boson mass exceeds the mass difference between the top and bottom quark, $m_{H^+} > m_t - m_b$, the charged Higgs boson is predominantly produced by the fusion of bottom and top quarks illustrated in figures 1 (middle) and (right) for the four-flavour scheme (4FS) and the five-flavour scheme (5FS), respectively. In the 4FS, there are no b quarks in the initial state, causing a different ordering of the perturbative terms at any finite order between the 4FS and 5FS [28–31]. The predictions of the 4FS and the 5FS cross sections calculated at next-to-leading order (NLO) are combined using the "Santander matching scheme" [32]. In the MSSM benchmark scenarios considered, the $H^+ \to \tau^+\nu_\tau$ decay mode dominates for $m_{H^+} < 220\,\text{GeV}$ [19], and for large values of both m_{H^+} and $\tan\beta$, the decay $H^+ \to t\bar{b}$ becomes dominant but the $H^+ \to \tau^+\nu_\tau$ decay mode still contributes. For the $H^+ \to \tau^+\nu_\tau$ decay mode, considering the final state with hadronic τ lepton and associated W boson decays, the current upper limits of 0.8–0.004 pb have been set on $\sigma(pp \to \bar{t}(b)H^+)\,\mathcal{B}(H^+ \to \tau^+\nu_\tau)$ by the ATLAS experiment for $m_{H^+} = 180$–$1000\,\text{GeV}$ using data at $\sqrt{s} = 8\,\text{TeV}$ [24].

In this paper, a search for the charged Higgs boson is performed in pp collisions at $\sqrt{s} = 8\,\text{TeV}$. The data were recorded by the CMS experiment at the LHC and correspond to an integrated luminosity of $19.7 \pm 0.5\,\text{fb}^{-1}$. The charged Higgs boson decay modes and final states discussed in this paper are summarized in table 1. Model-independent limits without any assumption on the charged Higgs boson branching fractions are calculated on $\mathcal{B}(t \to H^+b)\,\mathcal{B}(H^+ \to \tau^+\nu_\tau)$ and $\sigma(pp \to \bar{t}(b)H^+)\,\mathcal{B}(H^+ \to \tau^+\nu_\tau)$ for $m_{H^+} < m_t - m_b$ and $m_{H^+} > m_t - m_b$, respectively, with the analysis on the $H^+ \to \tau^+\nu_\tau$ decay mode in the τ_h+jets final state. Additionally, the $H^+ \to \tau^+\nu_\tau$ and $H^+ \to t\bar{b}$ decay modes are inclusively

JHEP11(2015)018

Decay mode	Signatures for $m_{H^+} < m_t - m_b$	Signatures for $m_{H^+} > m_t - m_b$
	$pp \to t\bar{t} \to bH^+\bar{b}H^-/bH^+\bar{b}W^-$	$pp \to \bar{t}(b)H^+$
$H^+ \to \tau^+\nu_\tau$	τ_h+jets[(5)]	τ_h+jets[(5)], $\mu\tau_h$[(6)], $\ell\ell'$[(7)]
$H^+ \to t\bar{b}$	—	$\mu\tau_h$[(6)], $\ell\ell'$[(7)], ℓ+jets[(8)]

Table 1. Overview of the charged Higgs boson production processes, decay modes, final states, and mass regions analysed in this paper ($\ell = e, \mu$). All final states contain additional jets from the hadronization of b quarks and missing transverse energy from undetected neutrinos. The index after each signature denotes the section where it is discussed.

studied in the $\mu\tau_h$, single lepton (ℓ+jets), and $\ell\ell'$ (ℓ' referring to the possible different flavour between the two leptons) final states for $m_{H^+} > m_t - m_b$. Combined limits for the $H^+ \to t\bar{b}$ decay mode are set on $\sigma(pp \to \bar{t}(b)H^+)$ by assuming either $\mathcal{B}(H^+ \to \tau^+\nu_\tau) = 1$ or $\mathcal{B}(H^+ \to t\bar{b}) = 1$. The τ_h+jets final state is not sensitive to the presence of charged Higgs boson decay modes other than $H^+ \to \tau^+\nu_\tau$, because any such decay mode would be estimated inclusively with the background through the measurement from data described in section 5.2.1. All the decay modes and final states considered are used to set exclusion limits in the m_{H^+}–tan β parameter space for different MSSM benchmark scenarios [29, 33]. To set these limits, the specific branching fractions predicted by those benchmark scenarios are applied. This paper includes the first results on the direct charged Higgs boson production for $m_{H^+} > m_t - m_b$ in the $H^+ \to t\bar{b}$ decay mode.

The CMS detector is briefly described in section 2, followed by details of the event reconstruction and simulation in sections 3 and 4, respectively. The event selection together with the background estimation is described in sections 5, 6, 7, and 8 for the τ_h+jets, $\mu\tau_h$, $\ell\ell'$, and ℓ+jets final states, respectively. The treatment of statistical and systematic uncertainties is described in section 9. The results are presented in section 10 and summarized in section 11.

2 The CMS detector

The central feature of the CMS apparatus is a superconducting solenoid of 6 m internal diameter, providing a magnetic field of 3.8 T. Within the superconducting solenoid volume are a silicon pixel and strip tracker, a lead tungstate crystal electromagnetic calorimeter (ECAL), and a brass and scintillator hadron calorimeter (HCAL), each composed of a barrel and two endcap sections. Muons are measured in gas-ionization detectors embedded in the steel flux-return yoke outside the solenoid. Forward calorimeters extend the pseudorapidity coverage provided by the barrel and endcap detectors up to $|\eta| < 5$. The first level (L1) of the CMS trigger system, composed of custom hardware processors, uses information from the calorimeters and muon detectors to select the most interesting events in a fixed time interval of less than 4 μs. The high-level trigger processor farm further decreases the event rate from around 100 kHz to around 1 kHz, before data storage. A more detailed description of the CMS detector, together with a definition of the coordinate system used and the relevant kinematic variables, can be found in ref. [34].

JHEP11(2015)018

3 Event reconstruction

In the data collected during 2012, an average of 21 proton-proton interactions occurred per LHC bunch crossing. To select the primary interaction vertex, the squared sum of the transverse momenta of the charged-particle tracks, $\sum p_{\mathrm{T}}^2$, associated with each interaction vertex is calculated. The interaction vertex with the largest $\sum p_{\mathrm{T}}^2$ value is taken as the primary interaction vertex in the event [35]. The other pp collisions are referred to as pileup.

Events are reconstructed with the particle-flow (PF) algorithm [36, 37], which combines information from all sub-detectors to identify and reconstruct individual electrons, muons, photons, and charged and neutral hadrons. Electrons are reconstructed from clusters of ECAL energy deposits matched to hits in the silicon tracker [38]. Muons are reconstructed by performing a simultaneous global track fit to hits in the silicon tracker and the muon system [39]. The energy of photons is directly obtained from the ECAL measurement, corrected for zero-suppression effects. The energy of charged hadrons is determined from a combination of their momentum measured in the tracker and the matching ECAL and HCAL energy deposits, corrected for zero-suppression effects and for the response function of the calorimeters to hadronic showers. Finally, the energy of neutral hadrons is obtained from the corresponding corrected ECAL and HCAL energy. The composite physics objects, such as jets, hadronic tau lepton decays, and missing transverse energy are reconstructed from these PF particles.

Jets are reconstructed from the PF particles clustered by the anti-k_{t} algorithm [40, 41] with a distance parameter of 0.5. The jet momentum is determined as the vectorial sum of all particle momenta in the jet, and is found in the simulation to be within 5–10% of the true momentum over the whole p_{T} spectrum and detector acceptance. An offset correction is applied to take into account the extra energy clustered in jets arising from pileup. Jet energy corrections are derived from simulation, and are confirmed by in situ measurements of the energy balance in dijet and photon+jet events [42]. Additional selection criteria are applied to each event to remove spurious jet-like features originating from isolated noise patterns in certain HCAL regions. Jets originating from pileup interactions are removed by a multivariate jet identification algorithm [43].

Jets from the hadronization of b quarks are identified (b tagged) with the "combined secondary vertex" algorithm [44, 45]. The algorithm consists of evaluating a likelihood-based discriminator which uses information from reconstructed decay vertices of short-lived mesons and transverse impact parameter measurements of charged particles. In the τ_{h}+jets final state, the algorithm is used to identify b-tagged jets with a mistagging probability, i.e. the probability that a jet from the fragmentation of light quarks (u, d, s, c) or gluons is misidentified as a b jet, of approximately 0.1% ("tight" working point). In the analyses of the $\mu\tau_{\mathrm{h}}$ and ℓ+jets final states, the b tagging algorithm used has a mistagging probability of 1% ("medium" working point), since the multijet background is smaller than in the τ_{h}+jets final state. In the analysis with the $\ell\ell'$ final state, the b tagging working point is adjusted to allow a 10% mistagging probability to enhance signal acceptance since the multijet background in this analysis is even smaller. The corresponding probability to identify a b jet is about 50, 70, and 85%, respectively. The difference in b tagging efficiency between

JHEP11(2015)018

data and simulation is corrected by applying data-to-simulation scale factors dependent on the jet p_{T} and the jet pseudorapidity (η).

The missing transverse momentum vector $\vec{p}_{\mathrm{T}}^{\,\mathrm{miss}}$ is defined as the projection of the negative vector sum of the momenta of all reconstructed PF particles in an event onto the plane perpendicular to the beams. Its magnitude is referred to as $E_{\mathrm{T}}^{\mathrm{miss}}$. The $E_{\mathrm{T}}^{\mathrm{miss}}$ reconstruction is improved by propagating the jet energy corrections to it. Further filter algorithms are used to reject events with anomalously large $E_{\mathrm{T}}^{\mathrm{miss}}$ resulting from instrumental effects [46].

The "hadron-plus-strips" algorithm [47] is used to reconstruct hadronically decaying τ leptons. The algorithm uses the constituents of the reconstructed jets to identify individual τ decay modes with one charged and up to two neutral pions, or three charged pions. The neutral pions are reconstructed by clustering the reconstructed photons in narrow strips along the azimuthal angle direction taking into account possible broadening of calorimeter depositions from photon conversions. The τ_{h} candidates compatible with electrons or muons are rejected. Jets originating from the hadronization of quarks and gluons are suppressed by requiring that the τ_{h} candidate is isolated as described below. The τ_{h} identification efficiency depends on $p_{\mathrm{T}}^{\tau_{\mathrm{h}}}$ and $\eta^{\tau_{\mathrm{h}}}$, and is on average 50% for $p_{\mathrm{T}}^{\tau_{\mathrm{h}}} > 20\,\mathrm{GeV}$ with a probability of approximately 1% for hadronic jets to be misidentified as a τ_{h}.

Electrons, muons, and hadronically decaying τ leptons are required to be isolated from other particles by considering transverse momenta of neutral and charged particles in a cone $\Delta R = \sqrt{(\Delta\phi)^2 + (\Delta\eta)^2}$, where ϕ is the azimuthal angle, around the charged lepton candidate momentum direction. The isolation variable for electrons, muons, and τ_{h} is defined as:

$$I^{\mathrm{e}} = \sum_{\mathrm{charged}} p_{\mathrm{T}} + \max\left(0, \sum_{\mathrm{neut.\ hadr.}} p_{\mathrm{T}} + \sum_{\gamma} p_{\mathrm{T}} - \rho_{\mathrm{neutral}}\, A_{\mathrm{eff.}}\right), \tag{3.1}$$

$$I^{\mu} = \sum_{\mathrm{charged}} p_{\mathrm{T}} + \max\left(0, \sum_{\mathrm{neut.\ hadr.}} p_{\mathrm{T}} + \sum_{\gamma} p_{\mathrm{T}} - 0.5 \sum_{\mathrm{charged,pileup}} p_{\mathrm{T}}\right), \tag{3.2}$$

$$I^{\tau_{\mathrm{h}}} = \sum_{\mathrm{charged}} p_{\mathrm{T}} + \max\left(0, \sum_{\gamma} p_{\mathrm{T}} - 0.46 \sum_{\mathrm{charged,pileup}} p_{\mathrm{T}}\right), \tag{3.3}$$

where $\sum_{\mathrm{charged}} p_{\mathrm{T}}$ is the scalar sum of the transverse momenta of charged hadrons, electrons, and muons originating from the primary interaction vertex, and $\sum_{\mathrm{neut.\ hadr.}} p_{\mathrm{T}}$ and $\sum_{\gamma} p_{\mathrm{T}}$ are the scalar sums over neutral hadron and photon transverse momenta, respectively, in the cone ΔR around the charged lepton candidate momentum direction. The presence of particles from pileup events is taken into account depending on the charged-lepton type. For electron candidates, the scalar sum of the p_{T} of photons and neutral hadrons from pileup events in the isolation cone is estimated as the product of the neutral-particle transverse momentum density and the effective cone area, $\rho_{\mathrm{neutral}}\, A_{\mathrm{eff.}}$. The ρ_{neutral} component is evaluated from all photons and neutral hadrons in the event, and $A_{\mathrm{eff.}}$ accounts for the presence of pileup events. For muons and hadronically decaying τ leptons, the scalar sum of the p_{T} of photons and neutral hadrons from pileup events is estimated from the scalar sum of the transverse momenta of charged hadrons from pileup events in

JHEP11(2015)018

the isolation cone, $\sum_{\text{charged,pileup}} p_{\mathrm{T}}$, by multiplying it by the average ratio of neutral- to charged-hadron production in inelastic pp collisions. Since the contribution from neutral hadrons is ignored when computing the τ_{h} isolation variable, the pileup correction factor is slightly smaller than that used for correcting the muon isolation variable.

For electrons, an isolation cone size of $\Delta R = 0.3$ or 0.4 is used, depending on the final state. For muons and hadronically decaying τ leptons, isolation cone sizes of $\Delta R = 0.4$ and 0.5 are used, respectively. Electrons and muons are considered isolated if the relative isolation variable $I^{\ell}_{\text{rel}} = I^{\ell}/p^{\ell}_{\mathrm{T}}$, where $\ell = \mathrm{e}, \mu$, is lower than 10–20%, depending on the final state. Hadronically decaying τ leptons are considered isolated if $I^{\tau_{\mathrm{h}}} < 1\,\text{GeV}$.

4 Simulation

The signal processes are generated with PYTHIA 6.426 [48]. The $\mathrm{t\bar{t}}$, W+jets, and Z+jets backgrounds are generated using the MADGRAPH 5.1.3.30 [49] event generator with matrix elements (ME) providing up to four additional partons, including b quarks. The event generator is interfaced with PYTHIA to provide the parton showering and to perform the matching of the soft radiation with the contributions from the ME. The single top quark production is generated with POWHEG 1.0 [50–54] and the quantum chromodynamics (QCD) multijet and diboson production processes WW, WZ, and ZZ are generated using PYTHIA. Both the MADGRAPH and POWHEG generators are interfaced with PYTHIA for parton shower and hadronization. The TAUOLA 27.121.5 [55] package is used to generate τ decays for the simulated signal, as well as background samples.

The events are passed through full CMS detector simulation based on GEANT4 [56, 57], followed by a detailed trigger simulation and event reconstruction. Simulated minimum bias events are superimposed upon the hard interactions to match the pileup distribution observed in data. The PYTHIA parameters for the underlying event are set according to the Z2* tune, which is derived from the Z1 tune [58], which uses the CTEQ5L parton distribution set, whereas Z2* adopts CTEQ6L [59].

The number of $\mathrm{t\bar{t}}$ events produced is normalized to the predicted $\mathrm{t\bar{t}}$ production cross section of $246.7^{+6.2}_{-8.4} \pm 11.4\,\text{pb}$ as calculated with the TOP++ v2.0 program to next-to-next-to-leading order (NNLO) in perturbative QCD, including soft-gluon resummation to next-to-next-to-leading-logarithmic (NNLL) order [60], and assuming $m_{\mathrm{t}} = 173.34\,\text{GeV}$ [61]. The first uncertainty originates from the independent variation of the factorization and renormalization scales, μ_F and μ_R, while the second is associated with variations in the parton density functions (PDFs) and strong coupling constant α_{S}, following the PDF4LHC prescription with the MSTW2008 68% CL NNLO, CT10 NNLO and NNPDF2.3 5-flavour fixed-flavour number (FFN) PDF sets [62–65]. The predicted cross section is in good agreement with the measurements by ATLAS and CMS [66, 67]. The top quark p_{T} spectrum in data is found to be softer than that predicted using the MADGRAPH MC generator [68]. To correct for this effect, the $\mathrm{t\bar{t}}$ events are reweighted to make the top quark p_{T} spectrum in simulation match that observed in data [69].

The NNLO SM prediction is calculated with FEWZ v3.1 for the W+jets and Z/γ^* backgrounds [70, 71]. The cross section for the t-channel single top quark sample is calcu-

JHEP11(2015)018

lated at next-to-leading order (NLO) in QCD with HATHOR v2.1 [72, 73] with PDF and α_S uncertainties calculated using the PDF4LHC prescription [62, 74]. For the single top quark s-channel and tW-channel cross section, the SM prediction at NNLL in QCD is taken from refs. [75, 76].

5 The τ_h+jets final state for $H^+ \to \tau^+\nu_\tau$

In this analysis, a charged Higgs boson is assumed to be produced through the $t\bar{t} \to bH^+\bar{b}H^-$, $t\bar{t} \to bH^+\bar{b}W^-$, and $pp \to \bar{t}(b)H^+$ processes and searched for in the $H^+ \to \tau^+\nu_\tau$ decay mode with a hadronic decay of the τ and a hadronic decay of the W boson that originates from the associated $\bar{t} \to \bar{b}W^-$ decay. In these events, the missing transverse momentum is expected to originate from the neutrinos in the decay of the charged Higgs boson, which allows the reconstruction of the transverse mass, m_T, of the charged Higgs boson:

$$m_T = \sqrt{2p_T^{\tau_h} E_T^{miss}(1 - \cos\Delta\phi(\vec{p}_T^{\,\tau_h}, \vec{p}_T^{\,miss}))}, \tag{5.1}$$

where $\vec{p}_T^{\,\tau_h}$ denotes the transverse momentum vector of the hadronically decaying τ lepton and $p_T^{\tau_h}$ its magnitude, and $\Delta\phi$ is the angle between the τ_h direction and the $\vec{p}_T^{\,miss}$ in the transverse plane. The presence of the two neutrinos from the charged Higgs boson decay smears the expected Jacobian peak somewhat, but leaves the kinematic edge at the charged Higgs boson mass intact. The search is performed as a shape analysis, using the transverse mass to infer the presence of a signal. The dominant background processes are the SM $t\bar{t}$ and single top quark production, and the electroweak (EW) processes: W+jets, Z+jets, and dibosons (WW, WZ, ZZ). The multijet background constitutes a subleading background.

5.1 Event selection

Events are selected with a trigger that requires the presence of a τ_h and large E_T^{miss}. First the events are required to have calorimetric $E_T^{miss} > 40\,GeV$ at the first level of the CMS trigger system. The calorimetric E_T^{miss} is defined as the E_T^{miss} calculated from the ECAL and HCAL energy deposits instead of the PF particles. At the high-level trigger, the events are required to have calorimetric $E_T^{miss} > 70\,GeV$, and a τ_h of $p_T^{\tau_h} > 35\,GeV$ and $|\eta^{\tau_h}| < 2.5$. The τ_h is required to be loosely isolated, to contain at least one track of $p_T > 20\,GeV$, and to have at most two tracks in total, targeting the τ lepton decays into a single charged pion and up to two neutral pions. The probability for a signal event to be accepted by the trigger amounts to 8–14% in the m_{H^+} range of 80–160 GeV, and 19–44% in the m_{H^+} range of 180–600 GeV with all tau decays considered.

The efficiency of the τ part of the trigger is evaluated as a function of $p_T^{\tau_h}$ using a "tag-and-probe" technique [47] from $Z/\gamma^* \to \tau_\mu\tau_h$ events, where τ_μ refers to a muonic τ lepton decay. The efficiency of the E_T^{miss} part of the trigger is evaluated from events with a $t\bar{t}$-like final state of τ_h+jets selected with a single-τ trigger. The trigger efficiencies in simulated events are corrected with data-to-simulation scale factors applied as function of $p_T^{\tau_h}$ for the τ_h part of the trigger and as function of E_T^{miss} for the E_T^{miss} part of the trigger. The scale factors range between 0.95–1.06 and 0.97–1.02 for the τ_h and E_T^{miss} parts of the trigger, respectively.

JHEP11(2015)018

Selected events are required to have at least one τ_h with $p_T^{\tau_h} > 41\,\text{GeV}$ within $|\eta| < 2.1$ and to be matched to a trigger-level τ_h object. These thresholds are chosen to be compatible with the single-muon trigger used for estimate of backgrounds with hadronic τ decays from control samples in data, as described in section 5.2.1. Only one charged hadron is allowed to be associated with the τ_h and its p_T is required to fulfill $p_T > 20\,\text{GeV}$. Background events with $W \to \tau\nu_\tau$ decays are suppressed by requiring $R_\tau = p^{\text{charged hadron}}/p^{\tau_h} > 0.7$. The R_τ observable is sensitive to different polarizations of τ leptons originating from decays of W bosons (spin 1) and from decays of H^+ (spin 0) [77].

A $t\bar{t}$-like event topology is selected by requiring at least three jets of $p_T > 30\,\text{GeV}$ and $|\eta| < 2.4$ in addition to the τ_h and by requiring at least one of the selected jets to be identified as originating from the hadronization of a b quark. To select a fully hadronic final state, events containing identified and isolated electrons (muons) with $p_T > 15$ (10) GeV are rejected. The electron (muon) candidates are considered to be isolated if the relative isolation $I^e_{\text{rel.}}$ ($I^\mu_{\text{rel.}}$), as described in section 3, is smaller than 15% (20%).

To suppress the multijet background, $E_T^{\text{miss}} > 60\,\text{GeV}$ is required. The lower E_T^{miss} threshold on the PF E_T^{miss} compared to the calorimetric E_T^{miss} requirement applied at the high-level trigger improves the signal acceptance for $m_{H^+} < m_t - m_b$. This approach can be used because the PF E_T^{miss} has better resolution than the calorimetric E_T^{miss} [46].

In the multijet events selected with the $\tau+E_T^{\text{miss}}$ trigger a hadronic jet is misidentified as the τ_h in the event. In addition, the τ_h typically has a recoiling jet in the opposite direction. The E_T^{miss} in these events arises from the mismeasurement of the momenta of these jets with the $\vec{p}_T^{\,\text{miss}}$ direction aligned with $\vec{p}_T^{\,\tau_h}$. The best performance for multijet background suppression and signal acceptance is obtained with two-dimensional circular selections instead of simple selections based on azimuthal angle differences. The variables used for the azimuthal angle selections are defined as

$$\begin{aligned} R^{\text{min}}_{\text{coll}} &= \min\left\{\sqrt{\left(\Delta\phi(\tau_h, \vec{p}_T^{\,\text{miss}})\right)^2 + \left(\pi - \Delta\phi(\text{jet}_n, \vec{p}_T^{\,\text{miss}})\right)^2}\right\}, \\ R^{\text{min}}_{\text{bb}} &= \min\left\{\sqrt{\left(\pi - \Delta\phi(\tau_h, \vec{p}_T^{\,\text{miss}})\right)^2 + \left(\Delta\phi(\text{jet}_n, \vec{p}_T^{\,\text{miss}})\right)^2}\right\}, \end{aligned} \tag{5.2}$$

where the index n refers to any of the three highest p_T jets in the event and $\Delta\phi$ denotes the azimuthal angle between the reconstructed $\vec{p}_T^{\,\text{miss}}$ and the τ_h or one of the three highest-p_T jets. The labels "coll" and "bb" denote the collinear and back-to-back systems of the τ_h and the E_T^{miss}, respectively. The selected events are required to satisfy $R^{\text{min}}_{\text{coll}} > 0.70$ and $R^{\text{min}}_{\text{bb}} > 0.70$.

The same event selection is used for all the m_{H^+} values considered.

5.2 Background measurements

The background contributions arise from three sources:

1. Irreducible background from EW processes — W+jets, Z+jets, and dibosons — as well as SM $t\bar{t}$ and single top quark production, where the selected τ_h originates from a hadronic decay of a τ lepton ("EW+$t\bar{t}$ with τ_h").

JHEP11(2015)018

2. Reducible background from multijet events with large mismeasured $E_{\mathrm{T}}^{\mathrm{miss}}$ and jets that mimic hadronic τ decays.

3. Reducible background from EW+$\mathrm{t\bar{t}}$ events, where an electron, muon, or a jet is misidentified as the τ_{h} ("EW+$\mathrm{t\bar{t}}$ no τ_{h}").

The two largest backgrounds, "EW+$\mathrm{t\bar{t}}$ with τ_{h}" and multijets, are measured from control samples in data, as explained in sections 5.2.1 and 5.2.2. The contribution from "EW+$\mathrm{t\bar{t}}$ no τ_{h}" is estimated from simulation and is described in section 5.2.3.

5.2.1 Measurement of the EW+$\mathrm{t\bar{t}}$ with hadronically decaying τ leptons background

The m_{T} distribution for the "EW+$\mathrm{t\bar{t}}$ with τ_{h}" background is modelled via an embedding technique. It uses a control data sample of μ+jets events selected with a single-μ trigger. The same jet selection as in the τ_{h}+jets sample is used, and events with electrons or additional muons are rejected. Then, the selected μ is replaced by a simulated τ lepton decay. The simulated τ lepton momentum is the same as that of the selected μ, and the reconstructed τ decay products are merged with the original μ+jets event, from which the reconstructed muon is removed. In these hybrid events, the jets are reclustered and the $E_{\mathrm{T}}^{\mathrm{miss}}$ is recalculated and then the events are subjected to the same event selection as the τ_{h}+jets sample, i.e. τ_{h} identification, b tagging, $E_{\mathrm{T}}^{\mathrm{miss}}$ requirement, and the azimuthal angle selections are applied.

To obtain the m_{T} distribution for the "EW+$\mathrm{t\bar{t}}$ with τ_{h}" background, the effect of the muon trigger and the muon offline reconstruction need to be unfolded, and the efficiency of the τ+$E_{\mathrm{T}}^{\mathrm{miss}}$ trigger must be taken into account. First, the weight of each hybrid event is increased by the inverse of the muon trigger and identification efficiencies. Then, the efficiency of the τ+$E_{\mathrm{T}}^{\mathrm{miss}}$ trigger is applied by weighting the events with the efficiencies of the τ part of the trigger and the first trigger level part of the $E_{\mathrm{T}}^{\mathrm{miss}}$ trigger. The rest of the $E_{\mathrm{T}}^{\mathrm{miss}}$ part of the trigger is taken into account by applying a requirement on a hybrid calorimetric $E_{\mathrm{T}}^{\mathrm{miss}}$ constructed from the original event and the simulated τ lepton decay.

After the trigger has been taken into account, further corrections are applied. In a fraction of the selected μ+jets events the μ originates from a decay of a τ lepton, leading to an overestimation of the EW+$\mathrm{t\bar{t}}$ background by a few percent. This bias is corrected for by applying to the hybrid events p_{T}^{μ}-dependent correction factors derived from simulated $\mathrm{t\bar{t}}$ events. A residual difference is seen in the m_{T} distribution between non-embedded τ+jets and embedded μ+jets events in simulated $\mathrm{t\bar{t}}$ events. This difference is corrected by weighting the hybrid events by m_{T}-dependent correction factors derived from simulated $\mathrm{t\bar{t}}$ events. The $\mathrm{t\bar{t}}$ events constitute about 85% of the "EW+$\mathrm{t\bar{t}}$ with τ_{h}" background.

It should be noted that the embedding technique allows the separation of signal from the $\mathrm{H}^{+} \to \tau^{+}\nu_{\tau}$ decay mode from other decay modes, such as $\mathrm{H}^{+} \to \mathrm{t\bar{b}}$, where the τ lepton originates from a W boson decay. Namely, in the other charged Higgs boson decays, τ leptons and muons are produced at equal rates causing the embedding technique to include the $\mathrm{H}^{+} \to \mathrm{t\bar{b}}$ signal from data (and other such signals) as part of the "EW+$\mathrm{t\bar{t}}$ with τ_{h}" background.

JHEP11(2015)018

5.2.2 Measurement of the multijet background

The multijet background is measured with a "τ_h misidentification rate" technique. An estimate of the multijet background is obtained by measuring the probability of the τ_h candidate to pass the nominal and inverted τ_h isolation criterion. The misidentification rate is measured in bins of τ_h transverse momentum, in an event sample that is obtained prior to applying the b tagging, E_T^{miss}, and R_{bb}^{min} parts of the event selection described in section 5.1. The event sample that passes the nominal τ_h isolation selection contains a nonnegligible contamination from EW+$t\bar{t}$ backgrounds with genuine and misidentified τ leptons. Therefore, the number of multijet and EW+$t\bar{t}$ events is determined by a maximum likelihood fit of the E_T^{miss} distribution. A fit is performed for each $p_T^{\tau_h}$ bin. For multijet events, the E_T^{miss} templates are obtained from the data sample with inverted τ_h isolation by subtracting a small contribution of simulated EW+$t\bar{t}$ events. The E_T^{miss} templates for the EW+$t\bar{t}$ events are taken from simulation in the nominal region. The misidentification rate probabilities w_j are defined as the ratio of the number of multijet events in the isolated sample and the inverted isolation sample. Their measured values vary between 0.050–0.061 depending on the $p_T^{\tau_h}$ bin with a statistical uncertainty smaller than 3%.

The measured τ_h misidentification rate probabilities are then applied as weights to multijet events passing all nominal event selection criteria, except that the isolation criterion applied on the τ_h is inverted. The number of multijet events is obtained by subtracting the number of simulated EW+$t\bar{t}$ events from data. The estimate for the number of multijet events in a given bin i of the m_T distribution ($N_i^{multijet}$) is obtained by summing these weighted events over the $p_T^{\tau_h}$ bins according to

$$N_i^{\text{multijet}} = \sum_j \left(N_{i,j}^{\text{data, inverted}} - N_{i,j}^{\text{EW+t}\bar{\text{t}}\text{, inverted}} \right) w_j, \tag{5.3}$$

where N is the number of events and i and j denote m_T and $p_T^{\tau_h}$ bins, respectively.

5.2.3 The EW+$t\bar{t}$ with misidentified τ leptons background

The "EW+$t\bar{t}$ no τ_h" background originates almost solely from jets that are misidentified as the τ_h with a small contribution from electrons and muons misidentified as the τ_h. About 85% of the "EW+$t\bar{t}$ no τ_h" background events come from $t\bar{t}$ and the rest from single top quark production in the tW- and t-channels. The number of selected simulated events in the single top quark samples is small and therefore the m_T distribution for them is estimated with a procedure where the probability of each event to pass the b tagging is applied as a per-event weight instead of applying the b tagging selection. This probability is evaluated for simulated events with the $t\bar{t}$-like final state as function of jet p_T and flavour.

5.3 Event yields

Figure 2 shows the event yields after each selection step starting from the requirement that a τ_h, no isolated electrons or muons, and at least three jets are present in the event. The multijet background and the "EW+$t\bar{t}$ with τ_h" background are shown as measured from data, while the "EW+$t\bar{t}$ no τ_h" background is shown as estimated from the simulation. The data agree with the sum of expected backgrounds within the total uncertainties.

JHEP11(2015)018

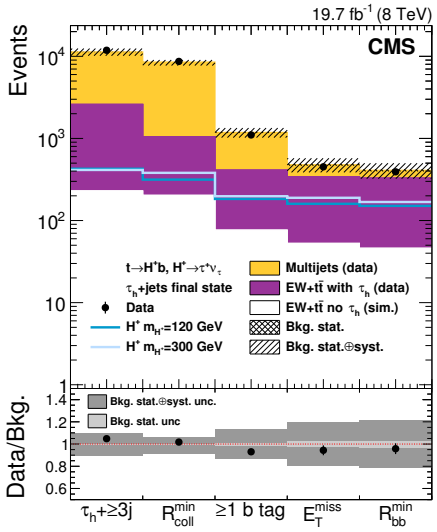

Figure 2. The event yield in the τ_h+jets final state after each selection step. For illustrative purposes, the expected signal yields are shown for $m_{H^+} = 120\,\text{GeV}$ normalized to $\mathcal{B}(t \to H^+b)\,\mathcal{B}(H^+ \to \tau^+\nu_\tau) = 0.01$ and for $m_{H^+} = 300\,\text{GeV}$ normalized to $\sigma(pp \to \bar{t}(b)H^+)\,\mathcal{B}(H^+ \to \tau^+\nu_\tau) = 1\,\text{pb}$, which are typical values for the sensitivity of this analysis. The bottom panel shows the ratio of data over the sum of expected backgrounds and its uncertainties. The cross-hatched (light grey) area in the upper (lower) part of the figure represents the statistical uncertainty, while the collinear-hatched (dark grey) area gives the total uncertainty in the background expectation.

The observed numbers of events after the full event selection are listed in table 2, along with those expected for the backgrounds and for the charged Higgs boson production. The systematic uncertainties listed in table 2 are discussed in section 9. The m_T distributions with all event selection criteria applied are shown in figure 3 for $m_{H^+} < m_t - m_b$ and $m_{H^+} > m_t - m_b$. In the $m_{H^+} > m_t - m_b$ region, the limited number of background events in the high-m_T tail is modelled by fitting an exponential function of the form $p_0 e^{-p_1(m_T - c)}$, where p_0 and p_1 are positive free parameters and where $c = 180\,\text{GeV}$ is the starting point of the fit. In the region of $m_T > 160\,\text{GeV}$ the event yields for the backgrounds are replaced by those obtained from this fit. The slight excess of observed events in the m_T spectrum for $m_{H^+} > m_t - m_b$ and limits on the production of the charged Higgs boson extracted from these distributions are discussed in section 10.

6 The $\mu\tau_h$ final state for $H^+ \to \tau^+\nu_\tau$ and $H^+ \to t\bar{b}$

In this analysis, a charged Higgs boson with $m_{H^+} > m_t - m_b$ is assumed to be produced through $pp \to \bar{t}(b)H^+$: this can result in a final state characterized by the presence of two leptons. Here we describe the $\mu\tau_h$ choice, whereas the $\ell\ell'$ ($\ell = e, \mu$) final state is discussed in section 7. The $\mu\tau_h$ final state is sensitive to the charged Higgs boson decay modes $H^+ \to \tau^+\nu_\tau$ and $H^+ \to t\bar{b}$.

In the first case, the τ decays hadronically and the final state is characterized by the leptonic decay of the W boson from the $\bar{t} \to \bar{b}W^-$ decay which results in a muon in the final state. In the second, at least one of the W bosons from the top quarks decays to a τ

JHEP11(2015)018

Source	$N_{\text{events}}(\pm\text{stat}\pm\text{syst})$
Signal, $m_{\mathrm{H}^+} = 120\,\text{GeV}$	$151 \pm 4\,^{+17}_{-18}$
Signal, $m_{\mathrm{H}^+} = 300\,\text{GeV}$	$168 \pm 2 \pm 16$
EW+$\mathrm{t\bar{t}}$ with τ_h (data)	$283 \pm 12\,^{+55}_{-54}$
Multijet background (data)	$80 \pm 3\,^{+9}_{-10}$
EW+$\mathrm{t\bar{t}}$ no τ_h (sim.)	$47 \pm 2\,^{+11}_{-10}$
Total expected	$410 \pm 12\,^{+57}_{-56}$
Data	392

Table 2. Numbers of expected signal and background events with their statistical and systematic uncertainties listed together with the number of observed events after the full event selection is applied in the τ_h+jets final state. For illustrative purposes, the expected signal yields are shown for $m_{\mathrm{H}^+} = 120\,\text{GeV}$ normalized to $\mathcal{B}(\mathrm{t} \to \mathrm{H}^+\mathrm{b})\,\mathcal{B}(\mathrm{H}^+ \to \tau^+\nu_\tau) = 0.01$ and for $m_{\mathrm{H}^+} = 300\,\text{GeV}$ normalized to $\sigma(\mathrm{pp} \to \bar{\mathrm{t}}(\mathrm{b})\mathrm{H}^+)\,\mathcal{B}(\mathrm{H}^+ \to \tau^+\nu_\tau) = 1\,\text{pb}$, which are typical values for the sensitivity of this analysis.

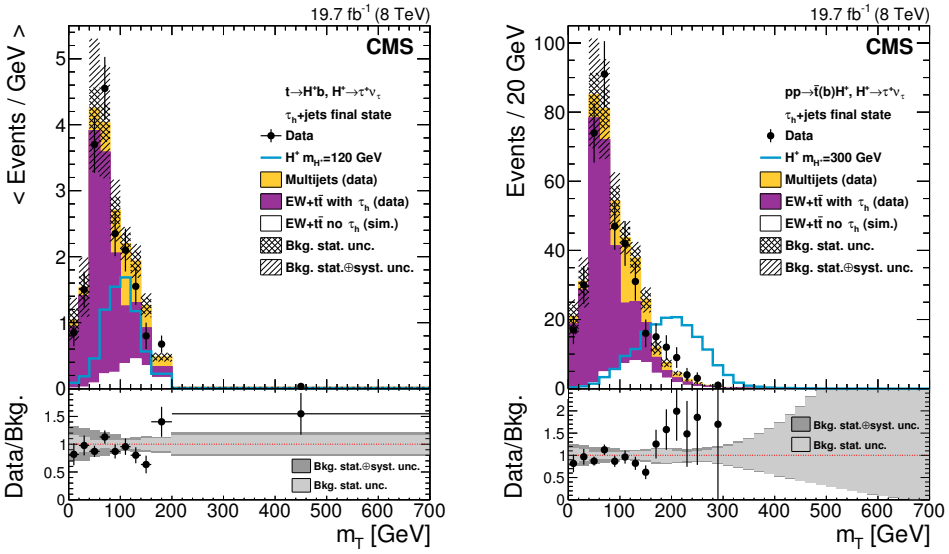

Figure 3. The transverse mass (m_T) distributions in the τ_h+jets final state for the H^+ mass hypotheses of 80–160 GeV (left) and 180–600 GeV (right). The event selection is the same in both left and right plots, but in the right plot the background expectation is replaced for $m_\mathrm{T} > 160\,\text{GeV}$ by a fit of the falling part of the m_T distribution. Since a variable bin width is used in the left plot the event yield in each bin has been divided by the bin width. For illustrative purposes, the expected signal yields are shown in the left plot for $m_{\mathrm{H}^+} = 120\,\text{GeV}$ normalized to $\mathcal{B}(\mathrm{t} \to \mathrm{H}^+\mathrm{b})\,\mathcal{B}(\mathrm{H}^+ \to \tau^+\nu_\tau) = 0.01$ and in the right plot for $m_{\mathrm{H}^+} = 300\,\text{GeV}$ normalized to $\sigma(\mathrm{pp} \to \bar{\mathrm{t}}(\mathrm{b})\mathrm{H}^+)\,\mathcal{B}(\mathrm{H}^+ \to \tau^+\nu_\tau) = 1\,\text{pb}$, which are typical values for the sensitivity of this analysis. The bottom panel shows the ratio of data over the sum of expected backgrounds along with the uncertainties. The cross-hatched (light grey) area in the upper (lower) part of the figure represents the statistical uncertainty, while the collinear-hatched (dark grey) area gives the total uncertainty in the background expectation.

JHEP11(2015)018

lepton which in turn decays to hadrons, whereas the other decays into a muon. Selecting the tau decay for one of the W bosons enhances the sensitivity to the $H^+ \to \tau^+\nu_\tau$ decay mode of the charged Higgs boson. In this final state, the charged Higgs boson production is characterized by a number of b-tagged jets larger than in the SM backgrounds, and consequently the shape of the b-tagged jet multiplicity distribution is used to infer the presence of a signal. The dominant SM background processes are from $t\bar{t} \to \mu\tau_h + X$, and other backgrounds where a jet is misidentified as a τ_h (mainly lepton+jet $t\bar{t}$ events and W+jet production).

6.1 Event selection

The event selection is similar to that used in the measurement of the top quark pair production cross section in dilepton final states containing a τ_h [78, 79]. A single-muon trigger with a threshold of $p_T > 24\,\text{GeV}$ and $|\eta| < 2.1$ is used to select the events.

Events are selected by requiring one isolated muon with $p_T > 30\,\text{GeV}$ and $|\eta| < 2.1$, one hadronically decaying τ with $p_T > 20\,\text{GeV}$ and $|\eta| < 2.4$, at least two jets with $p_T > 30\,\text{GeV}$ and $|\eta| < 2.4$, with at least one jet identified as originating from the hadronization of a b quark, and $E_T^{\text{miss}} > 40\,\text{GeV}$. The τ_h and the muon are required to have opposite electric charges. The muon candidate is considered to be isolated if the relative isolation, as defined in section 3, is $I_{\text{rel}} < 0.12$. The muon and the τ are required to be separated from each other and from any selected jet by a distance $\Delta R > 0.4$. The choice of the radius matches the lepton isolation cone. Events with an additional electron (muon) with $I_{\text{rel}} < 0.2$ and $p_T > 15(10)\,\text{GeV}$ are rejected.

6.2 Background estimate

There are three main background categories. The first includes backgrounds that contain a genuine muon and a genuine τ_h, and is constituted by $t\bar{t} \to \mu\tau_h + X$ production, associated $tW \to \mu\tau_h + X$ production, $Z \to \tau\tau \to \mu\tau_h$ Drell–Yan production, and $VV \to \mu\tau_h + X$ processes. The second category includes backgrounds with a genuine muon and an electron or muon misidentified as a τ_h, namely $t\bar{t} \to \mu\ell + X$, $Z \to \mu\mu$, associated $tW \to \mu\ell + X$ production and $VV \to \mu\ell + X$ production. The third category involves processes with a genuine muon and a jet misidentified as a τ_h, which include $t\bar{t} \to \mu$+jets, V+jets, single top quark, and $VV \to \mu$+jets events. Within those categories, all genuine muons come from W/Z decays, either direct ($W \to \mu\nu$, $Z \to \mu\mu$) or via intermediate τ decays ($W \to \tau\nu \to \mu + E_T^{\text{miss}}$, $Z \to \tau\tau \to \mu\tau_h + E_T^{\text{miss}}$).

The backgrounds from the first two categories are estimated using simulation, except for the background due to $Z/\gamma^* \to \tau\tau$ events with one τ_h and one τ decaying into a muon, which is estimated by taking for each variable the normalization from simulation and the shape from $Z \to \mu\mu$ events in data, where each muon has been replaced with reconstructed particles from a simulated τ lepton decay. The procedure is similar to the one described in section 5.2.1.

The backgrounds containing a jet misidentified as a τ_h come mostly from W+jets and from $t\bar{t} \to W^+W^-b\bar{b} \to \mu\nu q\bar{q}'b\bar{b}$ events, and are collectively labeled "misidentified τ_h" in the following tables and plots. This background is estimated by weighting each event in

JHEP11(2015)018

a $\mu+ \geq 3$ jets control sample by the probability for any jet in the event to mimic a τ_h. The contribution from $t\bar{t} \to \mu\ell + X$ events, where one jet fakes a τ_h, is estimated using simulation and is subtracted from the data driven estimate to avoid double counting. The probability that a jet is misidentified as a τ_h is measured from data as a function of jet p_T, η, and jet radius using W+jets and multijet events [47, 79]. Here, the estimate of the misidentified τ_h background is improved with respect to the method used in ref. [25] by weighting according to the quark and gluon jet compositions (from simulation) the estimates obtained in the W+jet and multijet samples [79]. This data driven estimate is different from the one described in section 5.2.2, where the control region is obtained by inverting isolation requirements on the reconstructed τ_h and only one control region is used. Here, estimating the fake rate in multijet events is not enough: the contamination from W+jets and $t\bar{t} \to W^+W^-b\bar{b} \to \mu\nu q\bar{q}'b\bar{b}$ events must be taken into account as well. The improvement in the central value of the estimate is verified with a closure test consisting in applying the data driven method to simulated events: the result of the closure test is compatible with the yields obtained from simulation, within the uncertainties. The systematic uncertainty associated to the data driven method is reduced by 30% with respect to the cited paper. The misidentified τ_h background measured from data is consistent with the expectations from simulation.

The fraction of events from SM $t\bar{t}$ production that is not included in the $t\bar{t} \to \mu\tau_h + X$ or misidentified τ_h contributions is labeled as "other $t\bar{t}$" in the following tables and plots. The $t\bar{t}$ events are categorized in order to separate the contribution from each decay mode, using the full information on the simulated particles.

The single lepton trigger efficiency and the muon isolation and identification efficiencies are corrected by multiplicative data-to-simulation scale factors that depend on the muon p_T and η. Those factors are derived using a "tag-and-probe" method [80, 81]. The trigger correction factors vary between 0.96 and 0.99, whereas the corrections to isolation and identification efficiency vary between 0.97 and 0.99.

6.3 Event yields

The numbers of expected events for the SM backgrounds, the expected number of signal events from the $pp \to \bar{t}(b)H^+$ process for $m_{H^+} = 250\,\text{GeV}$ for the decay modes $H^+ \to t\bar{b}$ and $H^+ \to \tau^+\nu_\tau$, and the number of observed events after all the selection requirements are summarized in table 3. Statistical and systematic uncertainties evaluated as described in section 9 are also shown. For illustrative purposes, the number of signal events is normalized, assuming a 100% branching fraction for each decay mode, to a cross section of 1 pb, which is typical of the cross section sensitivity of this analysis.

Data and simulated event yields at various steps of the event selection are shown in figure 4 (left). Since the background estimate is derived from data only after requiring one τ_h, the backgrounds here are normalized to the SM prediction obtained from the simulation. A good agreement ($\sim 1\%$ after the full selection) is found between data and the SM background expectations. The multijet background contribution is negligible at the final selection step. The expected signal event yields are shown as dashed lines.

JHEP11(2015)018

Source	$N_{\text{events}}(\pm\text{stat}\pm\text{syst})$
$H^+ \to \tau^+\nu_\tau$, $m_{H^+} = 250\,\text{GeV}$	$176 \pm 10 \pm 13$
$H^+ \to t\bar{b}$, $m_{H^+} = 250\,\text{GeV}$	$37 \pm 2 \pm 3$
$t\bar{t} \to \mu\tau_h + X$	$2913 \pm 14 \pm 242$
Misidentified τ_h	$1544 \pm 14 \pm 175$
$t\bar{t}$ dilepton	$101 \pm 10 \pm 27$
$Z/\gamma^* \to ee, \mu\mu$	$12 \pm 3 \pm 4$
$Z/\gamma^* \to \tau\tau$	$162 \pm 40 \pm 162$
Single top quark	$150 \pm 12 \pm 18$
Dibosons	$20 \pm 3 \pm 2$
Total SM backgrounds	$4903 \pm 45 \pm 341$
Data	4839

Table 3. Numbers of expected events in the $\mu\tau_h$ final state for the SM backgrounds and in the presence of a signal from $H^+ \to t\bar{b}$ and $H^+ \to \tau^+\nu_\tau$ decays for $m_{H^+} = 250\,\text{GeV}$ are shown together with the number of observed events after the final event selection. For illustrative purposes, the number of signal events is normalized, assuming a 100% branching fraction for each decay mode, to a cross section of 1 pb, which is typical of the cross section sensitivity of this analysis.

The b-tagged jet multiplicity after the full event selection is shown in figure 4 (right). Here the misidentified τ_h background is derived from data, as discussed in section 6.2. The ratio of the data to the sum of the expected SM background contributions is shown in the bottom panel. Limits on the production of the charged Higgs boson are extracted by exploiting this distribution.

7 The dilepton (ee/eμ/$\mu\mu$) final states for $H^+ \to \tau^+\nu_\tau$ and $H^+ \to t\bar{b}$

In this analysis, a charged Higgs boson with $m_{H^+} > m_t - m_b$ is assumed to be produced through $pp \to \bar{t}(b)H^+$ and is searched for in the $\ell\ell'$ final state. Assuming that the top quark produced in association with the charged Higgs boson decays as $\bar{t} \to \ell\nu b$, the dilepton final state is sensitive to charged Higgs boson decay modes $H^+ \to t\bar{b}$ (via leptonic decays of the top) or $H^+ \to \tau^+\nu_\tau$ (via leptonic decays of the tau lepton).

This leads to a final state similar to the SM $t\bar{t}$ dilepton final state, with the addition of one or two b jets. The shape of the b-tagged jet multiplicity distribution is used to infer the presence of a charged Higgs boson signal. The dominant SM backgrounds are from $t\bar{t}$ and single top quark production. An optimization procedure selected the b-tagged jet multiplicity variable as the most discriminating between the signal and the main backgrounds.

7.1 Event selection

The event selection is similar to that used for the measurement of the SM $t\bar{t}$ cross section and of the ratio $\mathcal{B}(t \to Wb)/\mathcal{B}(t \to Wq)$ in the dilepton channel [80, 82]. Data were collected with double-lepton triggers (ee/$\mu\mu$/eμ) with p_T thresholds of 17 GeV for the

JHEP11(2015)018

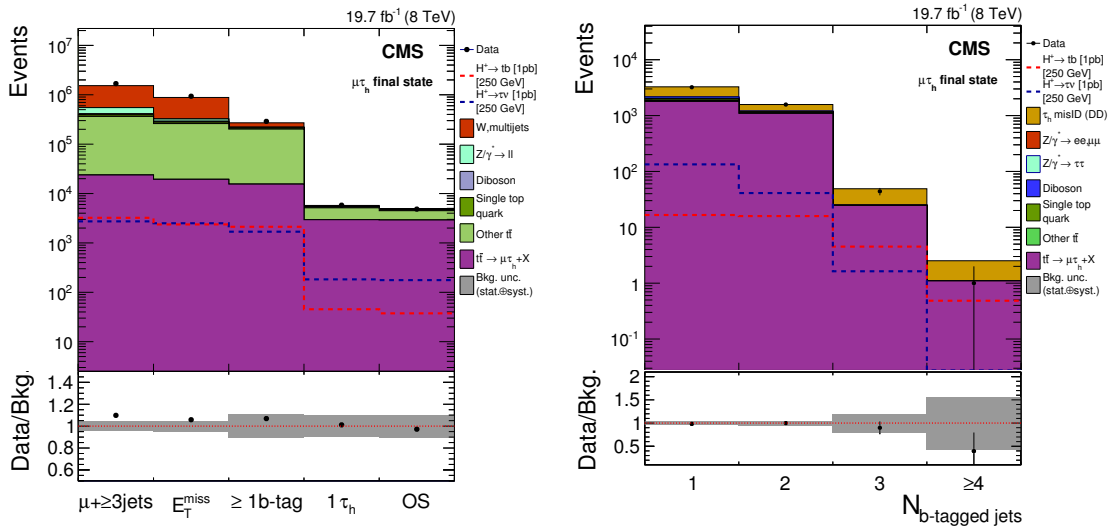

Figure 4. Left: event yields after each selection step, where OS indicates the requirement to have opposite electric charges for the τ_h and the μ. The backgrounds are estimated from simulation and normalized to the SM prediction. Right: the b-tagged jet multiplicity distribution after the full event selection. As opposed to the left plot, the "misidentified τ_h" component is estimated using the data-driven method and labeled "τ_h misID (DD)", while the remaining background contributions are from simulation normalized to the SM predicted values. For both distributions, the expected event yield in the presence of the $H^+ \to t\bar{b}$ and $H^+ \to \tau^+\nu_\tau$ decays is shown as dashed lines for $m_{H^+} = 250\,\text{GeV}$. For illustrative purposes, the number of signal events is normalized, assuming a 100% branching fraction for each decay mode, to a cross section of 1 pb, which is typical of the cross section sensitivity of this analysis. $\mathcal{B}(H^+ \to t\bar{b}) = 1$ and $\mathcal{B}(H^+ \to \tau^+\nu_\tau) = 1$, respectively. The bottom panel shows the ratio of data over the sum of the SM backgrounds; the shaded grey area shows the statistical and systematic uncertainties added in quadrature.

leading lepton and 8 GeV for the other. After offline reconstruction, events are required to have two isolated, oppositely charged, leptons (one electron and one muon, or two electrons, or two muons) with $p_T > 20\,\text{GeV}$ and $|\eta| < 2.5$ ($|\eta| < 2.4$) for electrons (muons), and at least two jets with $p_T > 30\,\text{GeV}$ and $|\eta| < 2.4$. The relative isolation requirement is $I_{rel} < 0.15(0.20)$ for electrons (muons). Jets are required to be separated by a distance $\Delta R = 0.4$ from the isolated leptons. A minimum dilepton invariant mass of 12 GeV is required to reject SM background from low-mass resonances. For the same flavour channels (ee, $\mu\mu$), events with dilepton invariant mass within 15 GeV from the Z boson mass are vetoed. In order to account for the presence of neutrinos, $E_T^{miss} > 40\,\text{GeV}$ is required. Finally, at least two b-tagged jets are required.

7.2 Background estimate

The main background comes from $t\bar{t}$ events in which both W bosons decay leptonically, and surpasses by more than one order of magnitude the sum of the remaining backgrounds. All backgrounds are estimated from simulation. The dilepton trigger efficiency is corrected by a multiplicative data-to-simulation scale factor dependent on the final state, in order to provide agreement between data and simulation; the corresponding scale factors are

JHEP11(2015)018

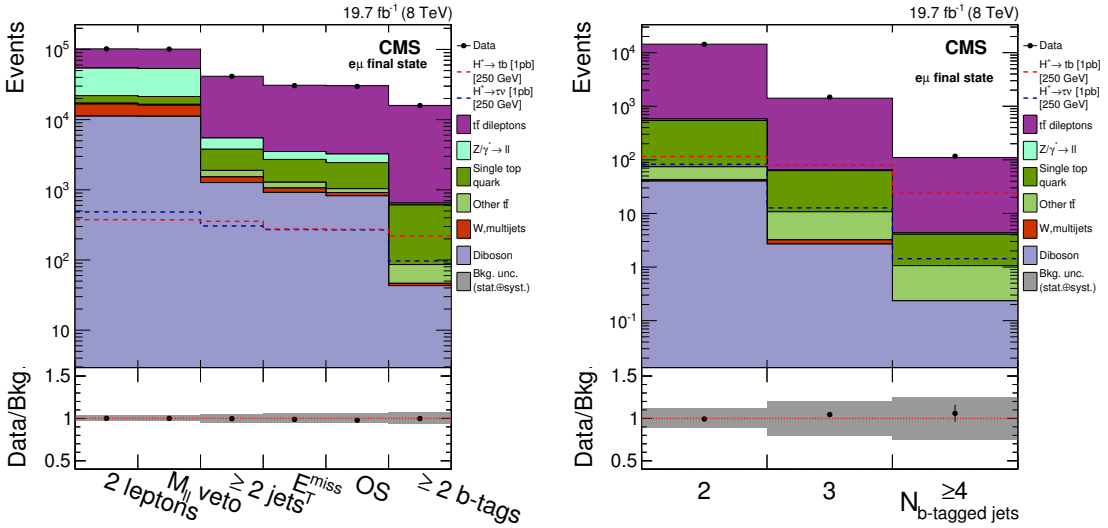

Figure 5. The event yields at different selection steps (left) and the b-tagged jet multiplicity after the full event selection for the eμ final state (right). For illustrative purposes, the number of signal events is normalized, assuming a 100% branching fraction for each decay mode, to a cross section of 1 pb, which is typical of the cross section sensitivity of this analysis. The bottom panel shows the ratio of data over the sum of the SM backgrounds; the shaded area shows the statistical and systematic uncertainties added in quadrature.

computed using the "tag-and-probe" method, and the resulting values are 0.97, 0.95, and 0.92 for the ee, eμ, and $\mu\mu$ final states, respectively. The data-to-simulation scale factors for the lepton identification and isolation efficiencies are defined using a second "tag-and-probe" method with $\mathrm{Z} \to \mathrm{e^+e^-}/\mu^+\mu^-$ events. For electrons (muons) with $p_\mathrm{T} > 20\,\mathrm{GeV}$, they are found to vary between 0.91 (0.97) and 1.0 (0.99).

7.3 Event yields

The number of data events after each selection requirement are in good agreement with the SM background expectations, and are shown in figure 5 (left), for the eμ final state as a representative example.

The number of expected events after all selections in the $\ell\ell'$ final state is summarized in table 4 for the SM background processes and for a charged Higgs boson with a mass of $m_{\mathrm{H^+}} = 250\,\mathrm{GeV}$. The main background comes from $\mathrm{t\bar{t}}$ production in the dilepton final state, including all three lepton flavours. Backgrounds from $\mathrm{t\bar{t}}$ production in the final states other than "$\mathrm{t\bar{t}}$ dilepton" (labelled "other $\mathrm{t\bar{t}}$") and other SM processes result in significantly smaller yields. Statistical and systematic uncertainties evaluated as described in section 9 are also shown. The data agree with the sum of expected backgrounds within the total uncertainties.

The b-tagged jet multiplicity distribution for the eμ final state, shown after the full event selection in figure 5 (right), is used to extract limits on the charged Higgs boson production.

JHEP11(2015)018

Source	ee	eμ	$\mu\mu$
$H^+ \to \tau^+\nu_\tau$, $m_{H^+} = 250\,GeV$	$39 \pm 3 \pm 3$	$97 \pm 4 \pm 5$	$40 \pm 3 \pm 3$
$H^+ \to t\bar{b}$, $m_{H^+} = 250\,GeV$	$85 \pm 3 \pm 2$	$219 \pm 5 \pm 5$	$90 \pm 3 \pm 2$
$t\bar{t}$ dilepton	$5692 \pm 17 \pm 520$	$15296 \pm 28 \pm 1364$	$6332 \pm 18 \pm 572$
Other $t\bar{t}$	$22 \pm 4 \pm 5$	$40 \pm 5 \pm 9$	$17 \pm 3 \pm 5$
$Z/\gamma^* \to \ell\ell$	$96 \pm 7 \pm 35$	$36 \pm 2 \pm 7$	$139 \pm 10 \pm 42$
W+jets, multijets	$6 \pm 2 \pm 1$	$3 \pm 1 \pm 1$	< 1
Single top quark	$199 \pm 10 \pm 21$	$522 \pm 15 \pm 54$	$228 \pm 10 \pm 26$
Dibosons	$15 \pm 1 \pm 2$	$43 \pm 2 \pm 6$	$20 \pm 1 \pm 3$
Total SM backgrounds	$6032 \pm 20 \pm 521$	$15941 \pm 32 \pm 1365$	$6736 \pm 23 \pm 575$
Data	6162	15902	6955

Table 4. Number of expected events for the SM backgrounds and for signal events with a charged Higgs boson mass of $m_{H^+} = 250\,GeV$ in the ee, eμ, and $\mu\mu$ dilepton final states after the final event selection. For illustrative purposes, the number of signal events is normalized, assuming a 100% branching fraction for each decay mode, to a cross section of 1 pb, which is typical of the cross section sensitivity of this analysis. Event yields are corrected with the trigger and selection efficiencies. Statistical and systematic uncertainties are shown.

8 The single-lepton (e/μ+jets) final states for $H^+ \to t\bar{b}$

In this analysis, a charged Higgs boson with $m_{H^+} > m_t - m_b$ and produced in association with a top quark $pp \to \bar{t}(b)H^+$, is searched for in the decay mode $H^+ \to t\bar{b}$. Of the two W bosons produced from the top quark decays, one decays leptonically, while the other decays hadronically, leading to the final state signature of one lepton, jets, and E_T^{miss}. These final states are similar to the SM $t\bar{t}$ semileptonic final states, with the addition of one or two b jets. While the dilepton analysis (section 7) uses the shape of the full b tagged jet multiplicity distribution to check for the presence of a signal, for this analysis, an optimization procedure led to use of the H_T distribution, defined as the scalar sum of the p_T of all selected jets, subdivided by b tagged jet multiplicity, to infer the presence of a charged Higgs signal. Due to the jet composition of the signal, the H_T distribution peaks at higher energies and has a less steeply falling high energy tail than the major backgrounds. The dominant backgrounds are $t\bar{t}$, W+jets, and single top quark production.

8.1 Event selection

Data were collected by the single-electron or a single-muon trigger with p_T thresholds of 27 and 24 GeV, respectively. The offline event selection requires the presence of exactly one isolated electron (muon) with $p_T > 30$ (27) GeV and $|\eta| < 2.5$ (2.4). The electrons (muons) are required to be isolated with $I^\ell_{rel} < 0.10$ (0.20), with I^ℓ_{rel} defined in section 3. Events with additional leptons are rejected. To maintain exclusivity with the other analyses included in this paper, events with one or more hadronic τ decays with $p_T^{\tau_h} > 20\,GeV$ and $|\eta_{\tau_h}| < 2.4$ are rejected. In addition, the presence of at least two jets with $p_T > 30\,GeV$ and $|\eta| < 2.4$ are required, with $p_T > 50\,GeV$ for the jet with the highest p_T. At least one

JHEP11(2015)018

of the selected jets is required to be b-tagged. The $E_{\mathrm{T}}^{\mathrm{miss}}$ must exceed 20 GeV to mimic the presence of a neutrino in the final event signature.

To account for differences in modelling of the lepton identification and trigger efficiency between simulation and data, η- and p_{T}-dependent scale factors are applied. The single-electron trigger correction factor is 0.973 (1.020) for $|\eta| \leq 1.5$ ($1.5 < |\eta| \leq 2.5$) and the single-muon trigger correction factors and corrections to identification efficiency are similar to those in section 6.2.

Events are classified into two categories, a signal region (SR) and a control region (CR). The CR is defined by having low reconstructed jet multiplicity, $2 \leq N_{\mathrm{jet}} \leq 3$, and is used to derive normalizations for dominant backgrounds from data. The SR is distinguished by its high jet multiplicity, and defined by the requirement $N_{\mathrm{jet}} \geq 4$. These categories are further subdivided according to the b-tagged jet multiplicities, $N_{\mathrm{b\ tag}}$, with the CR split into 3 subcategories ($N_{\mathrm{b\ tag}} = 0$, $N_{\mathrm{b\ tag}} = 1$, and $N_{\mathrm{b\ tag}} \geq 2$) and the SR split into two ($N_{\mathrm{b\ tag}} = 1$ and $N_{\mathrm{b\ tag}} \geq 2$). Distinguishing between electron and muon channels leads to a total of four SR categories and six CR categories.

8.2 Background estimate

The following background processes are considered: $\mathrm{t\bar{t}}$, W+jets, single top quark, Z/γ^{*}+jets, and dibosons (WW, WZ, and ZZ).

The backgrounds are subdivided into seven independent categories distinguished by their yields and shapes in the signal region. The six samples: $\mathrm{t\bar{t}}$, W+c (events with one or more c jet), W+b (events with one or more b jet), W+light-flavour (u, d, s, g) jets, single top quark, and multijets are defined as independent categories. The small backgrounds with similar H_{T} distributions from dibosons and Z/γ^{*}+jets are merged into the "$\mathrm{Z}/\gamma^{*}/\mathrm{VV}$" background. Additional contributions from $\mathrm{t\bar{t}}$+W and $\mathrm{t\bar{t}}$+Z are considered negligible. All H_{T} distributions are taken from simulation.

For the backgrounds which contribute little to the signal region (single top quark, diboson, Z+jets, and multijet production), the normalizations are taken directly from the simulation. For the four remaining processes which provide most of the background in the signal region ($\mathrm{t\bar{t}}$ production, W+c, W+b, and W+light-flavour jets), the normalization is initially taken from simulation, but is then determined by a simultaneous fit of the background distributions to the data. The normalization is allowed to float freely during the limit setting. Thus, the fit finds the best values for these normalizations, derived using simulated and observed yields from both the control and signal regions. The values obtained for these normalizations for the electron (muon) channel are 1.01 (1.01) for $\mathrm{t\bar{t}}$, 2.06 (1.62) for W+c, 1.90 (1.48) for W+b, and 1.18 (1.01) for W+light-flavour jets. The $\mathrm{t\bar{t}}$ background dominates and constitutes 80% of events with 1 b-tagged jet and 93% of events with 2 or more b-tagged jets, while W+c and W+b backgrounds contribute to 8% and 2%, respectively. Differences in normalizations between electron and muon channels are accounted for in the systematic uncertainties, as noted in table 9.

A closure test is performed to assess the validity of the assumption that the normalizations derived from the fit to data are not dependent on the jet multiplicities of the samples. A sample of events with at least four jets, none of which are b-tagged, is used for

JHEP11(2015)018

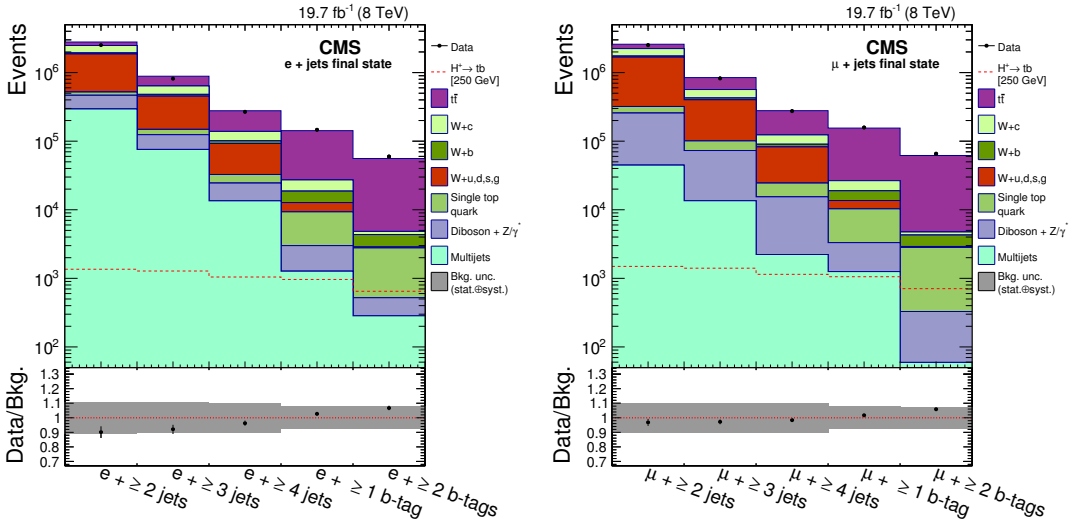

Figure 6. Event yields after different selection cuts for both the e+jets (left) and μ+jets (right) final state. Expectations for the charged Higgs boson for $m_{\mathrm{H}^+} = 250\,\mathrm{GeV}$, for the $\mathrm{H}^+ \to \mathrm{t\bar{b}}$ decays, are also shown. For illustrative purposes, the signal is normalized, assuming $\mathcal{B}(\mathrm{t} \to \mathrm{H}^+\mathrm{b}) = 1$, to a cross section of 1 pb, which is typical of the cross section sensitivity of this analysis. The bottom panel shows the ratio of data over the sum of the SM backgrounds with the total uncertainties.

the closure test. The agreement between observed and predicted events, using the post-fit values of the normalizations, across all bins in the high jet multiplicity region is found to be within 10%.

8.3 Event yields

The number of data events after different selection cuts are compared to expectations from SM backgrounds and are shown in figure 6 for both the electron and muon channels. Results are in good agreement with SM background expectations.

The number of expected events in the final selection for each subsample can be seen in table 5. The number of events for data, SM background processes, and a charged Higgs boson with a mass of $m_{\mathrm{H}^+} = 250\,\mathrm{GeV}$ are shown. The leading contributions to the SM background come from $\mathrm{t\bar{t}}$ events with a semi-leptonic final state, W boson production in association with heavy-flavour jets, and single top quark production. Statistical and systematic uncertainties are evaluated as described in section 9.

The H_{T} distributions for the two signal regions in the muon channel are shown in figure 7. Limits on the production cross section of the charged Higgs boson are extracted by exploiting these distributions.

9 Systematic uncertainties

The uncertainties common to the analyses are presented in section 9.1. The uncertainties specific to the individual analyses are discussed in sections 9.2–9.5.

JHEP11(2015)018

Source	$N_{\mathrm{b\ tag}} = 1$	$N_{\mathrm{b\ tag}} \geq 2$	$N_{\mathrm{b\ tag}} = 1$	$N_{\mathrm{b\ tag}} \geq 2$
	e+jets		μ+jets	
$\mathrm{H^+ \to t\bar{b}}$, $m_{\mathrm{H^+}} = 250\,\mathrm{GeV}$	315 ± 4 ± 17	647 ± 6 ± 34	348 ± 5 ± 19	707 ± 7 ± 37
$\mathrm{t\bar{t}}$	64111 ± 74 ± 5174	51059 ± 66 ± 4679	71593 ± 78 ± 5711	57094 ± 70 ± 5160
W+c	8031 ± 89 ± 1047	482 ± 21 ± 79	7156 ± 77 ± 11193	460 ± 18 ± 92
W+b	4470 ± 61 ± 1206	1486 ± 35 ± 404	3926 ± 53 ± 1386	1364 ± 32 ± 484
W+u,d,s,g	3326 ± 44 ± 598	90 ± 7 ± 21	3231 ± 39 ± 581	95 ± 7 ± 22
Single top quark	4059 ± 42 ± 463	2253 ± 30 ± 274	4496 ± 44 ± 524	2493 ± 32 ± 295
$\mathrm{Z}/\gamma^*/\mathrm{VV}$	1492 ± 54 ± 771	237 ± 21 ± 130	1792 ± 60 ± 942	269 ± 22 ± 140
Multijet background	990 ± 270 ± 1040	280 ± 160 ± 290	1220 ± 480 ± 1260	59 ± 34 ± 60
Total SM backgrounds	86480 ± 310 ± 5620	55890 ± 190 ± 4720	93410 ± 500 ± 6240	61836 ± 95 ± 5194
Data	86580	59637	92391	65472

Table 5. Number of expected events for the SM backgrounds and for signal events with a charged Higgs boson mass of $m_{\mathrm{H^+}} = 250\,\mathrm{GeV}$ in the ℓ+jets final states after the final event selection. Normalizations for W+light-flavour jets, W+c, W+b, and $\mathrm{t\bar{t}}$ are derived from data. Normalizations for other backgrounds are based on simulation. For illustrative purposes, the signal is normalized, assuming $\mathcal{B}(\mathrm{t} \to \mathrm{H^+b}) = 1$, to a cross section of 1 pb, which is typical of the cross section sensitivity of this analysis. Statistical and systematic uncertainties are shown.

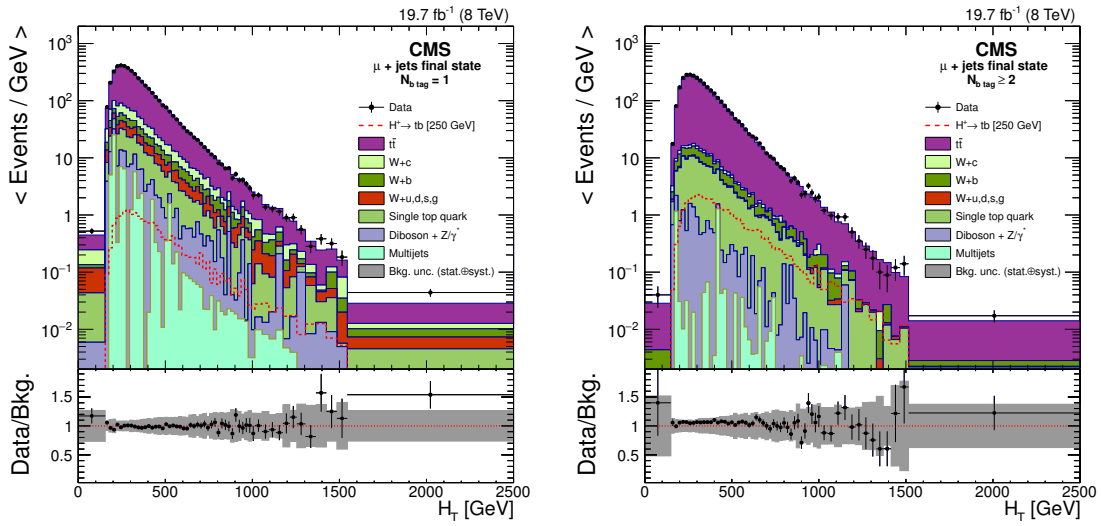

Figure 7. The H_{T} distributions observed in data and predicted for signal and background in the μ+jets channel with $N_{\mathrm{b\ tag}} = 1$ (left) and $N_{\mathrm{b\ tag}} \geq 2$ (right). Normalizations for $\mathrm{t\bar{t}}$, $\mathrm{W + c}$, $\mathrm{W + b}$, and W+light-flavour jets are derived from data. Normalizations for other backgrounds are based on simulation. Expectations for the charged Higgs boson for $m_{\mathrm{H^+}} = 250\,\mathrm{GeV}$, for the $\mathrm{H^+ \to t\bar{b}}$ decays, are also shown. For illustrative purposes, the signal is normalized, assuming $\mathcal{B}(\mathrm{t} \to \mathrm{H^+b}) = 1$, to a cross section of 1 pb, which is typical of the cross section sensitivity of this analysis. The bottom panel shows the ratio of data and the sum of the SM backgrounds with the total uncertainties. Bin contents are normalized to the bin width.

JHEP11(2015)018

9.1 Uncertainties common to the analyses

The sources of systematic uncertainties common to the analyses (unless specified otherwise) and affecting simulated samples only are as follows:

- Uncertainties in the lepton trigger, identification, and isolation efficiencies are calculated from independent samples with a "tag-and-probe" method. The uncertainties in the single electron, single muon, and dilepton triggers amount to 2%, 2%, and 3%, respectively. For the τ_h+jets final state, the treatment is detailed in section 9.2;
- The uncertainty in the efficiency and identification of electrons is 2% (1%) for $p_T >$ 20 (30) GeV. For muons, the uncertainty in the efficiency and identification is 1%;
- The uncertainty in τ_h identification efficiency is estimated to be 6% [83];
- The misidentification uncertainty in events with an electron misidentified as the τ_h is 20% (25%) for the barrel (endcap); for events with a muon (jet) misidentified as the τ_h an uncertainty of 30% (20%) is estimated [83];
- The uncertainty in the τ_h energy scale (τ_h ES) is estimated by varying the τ_h momentum by $\pm$3% [83];
- The uncertainties in the jet energy scale (JES), jet energy resolution (JER), and the contribution to E_T^{miss} scale from particles not clustered to jets ("unclustered E_T^{miss} scale") are estimated independently according to the prescription described in ref. [42], and found to within 1–6% for the signal and dominant simulated backgrounds in all the analyses. The variations of these quantities are also propagated to the E_T^{miss}. The uncertainty in JES is evaluated as a function of jet p_T and jet η, and takes into account JES variations due to parton flavour;
- The uncertainty arising from b tagging/mistagging efficiencies is estimated according to the description in ref. [44]. Values of 3–20% are found in the different analyses;
- A 100% uncertainty is assumed for the reweighting of the top quark p_T spectrum of each top quark in simulated SM $t\bar{t}$ events, discussed in section 4. The reweighting and uncertainty depends on the top quark decay [69];
- The uncertainty in pileup event modelling is estimated by varying the total inelastic cross section used to infer the pileup distribution in data by $\pm$5%;
- Uncertainties in the theoretical cross section normalization described in detail in section 4;
- For the $\mu\tau_h$, ℓ+jets, and $\ell\ell'$ final states, the uncertainties due to ME and parton shower (PS) matching, and those due to the factorization and renormalization scale choices are applied only to the dominant simulated $t\bar{t}$ backgrounds; they are estimated by varying by a factor of two the threshold between jet production at the ME level and via PS and by varying by a factor of four the nominal scale given by the momentum transfer of the hard process (Q^2) in the event;

JHEP11(2015)018

- For the $\mu\tau_h$ and $\ell\ell'$ final states, the uncertainty in the b-tagged jet multiplicity distribution shapes due to PDF variations is estimated separately for the dominant simulated $t\bar{t}$ backgrounds by varying independently the components of the PDF parameterization;

- For the $\mu\tau_h$ and $\ell\ell'$ final states, the uncertainty due to the modelling of the associated heavy-flavour production ($t\bar{t}$+$b\bar{b}$) is taken into account by assigning to each bin of the b-tagged jet multiplicity distribution of the $t\bar{t}$+$b\bar{b}$ events an uncorrelated bin-by-bin uncertainty of 44%. This uncertainty is based on the comparison between the observed and predicted ratios of $\sigma(t\bar{t}+b\bar{b})/\sigma(t\bar{t}+q\bar{q})$ [84];

- The uncertainty in the integrated luminosity is estimated to be 2.6% [85].

9.2 The τ_h+jets final state for $H^+ \to \tau^+\nu_\tau$

In the τ_h+jets final state, some of the systematic uncertainties related to simulated samples also affect the background measurements from data. In the multijet background, a small number of simulated EW+$t\bar{t}$ events is subtracted from the data to obtain the number of multijet events. The uncertainties affecting this small number of simulated events are taken into account, but their magnitudes are suppressed because they apply to only a fraction of the multijet background and a minus sign is assigned for them to denote anticorrelation. For the "EW+$t\bar{t}$ with τ_h" background, uncertainties related to the simulated τ lepton decays are taken into account.

In addition to the uncertainties already described in section 9.1, the following sources of systematic uncertainties are taken into account for the τ_h+jets final state:

- The uncertainties in the efficiencies of the τ part and E_T^{miss} part of the τ+E_T^{miss} trigger measured from data and simulation are considered separately. The simulated samples are affected by both sources of uncertainty, while the "EW+$t\bar{t}$ with τ_h" background, obtained with the "embedding" procedure, is affected only by the uncertainty in the trigger efficiency measured in data. Furthermore, for the "EW+$t\bar{t}$ with τ_h" background, the data part of the μ trigger efficiency is also considered, and a further 12% uncertainty is applied for approximating the E_T^{miss} of the high-level trigger by offline calorimeter-based E_T^{miss};

- The uncertainty in vetoing events with electrons and/or muons affecting only the simulated samples is estimated from the uncertainty in the electron and muon reconstruction, identification, and isolation efficiencies as 2% (1%) for electrons (muons);

- A 50% normalization uncertainty for the m_T distribution is assigned for the simulated single top quark samples in the "EW+$t\bar{t}$ no τ_h" background for assigning as event weight the probability to pass b tagging instead of applying the b tagging condition;

- The uncertainties in the "EW+$t\bar{t}$ with τ_h" background measurement method are described in the following. The uncertainty in the muon identification efficiency in data is found to be small. The contamination of the μ+jets control sample by

JHEP11(2015)018

multijet events is estimated with a μ enriched simulated multijet sample to be at most 2%, which is taken as a systematic uncertainty. The fraction of events with $W \to \tau\nu_\tau \to \mu\nu_\mu\nu_\tau$, discussed in section 5.2.1, is evaluated from simulated events and found to obey a functional form $(1-a)\, p_T^{-b}$, where a and b are positive constants and p_T is the transverse momentum of the selected muon. The systematic uncertainty for correcting the event yield for this effect amounts to 1.2%. A 100% uncertainty is assumed on the event weights accounting for the difference between the τ+jets and embedded μ+jets events from simulated $t\bar{t}$ events (denoted as "Non-emb. vs. emb. difference" in table 6) observed in the m_T distribution;

- The uncertainties in the multijet background measurement method are described in the following. The statistical uncertainty in the E_T^{miss} template fit that is performed in each bin of $p_T^{\tau_h}$, as described in section 5.2, is estimated to be 3% in each $p_T^{\tau_h}$ bin. The difference in the m_T distribution shapes between the nominal sample and the sample with inverted τ_h isolation criterion is taken as a systematic uncertainty. It is evaluated from the ratio of the event yields of the samples with nominal and inverted τ_h isolation criterion as a function of m_T after requiring the other τ_h selection criteria, the veto against electrons and muons, at least three jets, and the requirement on R_{coll}^{min}. The statistical uncertainty of the ratio of the event yields is found to account for the difference in the shape and its magnitude is taken as the systematic uncertainty. Its value ranges between 5–15% depending on the bin of the m_T distribution.

A summary of the systematic uncertainties is shown in table 6.

In the region where the background yields are taken from the exponential fit on m_T, the statistical uncertainties in the background distributions are given by the uncertainties on the fit parameters while the relative values of the systematic uncertainties are kept the same like in the unfitted m_T distribution.

The dominant systematic uncertainties for signal arise from τ_h identification, τ_h energy scale, b tagging, and the theoretical $t\bar{t}$ cross section uncertainty for $m_{H^+} < m_t - m_b$. For the backgrounds, the dominant uncertainties are those in τ_h identification, jet$\to\tau_h$ misidentification, treatment of the E_T^{miss} part of the trigger, and the difference between the transverse mass shapes of the τ+jets and embedded μ+jets events. In the region $m_{H^+} > 300\,\text{GeV}$ the sensitivity of the analysis is driven solely by the signal acceptance and the uncertainties in the signal.

9.3 The $\mu\tau_h$ final state for $H^+ \to \tau^+\nu_\tau$ and $H^+ \to t\bar{b}$

The dominant sources of systematic uncertainties are the τ_h identification and misidentification, the top quark p_T modelling, and the prediction of the $t\bar{t}$ cross section. In addition to the uncertainties described in section 9.1, an uncertainty associated with the misidentified τ_h background estimated from data is evaluated as half of the maximum variation between the "W+jet" and "multijet" estimates discussed in section 6.2. The statistical uncertainty associated with the number of events in the control region to which the final estimate is applied amounts to 1% and is taken into account in the limit computation.

JHEP11(2015)018

Source	Signal H^+H^-	Signal H^+W^-	Signal H^+	Multi-jets	EW+$t\bar{t}$ with τ_h	EW+$t\bar{t}$ no τ_h
τ part of trigger (data)	1.5–1.8	1.3–1.5	1.8–3.0	−0.5	1.2	1.4
τ part of trigger (simulation)	0.7–0.8	0.6–0.7	0.8–1.1	−0.2		0.8
E_T^{miss} part of trigger (data)	2.6–3.3	2.5–2.8	2.9–4.2	−1.2	2.5	2.8
E_T^{miss} part of trigger (simulation)	0.1	0.1	0.1	−0.1		0.4
Approximation in E_T^{miss} part of trigger					12	
Single μ trigger; data					−0.1	
Veto of events with e	0.1–0.2	0.2–0.3	0.2–0.3	<−0.1		0.4
Veto of events with μ	0.1	0.1–0.2	0.1	<−0.1		0.5
τ_h identification (S)	6.0	6.0	5.9–6.0	−0.8	6.0	
e misidentification as τ_h (S)	<0.1	<0.1	<0.1	−0.1		3.3
μ misidentification as τ_h (S)	<0.1	<0.1	<0.1	<−0.1		1.1
Jet misidentification as τ_h (S)	0.1	0.1–0.3	0.1	−6.9		17
τ_h energy scale (S)	0.3–2.6	2.7–5.2	0.3–2.7	−1.8	5.8	2.0
Jet energy scale	2.6–5.2	2.0–3.0	1.6–2.1	−1.4		3.2
Jet energy resolution	1.1–1.8	0.5–1.3	0.7–1.5	−0.2		3.2
Unclustered E_T^{miss} energy scale	0.1–0.4	0.1–0.9	0.1–0.4	−0.5		1.5
b-jet tagging (S)	5.9–20	4.7–5.3	4.6–5.4	−3.5		5.0
Top quark p_T modelling (S)				$^{+5.6}_{-6.8}$		$^{+11}_{-6.6}$
Pileup modelling	0.1–0.9	0.1–0.8	0.1–0.6	−0.1		2.9
μ identification; data					<−0.1	
Multijet contamination					2.0	
$W \to \tau\nu_\tau \to \mu\nu_\mu\nu_\tau$ fraction					1.2	
Non-emb. vs. emb. difference (S)					$^{+14}_{-12}$	
Multijet m_T distribution shape (S)				4.6		
Multijet template fit				3.0		
Probabilistic m_T in single top quark						6.8
$t\bar{t}$ cross section, scale	$^{+2.5}_{-3.4}$	$^{+2.5}_{-3.4}$		$^{+1.0}_{-0.7}$		$^{+2.2}_{-2.9}$
$t\bar{t}$ cross section, PDF+α_S	4.6	4.6		−1.6		4.0
Single top quark cross section						1.0
W+jets, Z/γ^*, VV cross section						0.1
Integrated luminosity	2.6	2.6	2.6	−0.8		2.6

Table 6. The systematic uncertainties (in %) on event yields for the charged Higgs boson signal processes $t\bar{t} \to bH^+\bar{b}H^-$ (H^+H^-), $t\bar{t} \to bH^+\bar{b}W^-$ (H^+W^-), and $pp \to \bar{t}(b)H^+$ (H^+) and for the background processes. The uncertainties which depend on the m_T distribution bin are marked with (S) and for these the maximum integrated value of the negative or positive variation is displayed. Empty cells indicate that an uncertainty does not affect the sample. The uncertainty values within the rows are considered to be fully correlated and the values within the columns are considered to be uncorrelated. A minus sign in front of an uncertainty value means anticorrelation with other values in the same row.

JHEP11(2015)018

Source	Signal	$t\bar{t} \to \mu\tau_h + X$	$t\bar{t}$ dilepton	τ_h mis-id	single top quark
Single μ trigger	2.0	2.0	2.0		
e identification	2.0	2.0	2.0		2.0
μ identification	1.0	1.0	1.0		1.0
τ_h identification	6.0	6.0			6.0
e misidentification as τ_h			3.0		
μ misidentification as τ_h			3.0		
Jet misidentification as τ_h			20		
τ_h energy scale (S)	0.6	2.4	4.4		4.1
Jet energy scale (S)	2.5	1.9	2.6		3.9
Jet energy resolution (S)	0.8	0.1	1.6		0.2
Unclustered E_T^{miss} energy scale (S)	0.8	0.1	1.8		0.2
b tagging (S)	1.8	1.8	2.7		3.2
udsg→b mistagging (S)	<0.1	<0.1	<0.1		0.1
Top quark p_T modelling (S)		5.4	5.2		
Pileup modelling	4.0	2.0	8.0		2.0
Misidentified τ_h background				11	
Cross sections		$^{+2.5}_{-3.4} \pm 4.6$	$^{+2.5}_{-3.4} \pm 4.6$		8.0
Matching scale (S)		12	5.1		
Fact./renorm. scale (S)		3.4	7.5		
PDF effect on shape		shape only	shape only		
Heavy flavours (S)		<0.1	<0.1		
Integrated luminosity	2.6	2.6	2.6		2.6

Table 7. The systematic uncertainties (in %) for the $\mu\tau_h$ final state for backgrounds, and for signal events from $H^+ \to t\bar{b}$ decays for $m_{H^+} = 250\,\text{GeV}$. These systematic uncertainties are given as the input to the exclusion limit calculation. The uncertainties that depend on the b-tagged jets multiplicity distribution bin are marked with (S) and for these the maximum integrated value of the negative or positive variation is displayed. Empty cells indicate that an uncertainty does not affect the sample. The uncertainty values within the rows are considered to be fully correlated and the values within the columns are considered to be uncorrelated. The uncertainties in the cross sections are to be considered uncorrelated for different samples and fully correlated for different final states of the same sample (e.g. the different $t\bar{t}$ decays).

The systematic uncertainties for the signal and background samples are summarized in table 7. The diboson and Drell-Yan background yields are small compared to the uncertainty on the $t\bar{t}$ background, and consequently are not used in the limit computation. Results are not sensitive to the inclusion of those backgrounds.

9.4 Dilepton (ee/eμ/$\mu\mu$) final states for $H^+ \to \tau^+\nu_\tau$ and $H^+ \to t\bar{b}$

The main sources of systematic uncertainties are the unclustered E_T^{miss} scale, the b tagging efficiency, and the prediction of the $t\bar{t}$ cross section.

The systematic uncertainties for signal and background events are summarized in table 8. The diboson, Z/γ^*, "other $t\bar{t}$", and W+jets backgrounds yields are small compared to the uncertainty on the $t\bar{t}$ background, and consequently are not used in the limit computation. Results are not sensitive to the inclusion of those backgrounds.

JHEP11(2015)018

Source	Signal	$t\bar{t}$ dilepton	$Z/\gamma^* \to \ell\ell$	single top quark
eμ trigger	3.0	3.0	3.0	3.0
e identification	2.0	2.0	2.0	2.0
μ identification	1.0	1.0	1.0	1.0
Jet energy scale (S)	1.4	1.1	1.7	1.4
Jet energy resolution (S)	0.3	0.3	0.4	0.4
Unclustered $E_{\mathrm{T}}^{\mathrm{miss}}$ energy scale (S)	1.3	2.1	11.7	2.6
b tagging (S)	2.4	3.7	10	4.3
udsg→b mistagging (S)	2.3	3.6	10	4.4
Top quark p_{T} modelling (S)		3.8		
Pileup modelling	0.6	0.4	1.2	1.2
Cross sections		$^{+2.5}_{-3.4} \pm 4.6$	4.0	8.0
Matching scale (S)		7.7		
Fact./renorm. scale (S)		8.4		
PDF shape		shape only		
Heavy flavours (S)		<0.1		
Integrated luminosity	2.6	2.6	2.6	2.6

Table 8. The systematic uncertainties (in %) for backgrounds, and for signal events from $H^+ \to t\bar{b}$ decays for the dilepton channels for a charged Higgs boson mass $m_{H^+} = 250\,\mathrm{GeV}$. The e$\mu$ final state is shown as a representative example. These systematic uncertainties are given as the input to the exclusion limit calculation. The uncertainties that depend on the b-tagged jets multiplicity distribution bin are marked with (S) and for these the maximum integrated value of the negative or positive variation is displayed. Empty cells indicate that an uncertainty does not affect the sample. The uncertainty values within the rows are considered to be fully correlated and the values within the columns are considered to be uncorrelated. The uncertainties in the cross sections are to be considered uncorrelated for different samples and fully correlated for different final states of the same sample (e.g. the different $t\bar{t}$ decay channels).

9.5 Single-lepton (e/μ+jets) final states for $H^+ \to t\bar{b}$

In addition to the uncertainties described earlier in this section, the following systematic uncertainties specific to the ℓ+jets final states, affecting the simulated samples only, are as follows:

- The normalizations for $t\bar{t}$, W+c, W+b, and W+light-flavour backgrounds are left unconstrained. Statistical and systematic uncertainties are applied to yields in the control regions described in section 3. These uncertainties are based on deviations of the fitted normalization factor when varying multijet and Z/γ^*+jets contributions by a factor of two, signal contamination by a factor of five, and by requiring either two or three jets in the control region. The total uncertainty in the normalization factors ranges between 5–35%.

- A 50% uncertainty [86–88] is applied to the Z/γ^*+jets and diboson backgrounds due to their small contribution to the signal region;

JHEP11(2015)018

Source	$H^+ \to t\bar{b}$	$t\bar{t}$	W+c	W+b	W+u,d,s,g	single top quark	$Z/\gamma^*/VV$	Multijets
Single-e trigger	2.0	2.0	2.0	2.0	2.0	2.0	2.0	2.0
Single-μ trigger	2.0	2.0	2.0	2.0	2.0	2.0	2.0	2.0
e identification	1.0	1.0	1.0	1.0	1.0	1.0	1.0	1.0
μ identification	1.0	1.0	1.0	1.0	1.0	1.0	1.0	1.0
Jet energy scale (S)	4.0	6.4	15	11	14	9.2	27	49
Jet energy resolution (S)	0.1	0.3	1.7	2.3	1.4	0.8	2.3	6.9
b tagging (S)	3.9	1.3	14	6.2	11	0.7	5.4	16
Top quark p_T modelling (S)		3.5						
Pileup modelling (S)	1.2	0.7	2.3	0.5	0.4	0.7	3.7	7.0
Normalization from data, e+jets		5.5*	4.9*	25*	9.6*			
Normalization from data, μ+jets		5.2*	10*	34*	10*			
Cross section						8.0	50	100
Fact./renorm. scales (S)		7.3						
Q^2 scale (S)		7.6						
Integrated Luminosity	2.6					2.6	2.6	2.6

Table 9. The systematic uncertainties (in %) for backgrounds, and for signal events from $H^+ \to t\bar{b}$ decays for the ℓ+jets channels for a charged Higgs boson mass $m_{H^+} = 250\,\text{GeV}$. The uncertainties that depend on the shape of the H_T distribution bin are marked with (S) and for these the maximum integrated value of the negative or positive variation is displayed. Empty cells indicate that an uncertainty does not affect the sample. The uncertainty values within the rows are considered to be fully correlated, with the exception of cross section and data-driven normalization, which are considered to be uncorrelated. The uncertainty values within the columns are considered to be uncorrelated. Uncertainties labelled with a "*" are only present in the CR with an implicit unconstrained parameter correlated across all bins (section 8.2). The values for these are assigned prior to the setting of limits.

- A 100% systematic uncertainty is applied to the QCD cross section normalization. This accounts for the maximal variation in the QCD normalization when left unconstrained in the background-only fit to data while constraining normalizations for other backgrounds to their systematic uncertainties.

The systematic uncertainties for signal and background events are summarized in table 9.

10 Results

A statistical analysis of the m_T (figure 3), b-tagged jet multiplicity (figure 4 (right) and figure 5 (right)), and H_T (figure 7) distributions has been performed using a binned maximum likelihood fit. The data agree with the SM prediction and consequently 95% CL upper limits on charged Higgs boson production are derived using the modified frequentist CL_s criterion [89, 90] with a test statistic based on the profile likelihood ratio with asymptotic approximation [91, 92].

The systematic uncertainties described in section 9 are incorporated via nuisance parameters following the frequentist paradigm. Correlations between the different sources of systematic uncertainty are taken into account. Uncertainties affecting the shape of the m_T, b-tagged jet multiplicity, or H_T distributions are represented by nuisance parameters whose variation results in a continuous perturbation of the distribution [93].

JHEP11(2015)018

10.1 Model-independent limits on charged Higgs boson production ($\mathrm{H}^+ \to \tau^+\nu_\tau$)

In the analysis of the $\mathrm{H}^+ \to \tau^+\nu_\tau$ decay mode with the τ_h+jets final state no assumption on the charged Higgs boson branching fractions is needed because subtracting the background from "EW+$\mathrm{t\bar{t}}$ with τ_h" will remove any potential $\mathrm{H}^+ \to \mathrm{t\bar{b}}$ and other such signals from data due to the embedding technique described in section 5.2.1. For $m_{\mathrm{H}^+} = 80$–$160\,\mathrm{GeV}$, the charged Higgs boson is produced most copiously through $\mathrm{t\bar{t}}$ production which can produce one ($\mathrm{t\bar{t}} \to \mathrm{bH^+\bar{b}W^-}$) or two charged Higgs bosons ($\mathrm{t\bar{t}} \to \mathrm{bH^+\bar{b}H^-}$) if $\mathcal{B}(\mathrm{t} \to \mathrm{H^+b}) > 0$. Furthermore, the presence of the charged Higgs boson suppresses the $\mathrm{t\bar{t}} \to \mathrm{bW^+\bar{b}W^-}$ yield compared to the SM prediction. Consequently, the number of events in a given bin of the m_T distribution depends on the signal strength parameter μ according to:

$$N(\mu) = \mu^2\, s(\mathrm{H^+H^-}) + 2\mu(1-\mu)\, s(\mathrm{H^+W^-}) + (1-\mu)^2\, b(\mathrm{W^+W^-}) + b, \tag{10.1}$$

where $\mu = \mathcal{B}(\mathrm{t} \to \mathrm{H^+b})\,\mathcal{B}(\mathrm{H^+} \to \tau^+\nu_\tau)$, $s(\mathrm{H^+H^-})$ and $s(\mathrm{H^+W^-})$ are the number of expected signal events for the $\mathrm{t\bar{t}} \to \mathrm{bH^+\bar{b}H^-}$ and $\mathrm{t\bar{t}} \to \mathrm{bH^+\bar{b}W^-}$ processes, respectively; $b(\mathrm{W^+W^-})$ is the expected number of events from the portion of $\mathrm{t\bar{t}} \to \mathrm{bW^+\bar{b}W^-}$ background that is estimated with simulation, and b is the expected number of other background events. The number of signal and $\mathrm{t\bar{t}} \to \mathrm{bW^+\bar{b}W^-}$ background events is normalized to the SM predicted cross section and by setting $\mathcal{B}(\mathrm{t} \to \mathrm{H^+b})\,\mathcal{B}(\mathrm{H^+} \to \tau^+\nu_\tau) = 1$ for a top quark decaying to a charged Higgs boson.

For $m_{\mathrm{H}^+} = 180$–$600\,\mathrm{GeV}$, the number of events in a given bin of the m_T distribution depends on the signal strength parameter according to:

$$N(\mu) = \mu\,\varepsilon_\mathrm{s}\mathcal{L} + b, \tag{10.2}$$

where $\mu = \sigma(\mathrm{pp} \to \mathrm{\bar{t}(b)H^+})\,\mathcal{B}(\mathrm{H^+} \to \tau^+\nu_\tau)$, ε_s is the event selection efficiency for signal events, $\mathcal{L}$ is the integrated luminosity, and b is the expected number of background events.

The upper limits on $\mathcal{B}(\mathrm{t} \to \mathrm{H^+b})\,\mathcal{B}(\mathrm{H^+} \to \tau^+\nu_\tau)$ and on $\sigma(\mathrm{pp} \to \mathrm{\bar{t}(b)H^+})\,\mathcal{B}(\mathrm{H^+} \to \tau^+\nu_\tau)$ are shown in figure 8 for the $\mathrm{H}^+ \to \tau^+\nu_\tau$ decay mode with the τ_h+jets final state for the ranges $m_{\mathrm{H}^+} = 80$–$160\,\mathrm{GeV}$ and $m_{\mathrm{H}^+} = 180$–$600\,\mathrm{GeV}$, respectively. The numerical values of the limits are given in table 10. At $m_{\mathrm{H}^+} = 250\,\mathrm{GeV}$ an excess of data is observed with a local p-value of 0.046 corresponding to significance of 1.7σ.

10.2 Limits on charged Higgs boson production with branching fraction assumed

In the presence of a charged Higgs boson and for $m_{\mathrm{H}^+} = 180$–$600\,\mathrm{GeV}$, the analyses of the $\mu\tau_\mathrm{h}$, ℓ+jets, and $\ell\ell'$ final states have sensitivity to both $\mathrm{H}^+ \to \tau^+\nu_\tau$ and $\mathrm{H}^+ \to \mathrm{t\bar{b}}$ decays. Consequently, a model-independent limit can neither be provided for $\sigma(\mathrm{pp} \to \mathrm{\bar{t}(b)H^+})\,\mathcal{B}(\mathrm{H^+} \to \tau^+\nu_\tau)$ nor for $\sigma(\mathrm{pp} \to \mathrm{\bar{t}(b)H^+})\,\mathcal{B}(\mathrm{H^+} \to \mathrm{t\bar{b}})$. Nevertheless, one can test models by fixing $\mathcal{B}(\mathrm{H^+} \to \tau^+\nu_\tau)$ and $\mathcal{B}(\mathrm{H^+} \to \mathrm{t\bar{b}})$. In this section, results are reported for a model with $\mathcal{B}(\mathrm{H^+} \to \mathrm{t\bar{b}}) = 1$, to which the τ_h+jets analysis is blind because of the estimates of the backgrounds from data like described in section 5.2.1. For

JHEP11(2015)018

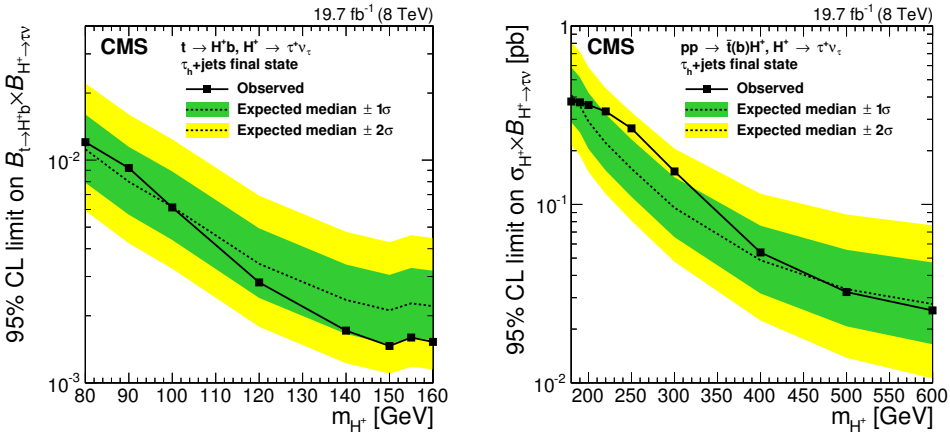

Figure 8. Expected and observed 95% CL model-independent upper limits on $\mathcal{B}(\mathrm{t} \to \mathrm{H}^+\mathrm{b})\,\mathcal{B}(\mathrm{H}^+ \to \tau^+\nu_\tau)$ with $m_{\mathrm{H}^+} = 80$–$160\,\mathrm{GeV}$ (left), and on $\sigma(\mathrm{pp} \to \bar{\mathrm{t}}(\mathrm{b})\mathrm{H}^+)\,\mathcal{B}(\mathrm{H}^+ \to \tau^+\nu_\tau)$ with $m_{\mathrm{H}^+} = 180$–$600\,\mathrm{GeV}$ (right) for the $\mathrm{H}^+ \to \tau^+\nu_\tau$ search in the τ_h+jets final state. The regions above the solid lines are excluded.

m_{H^+}	Expected limit					Observed
[GeV]	-2σ	-1σ	median	$+1\sigma$	$+2\sigma$	limit
95% CL upper limit on $\mathcal{B}(\mathrm{t} \to \mathrm{H}^+\mathrm{b})\,\mathcal{B}(\mathrm{H}^+ \to \tau^+\nu_\tau)$						
80	0.0059	0.0079	0.0112	0.0160	0.0221	0.0120
90	0.0042	0.0057	0.0080	0.0115	0.0160	0.0092
100	0.0033	0.0044	0.0062	0.0089	0.0124	0.0061
120	0.0018	0.0024	0.0034	0.0049	0.0069	0.0028
140	0.0012	0.0017	0.0024	0.0034	0.0048	0.0017
150	0.0011	0.0015	0.0021	0.0031	0.0043	0.0015
155	0.0012	0.0016	0.0023	0.0033	0.0046	0.0016
160	0.0011	0.0016	0.0022	0.0032	0.0045	0.0015
95% CL upper limit on $\sigma(\mathrm{pp} \to \bar{\mathrm{t}}(\mathrm{b})\mathrm{H}^+)\,\mathcal{B}(\mathrm{H}^+ \to \tau^+\nu_\tau)$ [pb]						
180	0.213	0.289	0.409	0.587	0.816	0.377
190	0.188	0.254	0.358	0.516	0.719	0.373
200	0.152	0.205	0.291	0.423	0.587	0.361
220	0.114	0.155	0.221	0.321	0.448	0.332
250	0.081	0.110	0.159	0.231	0.328	0.267
300	0.048	0.065	0.096	0.142	0.205	0.153
400	0.022	0.032	0.049	0.076	0.115	0.054
500	0.014	0.021	0.033	0.056	0.088	0.032
600	0.011	0.016	0.028	0.047	0.076	0.025

Table 10. Expected and observed 95% CL model-independent upper limits on $\mathcal{B}(\mathrm{t} \to \mathrm{H}^+\mathrm{b})\,\mathcal{B}(\mathrm{H}^+ \to \tau^+\nu_\tau)$ for $m_{\mathrm{H}^+} = 80$–$160\,\mathrm{GeV}$ (top), and on $\sigma(\mathrm{pp} \to \bar{\mathrm{t}}(\mathrm{b})\mathrm{H}^+)\,\mathcal{B}(\mathrm{H}^+ \to \tau^+\nu_\tau)$ for $m_{\mathrm{H}^+} = 180$–$600\,\mathrm{GeV}$ (bottom), for the $\mathrm{H}^+ \to \tau^+\nu_\tau$ search in the τ_h+jets final state.

JHEP11(2015)018

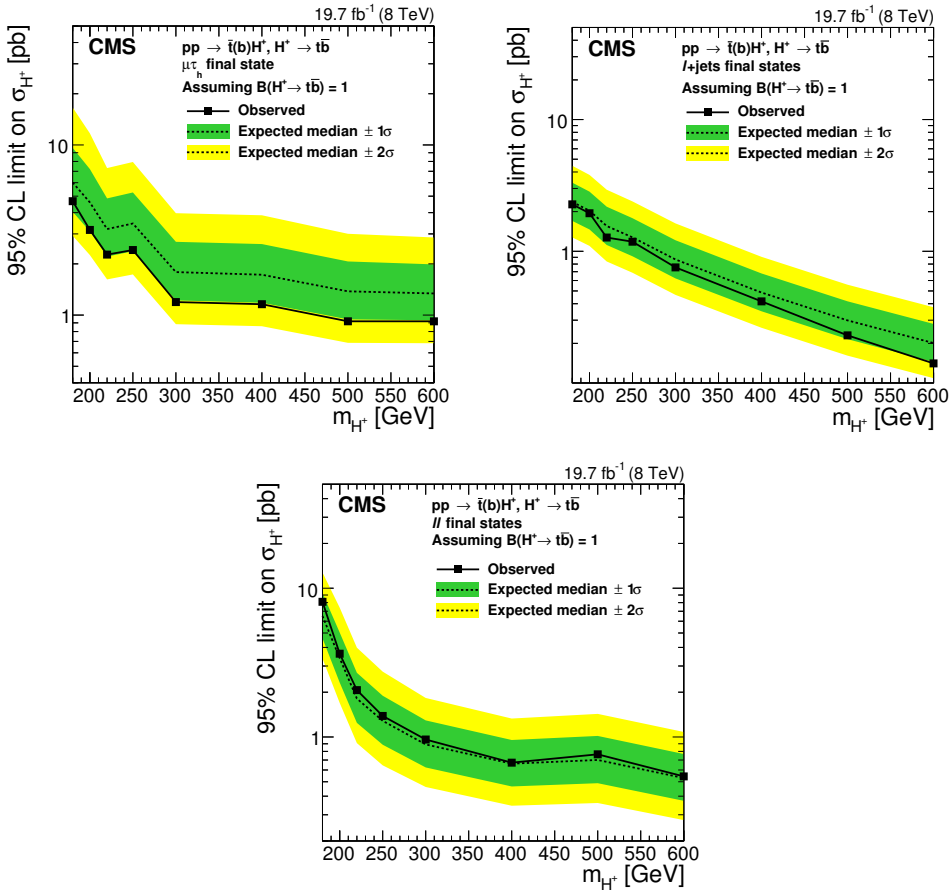

Figure 9. Expected and observed 95% CL upper limits on $\sigma(\mathrm{pp} \to \bar{\mathrm{t}}(\mathrm{b})\mathrm{H}^+)$ for the $\mu\tau_\mathrm{h}$ (upper left), ℓ+jets (upper right), and $\ell\ell'$ final states (bottom) assuming $\mathcal{B}(\mathrm{H}^+ \to \mathrm{t}\bar{\mathrm{b}}) = 1$. The regions above the solid lines are excluded.

$\mathcal{B}(\mathrm{H}^+ \to \tau^+\nu_\tau) = 1$, the sensitivity of the $\mu\tau_\mathrm{h}$ and $\ell\ell'$ final states analyses is found to be substantially weaker than that obtained in the τ_h+jets analysis.

Equation (10.2) is used to derive the limits by counting the number of events in bins of the b-tagged jet multiplicity distribution for the $\mu\tau_\mathrm{h}$ and $\ell\ell'$ final states, and in bins of the H_T distribution for the ℓ+jets final state. The upper limits on $\sigma(\mathrm{pp} \to \bar{\mathrm{t}}(\mathrm{b})\mathrm{H}^+)$ assuming $\mathcal{B}(\mathrm{H}^+ \to \mathrm{t}\bar{\mathrm{b}}) = 1$ are shown in figure 9 for the $\mu\tau_\mathrm{h}$ (top left), ℓ+jets (top right), and $\ell\ell'$ (bottom) final states.

The upper limit on $\sigma(\mathrm{pp} \to \bar{\mathrm{t}}(\mathrm{b})\mathrm{H}^+)$ for the combination of the $\mu\tau_\mathrm{h}$, ℓ+jets, and $\ell\ell'$ final states is shown in figure 10. The numerical values are reported in table 11. In the combination, the sensitivity is driven by the ℓ+jets final state.

10.3 Combined limits on $\tan\beta$ in MSSM benchmark scenarios

Using all decay modes and final states, exclusion regions have been set in the m_{H^+}–$\tan\beta$ plane according to the LHC Higgs cross section working group prescription for different MSSM benchmark scenarios [29, 33]: "updated $m_\mathrm{h}^{\mathrm{max}}$", "$m_\mathrm{h}^{\mathrm{mod+}}$", "$m_\mathrm{h}^{\mathrm{mod-}}$", "light stop", "light stau", "tau-phobic", and "low-M_H" scenarios. These MSSM benchmark scenarios

JHEP11(2015)018

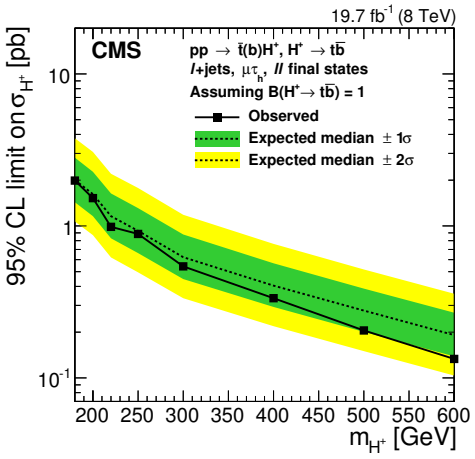

Figure 10. Expected and observed 95% CL upper limits on $\sigma(\mathrm{pp} \to \bar{\mathrm{t}}(\mathrm{b})\mathrm{H}^+)$ for the combination of the $\mu\tau_\mathrm{h}$, ℓ+jets, and $\ell\ell'$ final states assuming $\mathcal{B}(\mathrm{H}^+ \to \mathrm{t}\bar{\mathrm{b}}) = 1$. The region above the solid line is excluded.

m_{H^+}	Expected limit [pb]					Observed limit
[GeV]	-2σ	-1σ	median	$+1\sigma$	$+2\sigma$	[pb]
95% CL upper limit on $\sigma(\mathrm{pp} \to \bar{\mathrm{t}}(\mathrm{b})\mathrm{H}^+)$ with $\mathcal{B}(\mathrm{H}^+ \to \mathrm{t}\bar{\mathrm{b}}) = 1$						
180	1.07	1.43	2.01	2.81	3.78	1.99
200	0.87	1.16	1.62	2.27	3.07	1.52
220	0.62	0.83	1.16	1.64	2.20	0.99
250	0.49	0.66	0.93	1.31	1.78	0.89
300	0.33	0.45	0.62	0.88	1.18	0.54
400	0.22	0.29	0.40	0.57	0.76	0.33
500	0.15	0.20	0.28	0.39	0.52	0.21
600	0.10	0.14	0.19	0.27	0.36	0.13

Table 11. Expected and observed 95% CL upper limits on $\sigma(\mathrm{pp} \to \bar{\mathrm{t}}(\mathrm{b})\mathrm{H}^+)\,\mathcal{B}(\mathrm{H}^+ \to \mathrm{t}\bar{\mathrm{b}})$ assuming $\mathcal{B}(\mathrm{H}^+ \to \mathrm{t}\bar{\mathrm{b}}) = 1$ for the combination of the $\mu\tau_\mathrm{h}$, ℓ+jets, and $\ell\ell'$ final states.

are compatible with the properties of the recently discovered neutral scalar boson and with the current bounds on supersymmetric particle masses, and they are specified using low-energy MSSM parameters, i.e. no particular soft SUSY-breaking scenario is assumed. The updated $m_\mathrm{h}^{\mathrm{max}}$ scenario and $m_\mathrm{h}^{\mathrm{mod}}$ scenarios allow the discovered scalar boson to be interpreted as the light CP-even Higgs boson in large parts of the m_{H^+}–$\tan\beta$ plane. The light stop scenario leads to a suppressed rate for the Higgs boson production by gluon fusion, and the light stau scenario enhances the decay rate of the light CP-even Higgs boson to photons. A tau-phobic scenario has suppressed couplings to down-type fermions. In the low-M_H scenario, the discovered scalar boson is assumed to be the heavy CP-even Higgs boson and m_A is fixed to be 110 GeV causing m_{H^+} to be 132 GeV.

JHEP11(2015)018

Figure 11 shows the limits on the updated $m_{\mathrm{h}}^{\mathrm{max}}$ and $m_{\mathrm{h}}^{\text{mod-}}$ scenarios. For $m_{\mathrm{H}^+} = 90$–$160\,\mathrm{GeV}$, the analysis of the $\mathrm{H}^+ \to \tau^+\nu_\tau$ decay mode with the τ_{h}+jets final state described in section 5 is taken as input. The mass range starts here from $m_{\mathrm{H}^+} = 90\,\mathrm{GeV}$, as the lower values of a charged Higgs boson mass are not accessible in the considered MSSM scenarios. For $m_{\mathrm{H}^+} = 200$–$600\,\mathrm{GeV}$, a combination of all decay modes and final states is used to set the limits. In this combination, the signal yields from the $\mathrm{H}^+ \to \tau^+\nu_\tau$ and $\mathrm{H}^+ \to \mathrm{t\bar{b}}$ decay modes are defined by the branching fractions predicted by the model. If the limit on the charged Higgs boson production for a given m_{H^+}–$\tan\beta$ point is smaller than the cross section predicted by the model [28–31], the point is excluded. The mass range is chosen to start from $m_{\mathrm{H}^+} = 200\,\mathrm{GeV}$ to avoid the interference region where a charged Higgs boson is produced both from off-shell top quark decays and through direct production. In all these scenarios except for the low-M_{H} and light stop scenarios, a lower bound of about 155 GeV on the charged Higgs boson mass has been set assuming $m_{\mathrm{h}} = 125 \pm 3\,\mathrm{GeV}$. The light stop scenario is excluded for $m_{\mathrm{H}^+} < 160\,\mathrm{GeV}$ assuming $m_{\mathrm{h}} = 125 \pm 3\,\mathrm{GeV}$. For $m_{\mathrm{H}^+} > m_{\mathrm{t}} - m_{\mathrm{b}}$, the $\mathrm{H}^+ \to \mathrm{t\bar{b}}$ decay mode searches yield a lower limit on $\tan\beta$ while the upper limit on $\tan\beta$ is dominated by the results from the analysis of the $\mathrm{H}^+ \to \tau^+\nu_\tau$ decay mode with the τ_{h}+jets final state. The low-M_{H} scenario is completely excluded (figure 12) assuming the heavy CP-even MSSM Higgs boson mass is $m_{\mathrm{H}} = 125 \pm 3\,\mathrm{GeV}$.

In figures 11–12, theoretical systematic uncertainties affecting the expected signal event yields are added to the limit computation, modelled as nuisance parameters, in addition to the uncertainties discussed in section 9. The uncertainty in the branching fractions of the charged Higgs boson is estimated from the decay width uncertainties as in ref. [94] by scaling each partial width separately while fixing all others to their central values. This results in individual theoretical uncertainties for each branching fraction. The width uncertainties comprise the uncertainty from missing higher order corrections to beyond LO EW diagrams (5%), missing higher order corrections to NLO QCD (2%), and Δ_{b}-correction uncertainties (3%) [95]. The Δ_b-correction arises from the presence of squarks and gluino contributions in the charged Higgs boson Yukawa coupling to top and bottom quarks [96, 97].

For $m_{\mathrm{H}^+} = 90$–160 GeV, the theoretical uncertainties in the signal yield include the uncertainties in the branching fractions for $\mathrm{t} \to \mathrm{H}^+\mathrm{b}$ and $\mathrm{H}^+ \to \tau^+\nu_\tau$ totalling 0.1–5.0% depending on m_{H^+} and $\tan\beta$. Additionally, an uncertainty of 3% is added to the simulated $\mathrm{t\bar{t}}$ background to take into account higher order corrections to the $\mathrm{t\bar{t}}$ cross section. For $m_{\mathrm{H}^+} = 200$–$600\,\mathrm{GeV}$, the charged Higgs boson production cross section uncertainty and the uncertainty in the branching ratios are considered. The cross section uncertainty varies between 22–32% depending on m_{H^+}, $\tan\beta$, and the MSSM benchmark scenario. The uncertainty in $\mathcal{B}(\mathrm{H}^+ \to \tau^+\nu_\tau)$ varies between 0.4–5.0% for $\tan\beta = 10$–60 depending on m_{H^+} and the MSSM benchmark scenario. The $\mathcal{B}(\mathrm{H}^+ \to \mathrm{t\bar{b}})$ uncertainty varies between 0.1–5.0% for $\tan\beta = 1$–10 depending on m_{H^+} and the MSSM benchmark scenario. The theoretical branching fraction uncertainties for a given m_{H^+}–$\tan\beta$ point are summed linearly according to the LHC Higgs cross section working group prescription [94, 95], but the cross section and branching fraction uncertainties are treated as independent nuisances. The expected limit improves by no more than 2% if the theoretical uncertainties are treated in the statistical model as independent sources.

JHEP11(2015)018

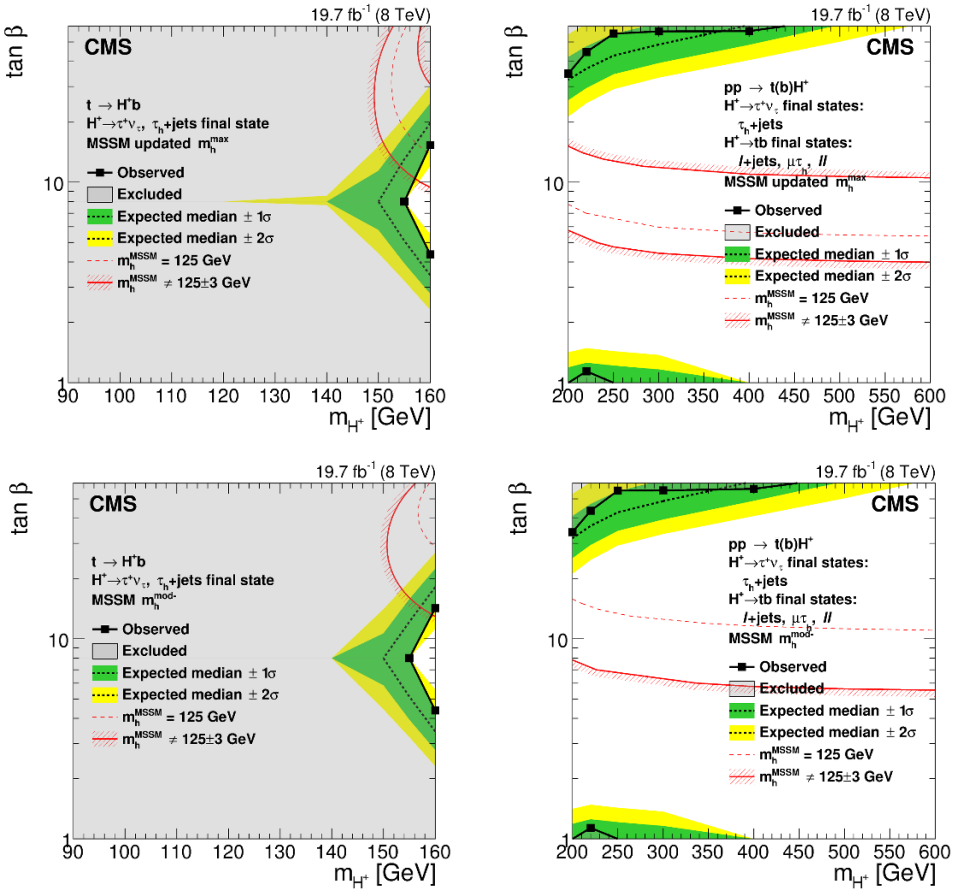

Figure 11. Exclusion region in the MSSM m_{H^+}–$\tan\beta$ parameter space for m_{H^+} = 80–160 GeV (left column) and for m_{H^+} = 180–600 GeV (right column) in the updated MSSM m_h^{max} scenario (top row) and m_h^{mod-} scenarios [29, 33] (bottom row). In the upper row plots the limit is derived from the $H^+ \to \tau^+\nu_\tau$ search with the τ_h+jets final state, and in the lower row plots the limit is derived from a combination of all the charged Higgs boson decay modes and final states considered. The $\pm1\sigma$ and $\pm2\sigma$ bands around the expected limit are also shown. The light-grey region is excluded. The red lines depict the allowed parameter space for the assumption that the discovered scalar boson is the lightest CP-even MSSM Higgs boson with a mass $m_h = 125 \pm 3$ GeV, where the uncertainty is the theoretical uncertainty in the Higgs boson mass calculation.

11 Summary

A search is performed for a charged Higgs boson with the CMS detector using a data sample corresponding to an integrated luminosity of $19.7 \pm 0.5\,\text{fb}^{-1}$ in proton-proton collisions at $\sqrt{s} = 8$ TeV. The charged Higgs boson production in $t\bar{t}$ decays and in $pp \to \bar{t}(b)H^+$ is studied assuming $H^+ \to \tau^+\nu_\tau$ and $H^+ \to t\bar{b}$ decay modes, using the τ_h+jets, $\mu\tau_h$, ℓ+jets, and $\ell\ell'$ final states. Data are found to agree with the SM expectations.

Model-independent limits without an assumption on the charged Higgs boson branching fractions are derived for the $H^+ \to \tau^+\nu_\tau$ decay mode in the τ_h+jets final state. Upper limits at 95% CL of $\mathcal{B}(t \to H^+b)\,\mathcal{B}(H^+ \to \tau^+\nu_\tau)$ = 1.2–0.15% and $\sigma(pp \to \bar{t}(b)H^+)\,\mathcal{B}(H^+ \to \tau^+\nu_\tau)$ = 0.38–0.025 pb are set for charged Higgs boson mass ranges m_{H^+} = 80–160 GeV and m_{H^+} = 180–600 GeV, respectively.

JHEP11(2015)018

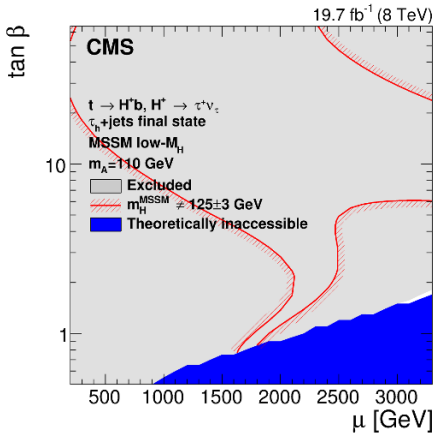

Figure 12. Exclusion region in the MSSM Higgsino mass parameter (μ) vs. $\tan\beta$ parameter space in the low-M_{H} scenario [29, 33] with $m_{\mathrm{A}} = 110\,\mathrm{GeV}$ for the $\mathrm{H}^+ \to \tau^+\nu_\tau$ search with the τ_{h}+jets final state. The light-grey region is excluded and the blue region is theoretically inaccessible. The area inside the red lines is the allowed parameter space for the assumption that the discovered scalar boson is the heavy CP-even MSSM Higgs boson with a mass $m_{\mathrm{H}} = 125 \pm 3\,\mathrm{GeV}$, where the uncertainty is the theoretical uncertainty in the Higgs boson mass calculation.

Assuming $\mathcal{B}(\mathrm{H}^+ \to \mathrm{t\bar{b}}) = 1$, a 95% CL upper limit of $\sigma(\mathrm{pp} \to \bar{\mathrm{t}}(\mathrm{b})\mathrm{H}^+) = 2.0$–$0.13\,\mathrm{pb}$ is set for a combination of the $\mu\tau_{\mathrm{h}}$, ℓ+jets, and $\ell\ell'$ final states for $m_{\mathrm{H}^+} = 180$–$600\,\mathrm{GeV}$. This is the first experimental result on the $\mathrm{H}^+ \to \mathrm{t\bar{b}}$ decay mode. Here, cross section $\sigma(\mathrm{pp} \to \mathrm{t}(\mathrm{b})\mathrm{H}^\pm)$ stands for the sum $\sigma(\mathrm{pp} \to \bar{\mathrm{t}}(\mathrm{b})\mathrm{H}^+) + \sigma(\mathrm{pp} \to \mathrm{t}(\bar{\mathrm{b}})\mathrm{H}^-)$.

The results are interpreted in different MSSM benchmark scenarios and used to set exclusion limits in the m_{H^+}–$\tan\beta$ parameter spaces. In the various models, a lower bound on the charged Higgs boson mass of about 155 GeV is set assuming $m_{\mathrm{h}} = 125 \pm 3\,\mathrm{GeV}$. The light-stop scenario is excluded for $m_{\mathrm{H}^+} < 160\,\mathrm{GeV}$ assuming $m_{\mathrm{h}} = 125 \pm 3\,\mathrm{GeV}$, and the low-$M_{\mathrm{H}}$ scenario defined in refs. [29, 33] is completely excluded assuming $m_{\mathrm{H}} = 125 \pm 3\,\mathrm{GeV}$.

Acknowledgments

We congratulate our colleagues in the CERN accelerator departments for the excellent performance of the LHC and thank the technical and administrative staffs at CERN and at other CMS institutes for their contributions to the success of the CMS effort. In addition, we gratefully acknowledge the computing centers and personnel of the Worldwide LHC Computing Grid for delivering so effectively the computing infrastructure essential to our analyses. Finally, we acknowledge the enduring support for the construction and operation of the LHC and the CMS detector provided by the following funding agencies: the Austrian Federal Ministry of Science, Research and Economy and the Austrian Science Fund; the Belgian Fonds de la Recherche Scientifique, and Fonds voor Wetenschappelijk Onderzoek; the Brazilian Funding Agencies (CNPq, CAPES, FAPERJ, and FAPESP); the Bulgarian Ministry of Education and Science; CERN; the Chinese Academy of Sciences, Ministry of Science and Technology, and National Natural Science Foundation of China; the Colombian Funding Agency (COLCIENCIAS); the Croatian Ministry of Science, Education and Sport,

JHEP11(2015)018

and the Croatian Science Foundation; the Research Promotion Foundation, Cyprus; the Ministry of Education and Research, Estonian Research Council via IUT23-4 and IUT23-6 and European Regional Development Fund, Estonia; the Academy of Finland, Finnish Ministry of Education and Culture, and Helsinki Institute of Physics; the Institut National de Physique Nucléaire et de Physique des Particules / CNRS, and Commissariat à l'Énergie Atomique et aux Énergies Alternatives / CEA, France; the Bundesministerium für Bildung und Forschung, Deutsche Forschungsgemeinschaft, and Helmholtz-Gemeinschaft Deutscher Forschungszentren, Germany; the General Secretariat for Research and Technology, Greece; the National Scientific Research Foundation, and National Innovation Office, Hungary; the Department of Atomic Energy and the Department of Science and Technology, India; the Institute for Studies in Theoretical Physics and Mathematics, Iran; the Science Foundation, Ireland; the Istituto Nazionale di Fisica Nucleare, Italy; the Ministry of Science, ICT and Future Planning, and National Research Foundation (NRF), Republic of Korea; the Lithuanian Aca We congratulate our colleagues in the CERN accelerator departments for the excellent performance of the LHC and thank the technical and administrative staffs at CERN and at other CMS institutes for their contributions to the success of the CMS effort. In addition, we gratefully acknowledge the computing centres and personnel of the Worldwide LHC Computing Grid for delivering so effectively the computing infrastructure essential to our analyses. Finally, we acknowledge the enduring support for the construction and operation of the LHC and the CMS detector provided by the following funding agencies: the Austrian Federal Ministry of Science, Research and Economy and the Austrian Science Fund; the Belgian Fonds de la Recherche Scientifique, and Fonds voor Wetenschappelijk Onderzoek; the Brazilian Funding Agencies (CNPq, CAPES, FAPERJ, and FAPESP); the Bulgarian Ministry of Education and Science; CERN; the Chinese Academy of Sciences, Ministry of Science and Technology, and National Natural Science Foundation of China; the Colombian Funding Agency (COLCIENCIAS); the Croatian Ministry of Science, Education and Sport, and the Croatian Science Foundation; the Research Promotion Foundation, Cyprus; the Ministry of Education and Research, Estonian Research Council via IUT23-4 and IUT23-6 and European Regional Development Fund, Estonia; the Academy of Finland, Finnish Ministry of Education and Culture, and Helsinki Institute of Physics; the Institut National de Physique Nucléaire et de Physique des Particules / CNRS, and Commissariat à l'Énergie Atomique et aux Énergies Alternatives / CEA, France; the Bundesministerium für Bildung und Forschung, Deutsche Forschungsgemeinschaft, and Helmholtz-Gemeinschaft Deutscher Forschungszentren, Germany; the General Secretariat for Research and Technology, Greece; the National Scientific Research Foundation, and National Innovation Office, Hungary; the Department of Atomic Energy and the Department of Science and Technology, India; the Institute for Studies in Theoretical Physics and Mathematics, Iran; the Science Foundation, Ireland; the Istituto Nazionale di Fisica Nucleare, Italy; the Ministry of Science, ICT and Future Planning, and National Research Foundation (NRF), Republic of Korea; the Lithuanian Academy of Sciences; the Ministry of Education, and University of Malaya (Malaysia); the Mexican Funding Agencies (CINVESTAV, CONACYT, SEP, and UASLP-FAI); the Ministry of Business, Innovation and Employment, New Zealand; the Pakistan Atomic Energy Commission; the Ministry of Science and Higher Education

JHEP11(2015)018

and the National Science Centre, Poland; the Fundação para a Ciência e a Tecnologia, Portugal; JINR, Dubna; the Ministry of Education and Science of the Russian Federation, the Federal Agency of Atomic Energy of the Russian Federation, Russian Academy of Sciences, and the Russian Foundation for Basic Research; the Ministry of Education, Science and Technological Development of Serbia; the Secretaría de Estado de Investigación, Desarrollo e Innovación and Programa Consolider-Ingenio 2010, Spain; the Swiss Funding Agencies (ETH Board, ETH Zurich, PSI, SNF, UniZH, Canton Zurich, and SER); the Ministry of Science and Technology, Taipei; the Thailand Center of Excellence in Physics, the Institute for the Promotion of Teaching Science and Technology of Thailand, Special Task Force for Activating Research and the National Science and Technology Development Agency of Thailand; the Scientific and Technical Research Council of Turkey, and Turkish Atomic Energy Authority; the National Academy of Sciences of Ukraine, and State Fund for Fundamental Researches, Ukraine; the Science and Technology Facilities Council, U.K.; the US Department of Energy, and the US National Science Foundation.

Individuals have received support from the Marie-Curie programme and the European Research Council and EPLANET (European Union); the Leventis Foundation; the A. P. Sloan Foundation; the Alexander von Humboldt Foundation; the Belgian Federal Science Policy Office; the Fonds pour la Formation à la Recherche dans l'Industrie et dans l'Agriculture (FRIA-Belgium); the Agentschap voor Innovatie door Wetenschap en Technologie (IWT-Belgium); the Ministry of Education, Youth and Sports (MEYS) of the Czech Republic; the Council of Science and Industrial Research, India; the HOMING PLUS programme of the Foundation for Polish Science, cofinanced from European Union, Regional Development Fund; the OPUS programme of the National Science Center (Poland); the Compagnia di San Paolo (Torino); the Consorzio per la Fisica (Trieste); MIUR project 20108T4XTM (Italy); the Thalis and Aristeia programmes cofinanced by EU-ESF and the Greek NSRF; the National Priorities Research Program by Qatar National Research Fund; the Rachadapisek Sompot Fund for Postdoctoral Fellowship, Chulalongkorn University (Thailand); and the Welch Foundation, contract C-1845.demy of Sciences; the Ministry of Education, and University of Malaya (Malaysia); the Mexican Funding Agencies (CINVESTAV, CONACYT, SEP, and UASLP-FAI); the Ministry of Business, Innovation and Employment, New Zealand; the Pakistan Atomic Energy Commission; the Ministry of Science and Higher Education and the National Science Centre, Poland; the Fundação para a Ciência e a Tecnologia, Portugal; JINR, Dubna; the Ministry of Education and Science of the Russian Federation, the Federal Agency of Atomic Energy of the Russian Federation, Russian Academy of Sciences, and the Russian Foundation for Basic Research; the Ministry of Education, Science and Technological Development of Serbia; the Secretaría de Estado de Investigación, Desarrollo e Innovación and Programa Consolider-Ingenio 2010, Spain; the Swiss Funding Agencies (ETH Board, ETH Zurich, PSI, SNF, UniZH, Canton Zurich, and SER); the Ministry of Science and Technology, Taipei; the Thailand Center of Excellence in Physics, the Institute for the Promotion of Teaching Science and Technology of Thailand, Special Task Force for Activating Research and the National Science and Technology Development Agency of Thailand; the Scientific and Technical Research Council of Turkey, and Turkish Atomic Energy Authority; the National Academy of Sciences of

JHEP11(2015)018

Ukraine, and State Fund for Fundamental Researches, Ukraine; the Science and Technology Facilities Council, U.K.; the US Department of Energy, and the US National Science Foundation. Individuals have received support from the Marie-Curie programme and the European Research Council and EPLANET (European Union); the Leventis Foundation; the A. P. Sloan Foundation; the Alexander von Humboldt Foundation; the Belgian Federal Science Policy Office; the Fonds pour la Formation à la Recherche dans l'Industrie et dans l'Agriculture (FRIA-Belgium); the Agentschap voor Innovatie door Wetenschap en Technologie (IWT-Belgium); the Ministry of Education, Youth and Sports (MEYS) of the Czech Republic; the Council of Science and Industrial Research, India; the HOMING PLUS programme of the Foundation for Polish Science, cofinanced from European Union, Regional Development Fund; the OPUS programme of the National Science Center (Poland); the Compagnia di San Paolo (Torino); the Consorzio per la Fisica (Trieste); MIUR project 20108T4XTM (Italy); the Thalis and Aristeia programmes cofinanced by EU-ESF and the Greek NSRF; the National Priorities Research Program by Qatar National Research Fund; the Rachadapisek Sompot Fund for Postdoctoral Fellowship, Chulalongkorn University (Thailand); and the Welch Foundation, contract C-1845.

JHEP11(2015)018

References

[1] ATLAS collaboration, *Observation of a new particle in the search for the standard model Higgs boson with the ATLAS detector at the LHC*, *Phys. Lett.* **B 716** (2013) 1 [arXiv:1207.7214] [INSPIRE].

[2] CMS collaboration, *Observation of a new boson at a mass of* 125 *GeV with the CMS experiment at the LHC*, *Phys. Lett.* **B 716** (2013) 30 [arXiv:1207.7235] [INSPIRE].

[3] CMS collaboration, *Observation of a new boson with mass near* 125 *GeV in pp collisions at* $\sqrt{s} = 7$ *and* 8 *TeV*, *JHEP* **06** (2013) 081 [arXiv:1303.4571] [INSPIRE].

[4] ATLAS collaboration, *Measurements of Higgs boson production and couplings in diboson final states with the ATLAS detector at the LHC*, *Phys. Lett.* **B 726** (2013) 88 [*Erratum ibid.* **B 734** (2014) 406] [arXiv:1307.1427] [INSPIRE].

[5] ATLAS collaboration, *Evidence for the spin-0 nature of the Higgs boson using ATLAS data*, *Phys. Lett.* **B 726** (2013) 120 [arXiv:1307.1432] [INSPIRE].

[6] CMS collaboration, *Study of the mass and spin-parity of the Higgs boson candidate via its decays to Z boson pairs*, *Phys. Rev. Lett.* **110** (2013) 081803 [arXiv:1212.6639] [INSPIRE].

[7] CMS collaboration, *Measurement of the properties of a Higgs boson in the four-lepton final state*, *Phys. Rev.* **D 89** (2014) 092007 [arXiv:1312.5353] [INSPIRE].

[8] CMS collaboration, *Constraints on the Higgs boson width from off-shell production and decay to Z-boson pairs*, *Phys. Lett.* **B 736** (2014) 64 [arXiv:1405.3455] [INSPIRE].

[9] CMS collaboration, *Precise determination of the mass of the Higgs boson and tests of compatibility of its couplings with the standard model predictions using proton collisions at 7 and 8 TeV*, *Eur. Phys. J.* **C 75** (2015) 212 [arXiv:1412.8662] [INSPIRE].

[10] T.D. Lee, *A theory of spontaneous T violation*, *Phys. Rev.* **D 8** (1973) 1226 [INSPIRE].

[11] P. Fayet, *Supergauge invariant extension of the Higgs mechanism and a model for the electron and its neutrino*, *Nucl. Phys.* **B 90** (1975) 104 [INSPIRE].

[12] P. Fayet, *Supersymmetry and weak, electromagnetic and strong interactions*, *Phys. Lett.* **B 64** (1976) 159 [INSPIRE].

[13] P. Fayet, *Spontaneously broken supersymmetric theories of weak, electromagnetic and strong interactions*, *Phys. Lett.* **B 69** (1977) 489 [INSPIRE].

[14] S. Dimopoulos and H. Georgi, *Softly broken supersymmetry and* SU(5), *Nucl. Phys.* **B 193** (1981) 150 [INSPIRE].

[15] N. Sakai, *Naturalness in supersymmetric guts*, *Z. Phys.* **C 11** (1981) 153 [INSPIRE].

[16] K. Inoue, A. Kakuto, H. Komatsu and S. Takeshita, *Low-energy parameters and particle masses in a supersymmetric grand unified model*, *Prog. Theor. Phys.* **67** (1982) 1889 [INSPIRE].

[17] K. Inoue, A. Kakuto, H. Komatsu and S. Takeshita, *Aspects of grand unified models with softly broken supersymmetry*, *Prog. Theor. Phys.* **68** (1982) 927 [*Erratum ibid.* **70** (1983) 330] [INSPIRE].

[18] K. Inoue, A. Kakuto, H. Komatsu and S. Takeshita, *Renormalization of supersymmetry breaking parameters revisited*, *Prog. Theor. Phys.* **71** (1984) 413 [INSPIRE].

[19] S. Heinemeyer, W. Hollik and G. Weiglein, *FeynHiggs: a program for the calculation of the masses of the neutral CP even Higgs bosons in the MSSM*, *Comput. Phys. Commun.* **124** (2000) 76 [hep-ph/9812320] [INSPIRE].

[20] ALEPH collaboration, A. Heister et al., *Search for charged Higgs bosons in e^+e^- collisions at energies up to $\sqrt{s} = 209$ GeV*, *Phys. Lett.* **B 543** (2002) 1 [hep-ex/0207054] [INSPIRE].

[21] DELPHI collaboration, J. Abdallah et al., *Search for charged Higgs bosons at LEP in general two Higgs doublet models*, *Eur. Phys. J.* **C 34** (2004) 399 [hep-ex/0404012] [INSPIRE].

[22] L3 collaboration, P. Achard et al., *Search for charged Higgs bosons at LEP*, *Phys. Lett.* **B 575** (2003) 208 [hep-ex/0309056] [INSPIRE].

[23] OPAL collaboration, G. Abbiendi et al., *Search for charged Higgs bosons in e^+e^- collisions at $\sqrt{s} = 189$–209 GeV*, *Eur. Phys. J.* **C 72** (2012) 2076 [arXiv:0812.0267] [INSPIRE].

[24] ATLAS collaboration, *Search for charged Higgs bosons decaying via $H^\pm \to \tau^\pm\nu$ in fully hadronic final states using pp collision data at $\sqrt{s} = 8$ TeV with the ATLAS detector*, *JHEP* **03** (2015) 088 [arXiv:1412.6663] [INSPIRE].

[25] CMS collaboration, *Search for a light charged Higgs boson in top quark decays in pp collisions at $\sqrt{s} = 7$ TeV*, *JHEP* **07** (2012) 143 [arXiv:1205.5736] [INSPIRE].

[26] ATLAS collaboration, *Search for charged Higgs bosons through the violation of lepton universality in $t\bar{t}$ events using pp collision data at $\sqrt{s} = 7$ TeV with the ATLAS experiment*, *JHEP* **03** (2013) 076 [arXiv:1212.3572] [INSPIRE].

JHEP11(2015)018

[27] ATLAS collaboration, *Search for a light charged Higgs boson in the decay channel $H^+ \to c\bar{s}$ in $t\bar{t}$ events using pp collisions at $\sqrt{s} = 7$ TeV with the ATLAS detector*, *Eur. Phys. J.* **C 73** (2013) 2465 [arXiv:1302.3694] [INSPIRE].

[28] M. Flechl, R. Klees, M. Krämer, M. Spira and M. Ubiali, *Improved cross-section predictions for heavy charged Higgs boson production at the LHC*, *Phys. Rev.* **D 91** (2015) 075015 [arXiv:1409.5615] [INSPIRE].

[29] LHC Higgs Cross Section Working Group collaboration, J.R. Andersen et al., *Handbook of LHC Higgs cross sections: 3. Higgs properties*, arXiv:1307.1347 [INSPIRE].

[30] S. Dittmaier, M. Krämer, M. Spira and M. Walser, *Charged-Higgs-boson production at the LHC: NLO supersymmetric QCD corrections*, *Phys. Rev.* **D 83** (2011) 055005 [arXiv:0906.2648] [INSPIRE].

[31] E.L. Berger, T. Han, J. Jiang and T. Plehn, *Associated production of a top quark and a charged Higgs boson*, *Phys. Rev.* **D 71** (2005) 115012 [hep-ph/0312286] [INSPIRE].

[32] R. Harlander, M. Krämer and M. Schumacher, *Bottom-quark associated Higgs-boson production: reconciling the four- and five-flavour scheme approach*, arXiv:1112.3478 [INSPIRE].

[33] M. Carena et al., *MSSM Higgs boson searches at the LHC: benchmark scenarios after the discovery of a Higgs-like particle*, *Eur. Phys. J.* **C 73** (2013) 2552 [arXiv:1302.7033] [INSPIRE].

[34] CMS collaboration, *The CMS experiment at the CERN LHC*, 2008 *JINST* **3** S08004 [INSPIRE].

[35] CMS collaboration, *Description and performance of track and primary-vertex reconstruction with the CMS tracker*, 2014 *JINST* **9** P10009 [arXiv:1405.6569] [INSPIRE].

[36] CMS collaboration, *Particle-flow event reconstruction in CMS and performance for jets, taus and MET*, CMS-PAS-PFT-09-001 (2009).

[37] CMS collaboration, *Commissioning of the particle-flow event reconstruction with the first LHC collisions recorded in the CMS detector*, CMS-PAS-PFT-10-001 (2010).

[38] CMS collaboration, *Performance of electron reconstruction and selection with the CMS detector in proton-proton collisions at $\sqrt{s} = 8$ TeV*, 2015 *JINST* **10** P06005 [arXiv:1502.02701] [INSPIRE].

[39] CMS collaboration, *Performance of CMS muon reconstruction in pp collision events at $\sqrt{s} = 7$ TeV*, 2012 *JINST* **7** P10002 [arXiv:1206.4071] [INSPIRE].

[40] M. Cacciari, G.P. Salam and G. Soyez, *The anti-k_t jet clustering algorithm*, *JHEP* **04** (2008) 063 [arXiv:0802.1189] [INSPIRE].

[41] M. Cacciari, G.P. Salam and G. Soyez, *FastJet user manual*, *Eur. Phys. J.* **C 72** (2012) 1896 [arXiv:1111.6097] [INSPIRE].

[42] CMS collaboration, *Determination of jet energy calibration and transverse momentum resolution in CMS*, 2011 *JINST* **6** P11002 [arXiv:1107.4277] [INSPIRE].

[43] CMS collaboration, *Pileup jet identification*, CMS-PAS-JME-13-005 (2013).

[44] CMS collaboration, *Performance of b tagging at $\sqrt{s} = 8$ TeV in multijet, ttbar and boosted topology events*, CMS-PAS-BTV-13-001 (2013).

JHEP11(2015)018

[45] CMS collaboration, *Identification of b-quark jets with the CMS experiment*, 2013 *JINST* **8** P04013 [arXiv:1211.4462] [INSPIRE].

[46] CMS collaboration, *Performance of the CMS missing transverse momentum reconstruction in pp data at $\sqrt{s} = 8$ TeV*, 2015 *JINST* **10** P02006 [arXiv:1411.0511] [INSPIRE].

[47] CMS collaboration, *Performance of τ-lepton reconstruction and identification in CMS*, 2012 *JINST* **7** P01001 [arXiv:1109.6034] [INSPIRE].

[48] T. Sjöstrand, S. Mrenna and P.Z. Skands, *PYTHIA 6.4 physics and manual*, *JHEP* **05** (2006) 026 [hep-ph/0603175] [INSPIRE].

[49] J. Alwall et al., *The automated computation of tree-level and next-to-leading order differential cross sections and their matching to parton shower simulations*, *JHEP* **07** (2014) 079 [arXiv:1405.0301] [INSPIRE].

[50] P. Nason, *A new method for combining NLO QCD with shower Monte Carlo algorithms*, *JHEP* **11** (2004) 040 [hep-ph/0409146] [INSPIRE].

[51] S. Frixione, P. Nason and C. Oleari, *Matching NLO QCD computations with parton shower simulations: the POWHEG method*, *JHEP* **11** (2007) 070 [arXiv:0709.2092] [INSPIRE].

[52] S. Alioli, P. Nason, C. Oleari and E. Re, *A general framework for implementing NLO calculations in shower Monte Carlo programs: the POWHEG BOX*, *JHEP* **06** (2010) 043 [arXiv:1002.2581] [INSPIRE].

[53] S. Alioli, P. Nason, C. Oleari and E. Re, *NLO single-top production matched with shower in POWHEG: s- and t-channel contributions*, *JHEP* **09** (2009) 111 [*Erratum ibid.* **1002** (2010) 011] [arXiv:0907.4076] [INSPIRE].

[54] E. Re, *Single-top Wt-channel production matched with parton showers using the POWHEG method*, *Eur. Phys. J.* **C 71** (2011) 1547 [arXiv:1009.2450] [INSPIRE].

[55] Z. Was, *TAUOLA the library for τ lepton decay and KKMC/KORALB/KORALZ/ status report*, *Nucl. Phys. Proc. Suppl.* **98** (2001) 96 [hep-ph/0011305] [INSPIRE].

[56] GEANT4 collaboration, S. Agostinelli et al., *GEANT4 — a simulation toolkit*, *Nucl. Instrum. Meth.* **A 506** (2003) 250 [INSPIRE].

[57] J. Allison et al., *GEANT4 developments and applications*, *IEEE Trans. Nucl. Sci.* **53** (2006) 270.

[58] R. Field, *Early LHC underlying event data — Findings and surprises*, in the proceedings of the 22nd *conference on Hadron collider physics (HCP2010)*, August 23–27, Toronto, Canada (2010), arXiv:1010.3558 [INSPIRE].

[59] J. Pumplin, D.R. Stump, J. Huston, H.L. Lai, P.M. Nadolsky and W.K. Tung, *New generation of parton distributions with uncertainties from global QCD analysis*, *JHEP* **07** (2002) 012 [hep-ph/0201195] [INSPIRE].

[60] M. Czakon and A. Mitov, *Top++: a program for the calculation of the top-pair cross-section at hadron colliders*, *Comput. Phys. Commun.* **185** (2014) 2930 [arXiv:1112.5675] [INSPIRE].

[61] ATLAS, CDF, CMS and D0 collaborations, *First combination of Tevatron and LHC measurements of the top-quark mass*, CMS-PAS-TOP-13-014 (2014).

[62] M. Botje et al., *The PDF4LHC working group interim recommendations*, arXiv:1101.0538 [INSPIRE].

JHEP11(2015)018

[63] A.D. Martin, W.J. Stirling, R.S. Thorne and G. Watt, *Uncertainties on α_s in global PDF analyses and implications for predicted hadronic cross sections*, *Eur. Phys. J.* **C 64** (2009) 653 [arXiv:0905.3531] [INSPIRE].

[64] J. Gao et al., *CT10 next-to-next-to-leading order global analysis of QCD*, *Phys. Rev.* **D 89** (2014) 033009 [arXiv:1302.6246] [INSPIRE].

[65] R.D. Ball et al., *Parton distributions with LHC data*, *Nucl. Phys.* **B 867** (2013) 244 [arXiv:1207.1303] [INSPIRE].

[66] ATLAS collaboration, *Measurement of the $t\bar{t}$ production cross-section using $e\mu$ events with b-tagged jets in pp collisions at $\sqrt{s} = 7$ and 8 TeV with the ATLAS detector*, *Eur. Phys. J.* **C 74** (2014) 3109 [arXiv:1406.5375] [INSPIRE].

[67] CMS collaboration, *Measurement of the $t\bar{t}$ production cross section in the dilepton channel in pp collisions at $\sqrt{s} = 8$ TeV*, *JHEP* **02** (2014) 024 [*Erratum ibid.* **1402** (2014) 102] [arXiv:1312.7582] [INSPIRE].

[68] CMS collaboration, *Measurement of differential top-quark pair production cross sections in pp colisions at $\sqrt{s} = 7$ TeV*, *Eur. Phys. J.* **C 73** (2013) 2339 [arXiv:1211.2220] [INSPIRE].

[69] CMS collaboration, *Measurement of the differential cross section for top quark pair production in pp collisions at $\sqrt{s} = 8$ TeV*, arXiv:1505.04480 [INSPIRE].

[70] K. Melnikov and F. Petriello, *Electroweak gauge boson production at hadron colliders through $O(\alpha_s^2)$*, *Phys. Rev.* **D 74** (2006) 114017 [hep-ph/0609070] [INSPIRE].

[71] K. Melnikov and F. Petriello, *The W boson production cross section at the LHC through $O(\alpha_s^2)$*, *Phys. Rev. Lett.* **96** (2006) 231803 [hep-ph/0603182] [INSPIRE].

[72] M. Aliev, H. Lacker, U. Langenfeld, S. Moch, P. Uwer and M. Wiedermann, *HATHOR: HAdronic Top and Heavy quarks crOss section calculatoR*, *Comput. Phys. Commun.* **182** (2011) 1034 [arXiv:1007.1327] [INSPIRE].

[73] P. Kant et al., *HatHor for single top-quark production: Updated predictions and uncertainty estimates for single top-quark production in hadronic collisions*, *Comput. Phys. Commun.* **191** (2015) 74 [arXiv:1406.4403] [INSPIRE].

[74] S. Alekhin et al., *The PDF4LHC working group interim report*, arXiv:1101.0536 [INSPIRE].

[75] N. Kidonakis, *NNLL resummation for s-channel single top quark production*, *Phys. Rev.* **D 81** (2010) 054028 [arXiv:1001.5034] [INSPIRE].

[76] N. Kidonakis, *Two-loop soft anomalous dimensions for single top quark associated production with a W^- or H^-*, *Phys. Rev.* **D 82** (2010) 054018 [arXiv:1005.4451] [INSPIRE].

[77] D.P. Roy, *The hadronic τ decay signature of a heavy charged Higgs boson at LHC*, *Phys. Lett.* **B 459** (1999) 607 [hep-ph/9905542] [INSPIRE].

[78] CMS collaboration, *Measurement of the top quark pair production cross section in pp collisions at $\sqrt{s} = 7$ TeV in dilepton final states containing a τ*, *Phys. Rev.* **D 85** (2012) 112007 [arXiv:1203.6810] [INSPIRE].

[79] CMS collaboration, *Measurement of the $t\bar{t}$ production cross section in pp collisions at $\sqrt{s} = 8$ TeV in dilepton final states containing one τ lepton*, *Phys. Lett.* **B 739** (2014) 23 [arXiv:1407.6643] [INSPIRE].

[80] CMS collaboration, *Measurement of the $t\bar{t}$ production cross section in the dilepton channel in pp collisions at $\sqrt{s} = 7$ TeV*, *JHEP* **11** (2012) 067 [arXiv:1208.2671] [INSPIRE].

JHEP11(2015)018

[81] CMS collaboration, *Measurements of inclusive W and Z cross sections in pp collisions at $\sqrt{s} = 7$ TeV*, *JHEP* **01** (2011) 080 [arXiv:1012.2466] [INSPIRE].

[82] CMS collaboration, *Measurement of the ratio $B(t \to Wb)/B(t \to Wq)$ in pp collisions at $\sqrt{s} = 8$ TeV*, *Phys. Lett.* **B 736** (2014) 33 [arXiv:1404.2292] [INSPIRE].

[83] CMS collaboration, *Search for neutral MSSM Higgs bosons decaying to a pair of τ leptons in pp collisions*, *JHEP* **10** (2014) 160 [arXiv:1408.3316] [INSPIRE].

[84] CMS collaboration, *Measurement of the cross section ratio $\sigma_{t\bar{t}b\bar{b}}/\sigma_{t\bar{t}jj}$ in pp collisions at $\sqrt{s} = 8$ TeV*, *Phys. Lett.* **B 746** (2015) 132 [arXiv:1411.5621] [INSPIRE].

[85] CMS collaboration, *CMS luminosity based on pixel cluster counting — Summer 2013 update*, CMS-PAS-LUM-13-001 (2013).

[86] ATLAS collaboration, *Measurement of the $W^{\pm}Z$ production cross section and limits on anomalous triple gauge couplings in proton-proton collisions at $\sqrt{s} = 7$ TeV with the ATLAS detector*, *Phys. Lett.* **B 709** (2013) 341 [arXiv:1111.5570] [INSPIRE].

[87] J.M. Campbell, R.K. Ellis and C. Williams, *Vector boson pair production at the LHC*, *JHEP* **07** (2011) 018 [arXiv:1105.0020] [INSPIRE].

[88] J.M. Campbell and R.K. Ellis, *$t\bar{t}W^{\pm}$ production and decay at NLO*, *JHEP* **07** (2012) 052 [arXiv:1204.5678] [INSPIRE].

[89] T. Junk, *Confidence level computation for combining searches with small statistics*, *Nucl. Instrum. Meth.* **A 434** (1999) 435 [hep-ex/9902006] [INSPIRE].

[90] A.L. Read, *Presentation of search results: the CL(s) technique*, *J. Phys.* **G 28** (2002) 2693 [INSPIRE].

[91] G. Cowan, K. Cranmer, E. Gross and O. Vitells, *Asymptotic formulae for likelihood-based tests of new physics*, *Eur. Phys. J.* **C 71** (2011) 1554 [*Erratum ibid.* **C 73** (2013) 2501] [arXiv:1007.1727] [INSPIRE].

[92] ATLAS collaboration, *Procedure for the LHC Higgs boson search combination in summer 2011*, ATL-PHYS-PUB-2011-011 (2011).

[93] J.S. Conway, *Nuisance parameters in likelihoods for multisource spectra*, in the proceedings of *PHYSTAT 2011 Workshop on Statistical Issues Related to Discovery Claims in Search Experiments and Unfolding*, January 17–20, CERN, Geneva, Switzerland (2011), CERN-2011-006 (2011).

[94] A. Denner, S. Heinemeyer, I. Puljak, D. Rebuzzi and M. Spira, *Standard model Higgs-boson branching ratios with uncertainties*, *Eur. Phys. J.* **C 71** (2011) 1753 [arXiv:1107.5909] [INSPIRE].

[95] S. Dittmaier et al., *Handbook of LHC Higgs cross sections: 2. Differential distributions*, arXiv:1201.3084 [INSPIRE].

[96] LHC Higgs Cross Section Working Group collaboration, S. Dittmaier et al., *Handbook of LHC Higgs cross sections: 1. Inclusive observables*, arXiv:1101.0593 [INSPIRE].

[97] L. Hofer, U. Nierste and D. Scherer, *Resummation of tan-beta-enhanced supersymmetric loop corrections beyond the decoupling limit*, *JHEP* **10** (2009) 081 [arXiv:0907.5408] [INSPIRE].

JHEP11(2015)018

The CMS collaboration

Yerevan Physics Institute, Yerevan, Armenia

V. Khachatryan, A.M. Sirunyan, A. Tumasyan

Institut für Hochenergiephysik der OeAW, Wien, Austria

W. Adam, E. Asilar, T. Bergauer, J. Brandstetter, E. Brondolin, M. Dragicevic, J. Erö, M. Flechl, M. Friedl, R. Frühwirth[1], V.M. Ghete, C. Hartl, N. Hörmann, J. Hrubec, M. Jeitler[1], V. Knünz, A. König, M. Krammer[1], I. Krätschmer, D. Liko, T. Matsushita, I. Mikulec, D. Rabady[2], B. Rahbaran, H. Rohringer, J. Schieck[1], R. Schöfbeck, J. Strauss, W. Treberer-Treberspurg, W. Waltenberger, C.-E. Wulz[1]

National Centre for Particle and High Energy Physics, Minsk, Belarus

V. Mossolov, N. Shumeiko, J. Suarez Gonzalez

Universiteit Antwerpen, Antwerpen, Belgium

S. Alderweireldt, T. Cornelis, E.A. De Wolf, X. Janssen, A. Knutsson, J. Lauwers, S. Luyckx, R. Rougny, M. Van De Klundert, H. Van Haevermaet, P. Van Mechelen, N. Van Remortel, A. Van Spilbeeck

Vrije Universiteit Brussel, Brussel, Belgium

S. Abu Zeid, F. Blekman, J. D'Hondt, N. Daci, I. De Bruyn, K. Deroover, N. Heracleous, J. Keaveney, S. Lowette, L. Moreels, A. Olbrechts, Q. Python, D. Strom, S. Tavernier, W. Van Doninck, P. Van Mulders, G.P. Van Onsem, I. Van Parijs

Université Libre de Bruxelles, Bruxelles, Belgium

P. Barria, H. Brun, C. Caillol, B. Clerbaux, G. De Lentdecker, G. Fasanella, L. Favart, A. Grebenyuk, G. Karapostoli, T. Lenzi, A. Léonard, T. Maerschalk, A. Marinov, L. Perniè, A. Randle-conde, T. Reis, T. Seva, C. Vander Velde, P. Vanlaer, R. Yonamine, F. Zenoni, F. Zhang[3]

Ghent University, Ghent, Belgium

K. Beernaert, L. Benucci, A. Cimmino, S. Crucy, D. Dobur, A. Fagot, G. Garcia, M. Gul, J. Mccartin, A.A. Ocampo Rios, D. Poyraz, D. Ryckbosch, S. Salva, M. Sigamani, N. Strobbe, M. Tytgat, W. Van Driessche, E. Yazgan, N. Zaganidis

Université Catholique de Louvain, Louvain-la-Neuve, Belgium

S. Basegmez, C. Beluffi[4], O. Bondu, S. Brochet, G. Bruno, A. Caudron, L. Ceard, G.G. Da Silveira, C. Delaere, D. Favart, L. Forthomme, A. Giammanco[5], J. Hollar, A. Jafari, P. Jez, M. Komm, V. Lemaitre, A. Mertens, C. Nuttens, L. Perrini, A. Pin, K. Piotrzkowski, A. Popov[6], L. Quertenmont, M. Selvaggi, M. Vidal Marono

Université de Mons, Mons, Belgium

N. Beliy, G.H. Hammad

Centro Brasileiro de Pesquisas Fisicas, Rio de Janeiro, Brazil

W.L. Aldá Júnior, G.A. Alves, L. Brito, M. Correa Martins Junior, M. Hamer, C. Hensel, C. Mora Herrera, A. Moraes, M.E. Pol, P. Rebello Teles

JHEP11(2015)018

Universidade do Estado do Rio de Janeiro, Rio de Janeiro, Brazil

E. Belchior Batista Das Chagas, W. Carvalho, J. Chinellato[7], A. Custódio, E.M. Da Costa, D. De Jesus Damiao, C. De Oliveira Martins, S. Fonseca De Souza, L.M. Huertas Guativa, H. Malbouisson, D. Matos Figueiredo, L. Mundim, H. Nogima, W.L. Prado Da Silva, A. Santoro, A. Sznajder, E.J. Tonelli Manganote[7], A. Vilela Pereira

Universidade Estadual Paulista [a], Universidade Federal do ABC [b], São Paulo, Brazil

S. Ahuja[a], C.A. Bernardes[b], A. De Souza Santos[b], S. Dogra[a], T.R. Fernandez Perez Tomei[a], E.M. Gregores[b], P.G. Mercadante[b], C.S. Moon[a,8], S.F. Novaes[a], Sandra S. Padula[a], D. Romero Abad, J.C. Ruiz Vargas

Institute for Nuclear Research and Nuclear Energy, Sofia, Bulgaria

A. Aleksandrov, R. Hadjiiska, P. Iaydjiev, M. Rodozov, S. Stoykova, G. Sultanov, M. Vutova

University of Sofia, Sofia, Bulgaria

A. Dimitrov, I. Glushkov, L. Litov, B. Pavlov, P. Petkov

Institute of High Energy Physics, Beijing, China

M. Ahmad, J.G. Bian, G.M. Chen, H.S. Chen, M. Chen, T. Cheng, R. Du, C.H. Jiang, R. Plestina[9], F. Romeo, S.M. Shaheen, J. Tao, C. Wang, Z. Wang, H. Zhang

State Key Laboratory of Nuclear Physics and Technology, Peking University, Beijing, China

C. Asawatangtrakuldee, Y. Ban, Q. Li, S. Liu, Y. Mao, S.J. Qian, D. Wang, Z. Xu

Universidad de Los Andes, Bogota, Colombia

C. Avila, A. Cabrera, L.F. Chaparro Sierra, C. Florez, J.P. Gomez, B. Gomez Moreno, J.C. Sanabria

University of Split, Faculty of Electrical Engineering, Mechanical Engineering and Naval Architecture, Split, Croatia

N. Godinovic, D. Lelas, I. Puljak, P.M. Ribeiro Cipriano

University of Split, Faculty of Science, Split, Croatia

Z. Antunovic, M. Kovac

Institute Rudjer Boskovic, Zagreb, Croatia

V. Brigljevic, K. Kadija, J. Luetic, S. Micanovic, L. Sudic

University of Cyprus, Nicosia, Cyprus

A. Attikis, G. Mavromanolakis, J. Mousa, C. Nicolaou, F. Ptochos, P.A. Razis, H. Rykaczewski

Charles University, Prague, Czech Republic

M. Bodlak, M. Finger[10], M. Finger Jr.[10]

JHEP11(2015)018

Academy of Scientific Research and Technology of the Arab Republic of Egypt, Egyptian Network of High Energy Physics, Cairo, Egypt
E. El-khateeb[11,11], T. Elkafrawy[11], A. Mohamed[12], A. Radi[13,11], E. Salama[13,11]

National Institute of Chemical Physics and Biophysics, Tallinn, Estonia
B. Calpas, M. Kadastik, M. Murumaa, M. Raidal, A. Tiko, C. Veelken

Department of Physics, University of Helsinki, Helsinki, Finland
P. Eerola, J. Pekkanen, M. Voutilainen

Helsinki Institute of Physics, Helsinki, Finland
J. Härkönen, V. Karimäki, R. Kinnunen, T. Lampén, K. Lassila-Perini, S. Laurila, S. Lehti, T. Lindén, P. Luukka, T. Mäenpää, T. Peltola, E. Tuominen, J. Tuominiemi, E. Tuovinen, L. Wendland

Lappeenranta University of Technology, Lappeenranta, Finland
J. Talvitie, T. Tuuva

DSM/IRFU, CEA/Saclay, Gif-sur-Yvette, France
M. Besancon, F. Couderc, M. Dejardin, D. Denegri, B. Fabbro, J.L. Faure, C. Favaro, F. Ferri, S. Ganjour, A. Givernaud, P. Gras, G. Hamel de Monchenault, P. Jarry, E. Locci, M. Machet, J. Malcles, J. Rander, A. Rosowsky, M. Titov, A. Zghiche

Laboratoire Leprince-Ringuet, Ecole Polytechnique, IN2P3-CNRS, Palaiseau, France
I. Antropov, S. Baffioni, F. Beaudette, P. Busson, L. Cadamuro, E. Chapon, C. Charlot, T. Dahms, O. Davignon, N. Filipovic, A. Florent, R. Granier de Cassagnac, S. Lisniak, L. Mastrolorenzo, P. Miné, I.N. Naranjo, M. Nguyen, C. Ochando, G. Ortona, P. Paganini, P. Pigard, S. Regnard, R. Salerno, J.B. Sauvan, Y. Sirois, T. Strebler, Y. Yilmaz, A. Zabi

Institut Pluridisciplinaire Hubert Curien, Université de Strasbourg, Université de Haute Alsace Mulhouse, CNRS/IN2P3, Strasbourg, France
J.-L. Agram[14], J. Andrea, A. Aubin, D. Bloch, J.-M. Brom, M. Buttignol, E.C. Chabert, N. Chanon, C. Collard, E. Conte[14], X. Coubez, J.-C. Fontaine[14], D. Gelé, U. Goerlach, C. Goetzmann, A.-C. Le Bihan, J.A. Merlin[2], K. Skovpen, P. Van Hove

Centre de Calcul de l'Institut National de Physique Nucleaire et de Physique des Particules, CNRS/IN2P3, Villeurbanne, France
S. Gadrat

Université de Lyon, Université Claude Bernard Lyon 1, CNRS-IN2P3, Institut de Physique Nucléaire de Lyon, Villeurbanne, France
S. Beauceron, C. Bernet, G. Boudoul, E. Bouvier, C.A. Carrillo Montoya, R. Chierici, D. Contardo, B. Courbon, P. Depasse, H. El Mamouni, J. Fan, J. Fay, S. Gascon, M. Gouzevitch, B. Ille, F. Lagarde, I.B. Laktineh, M. Lethuillier, L. Mirabito, A.L. Pequegnot, S. Perries, J.D. Ruiz Alvarez, D. Sabes, L. Sgandurra, V. Sordini, M. Vander Donckt, P. Verdier, S. Viret

JHEP11(2015)018

Georgian Technical University, Tbilisi, Georgia
T. Toriashvili[15]

Tbilisi State University, Tbilisi, Georgia
Z. Tsamalaidze[10]

RWTH Aachen University, I. Physikalisches Institut, Aachen, Germany
C. Autermann, S. Beranek, M. Edelhoff, L. Feld, A. Heister, M.K. Kiesel, K. Klein, M. Lipinski, A. Ostapchuk, M. Preuten, F. Raupach, S. Schael, J.F. Schulte, T. Verlage, H. Weber, B. Wittmer, V. Zhukov[6]

RWTH Aachen University, III. Physikalisches Institut A, Aachen, Germany
M. Ata, M. Brodski, E. Dietz-Laursonn, D. Duchardt, M. Endres, M. Erdmann, S. Erdweg, T. Esch, R. Fischer, A. Güth, T. Hebbeker, C. Heidemann, K. Hoepfner, D. Klingebiel, S. Knutzen, P. Kreuzer, M. Merschmeyer, A. Meyer, P. Millet, M. Olschewski, K. Padeken, P. Papacz, T. Pook, M. Radziej, H. Reithler, M. Rieger, F. Scheuch, L. Sonnenschein, D. Teyssier, S. Thüer

RWTH Aachen University, III. Physikalisches Institut B, Aachen, Germany
V. Cherepanov, Y. Erdogan, G. Flügge, H. Geenen, M. Geisler, F. Hoehle, B. Kargoll, T. Kress, Y. Kuessel, A. Künsken, J. Lingemann[2], A. Nehrkorn, A. Nowack, I.M. Nugent, C. Pistone, O. Pooth, A. Stahl

Deutsches Elektronen-Synchrotron, Hamburg, Germany
M. Aldaya Martin, I. Asin, N. Bartosik, O. Behnke, U. Behrens, A.J. Bell, K. Borras, A. Burgmeier, A. Cakir, L. Calligaris, A. Campbell, S. Choudhury, F. Costanza, C. Diez Pardos, G. Dolinska, S. Dooling, T. Dorland, G. Eckerlin, D. Eckstein, T. Eichhorn, G. Flucke, E. Gallo[16], J. Garay Garcia, A. Geiser, A. Gizhko, P. Gunnellini, J. Hauk, M. Hempel[17], H. Jung, A. Kalogeropoulos, O. Karacheban[17], M. Kasemann, P. Katsas, J. Kieseler, C. Kleinwort, I. Korol, W. Lange, J. Leonard, K. Lipka, A. Lobanov, W. Lohmann[17], R. Mankel, I. Marfin[17], I.-A. Melzer-Pellmann, A.B. Meyer, G. Mittag, J. Mnich, A. Mussgiller, S. Naumann-Emme, A. Nayak, E. Ntomari, H. Perrey, D. Pitzl, R. Placakyte, A. Raspereza, B. Roland, M.Ö. Sahin, P. Saxena, T. Schoerner-Sadenius, M. Schröder, C. Seitz, S. Spannagel, K.D. Trippkewitz, R. Walsh, C. Wissing

University of Hamburg, Hamburg, Germany
V. Blobel, M. Centis Vignali, A.R. Draeger, J. Erfle, E. Garutti, K. Goebel, D. Gonzalez, M. Görner, J. Haller, M. Hoffmann, R.S. Höing, A. Junkes, R. Klanner, R. Kogler, T. Lapsien, T. Lenz, I. Marchesini, D. Marconi, M. Meyer, D. Nowatschin, J. Ott, F. Pantaleo[2], T. Peiffer, A. Perieanu, N. Pietsch, J. Poehlsen, D. Rathjens, C. Sander, H. Schettler, P. Schleper, E. Schlieckau, A. Schmidt, J. Schwandt, M. Seidel, V. Sola, H. Stadie, G. Steinbrück, H. Tholen, D. Troendle, E. Usai, L. Vanelderen, A. Vanhoefer, B. Vormwald

Institut für Experimentelle Kernphysik, Karlsruhe, Germany
M. Akbiyik, C. Barth, C. Baus, J. Berger, C. Böser, E. Butz, T. Chwalek, F. Colombo, W. De Boer, A. Descroix, A. Dierlamm, S. Fink, F. Frensch, M. Giffels, A. Gilbert,

JHEP11(2015)018

F. Hartmann[2], S.M. Heindl, U. Husemann, I. Katkov[6], A. Kornmayer[2], P. Lobelle Pardo, B. Maier, H. Mildner, M.U. Mozer, T. Müller, Th. Müller, M. Plagge, G. Quast, K. Rabbertz, S. Röcker, F. Roscher, H.J. Simonis, F.M. Stober, R. Ulrich, J. Wagner-Kuhr, S. Wayand, M. Weber, T. Weiler, C. Wöhrmann, R. Wolf

Institute of Nuclear and Particle Physics (INPP), NCSR Demokritos, Aghia Paraskevi, Greece

G. Anagnostou, G. Daskalakis, T. Geralis, V.A. Giakoumopoulou, A. Kyriakis, D. Loukas, A. Psallidas, I. Topsis-Giotis

University of Athens, Athens, Greece

A. Agapitos, S. Kesisoglou, A. Panagiotou, N. Saoulidou, E. Tziaferi

University of Ioánnina, Ioánnina, Greece

I. Evangelou, G. Flouris, C. Foudas, P. Kokkas, N. Loukas, N. Manthos, I. Papadopoulos, E. Paradas, J. Strologas

Wigner Research Centre for Physics, Budapest, Hungary

G. Bencze, C. Hajdu, A. Hazi, P. Hidas, D. Horvath[18], F. Sikler, V. Veszpremi, G. Vesztergombi[19], A.J. Zsigmond

Institute of Nuclear Research ATOMKI, Debrecen, Hungary

N. Beni, S. Czellar, J. Karancsi[20], J. Molnar, Z. Szillasi

University of Debrecen, Debrecen, Hungary

M. Bartók[21], A. Makovec, P. Raics, Z.L. Trocsanyi, B. Ujvari

National Institute of Science Education and Research, Bhubaneswar, India

P. Mal, K. Mandal, D.K. Sahoo, N. Sahoo, S.K. Swain

Panjab University, Chandigarh, India

S. Bansal, S.B. Beri, V. Bhatnagar, R. Chawla, R. Gupta, U.Bhawandeep, A.K. Kalsi, A. Kaur, M. Kaur, R. Kumar, A. Mehta, M. Mittal, J.B. Singh, G. Walia

University of Delhi, Delhi, India

Ashok Kumar, A. Bhardwaj, B.C. Choudhary, R.B. Garg, A. Kumar, S. Malhotra, M. Naimuddin, N. Nishu, K. Ranjan, R. Sharma, V. Sharma

Saha Institute of Nuclear Physics, Kolkata, India

S. Bhattacharya, K. Chatterjee, S. Dey, S. Dutta, Sa. Jain, N. Majumdar, A. Modak, K. Mondal, S. Mukherjee, S. Mukhopadhyay, A. Roy, D. Roy, S. Roy Chowdhury, S. Sarkar, M. Sharan

Bhabha Atomic Research Centre, Mumbai, India

A. Abdulsalam, R. Chudasama, D. Dutta, V. Jha, V. Kumar, A.K. Mohanty[2], L.M. Pant, P. Shukla, A. Topkar

Tata Institute of Fundamental Research, Mumbai, India

T. Aziz, S. Banerjee, S. Bhowmik[22], R.M. Chatterjee, R.K. Dewanjee, S. Dugad, S. Ganguly, S. Ghosh, M. Guchait, A. Gurtu[23], G. Kole, S. Kumar, B. Mahakud, M. Maity[22],

JHEP11(2015)018

G. Majumder, K. Mazumdar, S. Mitra, G.B. Mohanty, B. Parida, T. Sarkar[22], K. Sudhakar, N. Sur, B. Sutar, N. Wickramage[24]

Indian Institute of Science Education and Research (IISER), Pune, India
S. Chauhan, S. Dube, S. Sharma

Institute for Research in Fundamental Sciences (IPM), Tehran, Iran
H. Bakhshiansohi, H. Behnamian, S.M. Etesami[25], A. Fahim[26], R. Goldouzian, M. Khakzad, M. Mohammadi Najafabadi, M. Naseri, S. Paktinat Mehdiabadi, F. Rezaei Hosseinabadi, B. Safarzadeh[27], M. Zeinali

University College Dublin, Dublin, Ireland
M. Felcini, M. Grunewald

INFN Sezione di Bari [a], Università di Bari [b], Politecnico di Bari [c], Bari, Italy
M. Abbrescia[a,b], C. Calabria[a,b], C. Caputo[a,b], A. Colaleo[a], D. Creanza[a,c], L. Cristella[a,b], N. De Filippis[a,c], M. De Palma[a,b], L. Fiore[a], G. Iaselli[a,c], G. Maggi[a,c], M. Maggi[a], G. Miniello[a,b], S. My[a,c], S. Nuzzo[a,b], A. Pompili[a,b], G. Pugliese[a,c], R. Radogna[a,b], A. Ranieri[a], G. Selvaggi[a,b], L. Silvestris[a,2], R. Venditti[a,b], P. Verwilligen[a]

INFN Sezione di Bologna [a], Università di Bologna [b], Bologna, Italy
G. Abbiendi[a], C. Battilana[2], A.C. Benvenuti[a], D. Bonacorsi[a,b], S. Braibant-Giacomelli[a,b], L. Brigliadori[a,b], R. Campanini[a,b], P. Capiluppi[a,b], A. Castro[a,b], F.R. Cavallo[a], S.S. Chhibra[a,b], G. Codispoti[a,b], M. Cuffiani[a,b], G.M. Dallavalle[a], F. Fabbri[a], A. Fanfani[a,b], D. Fasanella[a,b], P. Giacomelli[a], C. Grandi[a], L. Guiducci[a,b], S. Marcellini[a], G. Masetti[a], A. Montanari[a], F.L. Navarria[a,b], A. Perrotta[a], A.M. Rossi[a,b], T. Rovelli[a,b], G.P. Siroli[a,b], N. Tosi[a,b], R. Travaglini[a,b]

INFN Sezione di Catania [a], Università di Catania [b], CSFNSM [c], Catania, Italy
G. Cappello[a], M. Chiorboli[a,b], S. Costa[a,b], F. Giordano[a,b], R. Potenza[a,b], A. Tricomi[a,b], C. Tuve[a,b]

INFN Sezione di Firenze [a], Università di Firenze [b], Firenze, Italy
G. Barbagli[a], V. Ciulli[a,b], C. Civinini[a], R. D'Alessandro[a,b], E. Focardi[a,b], S. Gonzi[a,b], V. Gori[a,b], P. Lenzi[a,b], M. Meschini[a], S. Paoletti[a], G. Sguazzoni[a], A. Tropiano[a,b], L. Viliani[a,b]

INFN Laboratori Nazionali di Frascati, Frascati, Italy
L. Benussi, S. Bianco, F. Fabbri, D. Piccolo, F. Primavera

INFN Sezione di Genova [a], Università di Genova [b], Genova, Italy
V. Calvelli[a,b], F. Ferro[a], M. Lo Vetere[a,b], M.R. Monge[a,b], E. Robutti[a], S. Tosi[a,b]

INFN Sezione di Milano-Bicocca [a], Università di Milano-Bicocca [b], Milano, Italy
L. Brianza, M.E. Dinardo[a,b], S. Fiorendi[a,b], S. Gennai[a], R. Gerosa[a,b], A. Ghezzi[a,b], P. Govoni[a,b], S. Malvezzi[a], R.A. Manzoni[a,b], B. Marzocchi[a,b,2], D. Menasce[a], L. Moroni[a], M. Paganoni[a,b], D. Pedrini[a], S. Ragazzi[a,b], N. Redaelli[a], T. Tabarelli de Fatis[a,b]

JHEP11(2015)018

INFN Sezione di Napoli [a], Università di Napoli 'Federico II' [b], Napoli, Italy, Università della Basilicata [c], Potenza, Italy, Università G. Marconi [d], Roma, Italy

S. Buontempo[a], N. Cavallo[a,c], S. Di Guida[a,d,2], M. Esposito[a,b], F. Fabozzi[a,c], A.O.M. Iorio[a,b], G. Lanza[a], L. Lista[a], S. Meola[a,d,2], M. Merola[a], P. Paolucci[a,2], C. Sciacca[a,b], F. Thyssen

INFN Sezione di Padova [a], Università di Padova [b], Padova, Italy, Università di Trento [c], Trento, Italy

P. Azzi[a,2], N. Bacchetta[a], L. Benato[a,b], D. Bisello[a,b], A. Boletti[a,b], A. Branca[a,b], R. Carlin[a,b], P. Checchia[a], M. Dall'Osso[a,b,2], T. Dorigo[a], U. Dosselli[a], F. Gasparini[a,b], U. Gasparini[a,b], A. Gozzelino[a], S. Lacaprara[a], M. Margoni[a,b], A.T. Meneguzzo[a,b], F. Montecassiano[a], M. Passaseo[a], J. Pazzini[a,b], N. Pozzobon[a,b], P. Ronchese[a,b], F. Simonetto[a,b], E. Torassa[a], M. Tosi[a,b], M. Zanetti, P. Zotto[a,b], A. Zucchetta[a,b,2], G. Zumerle[a,b]

INFN Sezione di Pavia [a], Università di Pavia [b], Pavia, Italy

A. Braghieri[a], A. Magnani[a], P. Montagna[a,b], S.P. Ratti[a,b], V. Re[a], C. Riccardi[a,b], P. Salvini[a], I. Vai[a], P. Vitulo[a,b]

INFN Sezione di Perugia [a], Università di Perugia [b], Perugia, Italy

L. Alunni Solestizi[a,b], M. Biasini[a,b], G.M. Bilei[a], D. Ciangottini[a,b,2], L. Fanò[a,b], P. Lariccia[a,b], G. Mantovani[a,b], M. Menichelli[a], A. Saha[a], A. Santocchia[a,b], A. Spiezia[a,b]

INFN Sezione di Pisa [a], Università di Pisa [b], Scuola Normale Superiore di Pisa [c], Pisa, Italy

K. Androsov[a,28], P. Azzurri[a], G. Bagliesi[a], J. Bernardini[a], T. Boccali[a], G. Broccolo[a,c], R. Castaldi[a], M.A. Ciocci[a,28], R. Dell'Orso[a], S. Donato[a,c,2], G. Fedi, L. Foà[a,c†], A. Giassi[a], M.T. Grippo[a,28], F. Ligabue[a,c], T. Lomtadze[a], L. Martini[a,b], A. Messineo[a,b], F. Palla[a], A. Rizzi[a,b], A. Savoy-Navarro[a,29], A.T. Serban[a], P. Spagnolo[a], P. Squillacioti[a,28], R. Tenchini[a], G. Tonelli[a,b], A. Venturi[a], P.G. Verdini[a]

INFN Sezione di Roma [a], Università di Roma [b], Roma, Italy

L. Barone[a,b], F. Cavallari[a], G. D'imperio[a,b,2], D. Del Re[a,b], M. Diemoz[a], S. Gelli[a,b], C. Jorda[a], E. Longo[a,b], F. Margaroli[a,b], P. Meridiani[a], G. Organtini[a,b], R. Paramatti[a], F. Preiato[a,b], S. Rahatlou[a,b], C. Rovelli[a], F. Santanastasio[a,b], P. Traczyk[a,b,2]

INFN Sezione di Torino [a], Università di Torino [b], Torino, Italy, Università del Piemonte Orientale [c], Novara, Italy

N. Amapane[a,b], R. Arcidiacono[a,c,2], S. Argiro[a,b], M. Arneodo[a,c], R. Bellan[a,b], C. Biino[a], N. Cartiglia[a], M. Costa[a,b], R. Covarelli[a,b], A. Degano[a,b], N. Demaria[a], L. Finco[a,b,2], B. Kiani[a,b], C. Mariotti[a], S. Maselli[a], E. Migliore[a,b], V. Monaco[a,b], E. Monteil[a,b], M. Musich[a], M.M. Obertino[a,b], L. Pacher[a,b], N. Pastrone[a], M. Pelliccioni[a], G.L. Pinna Angioni[a,b], F. Ravera[a,b], A. Romero[a,b], M. Ruspa[a,c], R. Sacchi[a,b], A. Solano[a,b], A. Staiano[a], U. Tamponi[a]

JHEP11(2015)018

INFN Sezione di Trieste [a], Università di Trieste [b], Trieste, Italy
S. Belforte[a], V. Candelise[a,b,2], M. Casarsa[a], F. Cossutti[a], G. Della Ricca[a,b], B. Gobbo[a], C. La Licata[a,b], M. Marone[a,b], A. Schizzi[a,b], A. Zanetti[a]

Kangwon National University, Chunchon, Korea
A. Kropivnitskaya, S.K. Nam

Kyungpook National University, Daegu, Korea
D.H. Kim, G.N. Kim, M.S. Kim, D.J. Kong, S. Lee, Y.D. Oh, A. Sakharov, D.C. Son

Chonbuk National University, Jeonju, Korea
J.A. Brochero Cifuentes, H. Kim, T.J. Kim, M.S. Ryu

Chonnam National University, Institute for Universe and Elementary Particles, Kwangju, Korea
S. Song

Korea University, Seoul, Korea
S. Choi, Y. Go, D. Gyun, B. Hong, M. Jo, H. Kim, Y. Kim, B. Lee, K. Lee, K.S. Lee, S. Lee, S.K. Park, Y. Roh

Seoul National University, Seoul, Korea
H.D. Yoo

University of Seoul, Seoul, Korea
M. Choi, H. Kim, J.H. Kim, J.S.H. Lee, I.C. Park, G. Ryu

Sungkyunkwan University, Suwon, Korea
Y. Choi, J. Goh, D. Kim, E. Kwon, J. Lee, I. Yu

Vilnius University, Vilnius, Lithuania
A. Juodagalvis, J. Vaitkus

National Centre for Particle Physics, Universiti Malaya, Kuala Lumpur, Malaysia
I. Ahmed, Z.A. Ibrahim, J.R. Komaragiri, M.A.B. Md Ali[30], F. Mohamad Idris[31], W.A.T. Wan Abdullah, M.N. Yusli

Centro de Investigacion y de Estudios Avanzados del IPN, Mexico City, Mexico
E. Casimiro Linares, H. Castilla-Valdez, E. De La Cruz-Burelo, I. Heredia-de La Cruz[32], A. Hernandez-Almada, R. Lopez-Fernandez, A. Sanchez-Hernandez

Universidad Iberoamericana, Mexico City, Mexico
S. Carrillo Moreno, F. Vazquez Valencia

Benemerita Universidad Autonoma de Puebla, Puebla, Mexico
I. Pedraza, H.A. Salazar Ibarguen

Universidad Autónoma de San Luis Potosí, San Luis Potosí, Mexico
A. Morelos Pineda

JHEP11(2015)018

University of Auckland, Auckland, New Zealand
D. Krofcheck

University of Canterbury, Christchurch, New Zealand
P.H. Butler

National Centre for Physics, Quaid-I-Azam University, Islamabad, Pakistan
A. Ahmad, M. Ahmad, Q. Hassan, H.R. Hoorani, W.A. Khan, T. Khurshid, M. Shoaib

National Centre for Nuclear Research, Swierk, Poland
H. Bialkowska, M. Bluj, B. Boimska, T. Frueboes, M. Górski, M. Kazana, K. Nawrocki, K. Romanowska-Rybinska, M. Szleper, P. Zalewski

Institute of Experimental Physics, Faculty of Physics, University of Warsaw, Warsaw, Poland
G. Brona, K. Bunkowski, A. Byszuk[33], K. Doroba, A. Kalinowski, M. Konecki, J. Krolikowski, M. Misiura, M. Olszewski, M. Walczak

Laboratório de Instrumentação e Física Experimental de Partículas, Lisboa, Portugal
P. Bargassa, C. Beirão Da Cruz E Silva, A. Di Francesco, P. Faccioli, P.G. Ferreira Parracho, M. Gallinaro, N. Leonardo, L. Lloret Iglesias, F. Nguyen, J. Rodrigues Antunes, J. Seixas, O. Toldaiev, D. Vadruccio, J. Varela, P. Vischia

Joint Institute for Nuclear Research, Dubna, Russia
S. Afanasiev, P. Bunin, M. Gavrilenko, I. Golutvin, I. Gorbunov, A. Kamenev, V. Karjavin, V. Konoplyanikov, A. Lanev, A. Malakhov, V. Matveev[34], P. Moisenz, V. Palichik, V. Perelygin, S. Shmatov, S. Shulha, N. Skatchkov, V. Smirnov, A. Zarubin

Petersburg Nuclear Physics Institute, Gatchina (St. Petersburg), Russia
V. Golovtsov, Y. Ivanov, V. Kim[35], E. Kuznetsova, P. Levchenko, V. Murzin, V. Oreshkin, I. Smirnov, V. Sulimov, L. Uvarov, S. Vavilov, A. Vorobyev

Institute for Nuclear Research, Moscow, Russia
Yu. Andreev, A. Dermenev, S. Gninenko, N. Golubev, A. Karneyeu, M. Kirsanov, N. Krasnikov, A. Pashenkov, D. Tlisov, A. Toropin

Institute for Theoretical and Experimental Physics, Moscow, Russia
V. Epshteyn, V. Gavrilov, N. Lychkovskaya, V. Popov, I. Pozdnyakov, G. Safronov, A. Spiridonov, E. Vlasov, A. Zhokin

National Research Nuclear University 'Moscow Engineering Physics Institute' (MEPhI), Moscow, Russia
A. Bylinkin

P.N. Lebedev Physical Institute, Moscow, Russia
V. Andreev, M. Azarkin[36], I. Dremin[36], M. Kirakosyan, A. Leonidov[36], G. Mesyats, S.V. Rusakov, A. Vinogradov

JHEP11(2015)018

Skobeltsyn Institute of Nuclear Physics, Lomonosov Moscow State University, Moscow, Russia

A. Baskakov, A. Belyaev, E. Boos, V. Bunichev, M. Dubinin[37], L. Dudko, A. Ershov, V. Klyukhin, O. Kodolova, I. Lokhtin, I. Myagkov, S. Obraztsov, M. Perfilov, S. Petrushanko, V. Savrin

State Research Center of Russian Federation, Institute for High Energy Physics, Protvino, Russia

I. Azhgirey, I. Bayshev, S. Bitioukov, V. Kachanov, A. Kalinin, D. Konstantinov, V. Krychkine, V. Petrov, R. Ryutin, A. Sobol, L. Tourtchanovitch, S. Troshin, N. Tyurin, A. Uzunian, A. Volkov

University of Belgrade, Faculty of Physics and Vinca Institute of Nuclear Sciences, Belgrade, Serbia

P. Adzic[38], M. Ekmedzic, J. Milosevic, V. Rekovic

Centro de Investigaciones Energéticas Medioambientales y Tecnológicas (CIEMAT), Madrid, Spain

J. Alcaraz Maestre, E. Calvo, M. Cerrada, M. Chamizo Llatas, N. Colino, B. De La Cruz, A. Delgado Peris, D. Domínguez Vázquez, A. Escalante Del Valle, C. Fernandez Bedoya, J.P. Fernández Ramos, J. Flix, M.C. Fouz, P. Garcia-Abia, O. Gonzalez Lopez, S. Goy Lopez, J.M. Hernandez, M.I. Josa, E. Navarro De Martino, A. Pérez-Calero Yzquierdo, J. Puerta Pelayo, A. Quintario Olmeda, I. Redondo, L. Romero, M.S. Soares

Universidad Autónoma de Madrid, Madrid, Spain

C. Albajar, J.F. de Trocóniz, M. Missiroli, D. Moran

Universidad de Oviedo, Oviedo, Spain

J. Cuevas, J. Fernandez Menendez, S. Folgueras, I. Gonzalez Caballero, E. Palencia Cortezon, J.M. Vizan Garcia

Instituto de Física de Cantabria (IFCA), CSIC-Universidad de Cantabria, Santander, Spain

I.J. Cabrillo, A. Calderon, J.R. Castiñeiras De Saa, P. De Castro Manzano, J. Duarte Campderros, M. Fernandez, J. Garcia-Ferrero, G. Gomez, A. Lopez Virto, J. Marco, R. Marco, C. Martinez Rivero, F. Matorras, F.J. Munoz Sanchez, J. Piedra Gomez, T. Rodrigo, A.Y. Rodríguez-Marrero, A. Ruiz-Jimeno, L. Scodellaro, I. Vila, R. Vilar Cortabitarte

CERN, European Organization for Nuclear Research, Geneva, Switzerland

D. Abbaneo, E. Auffray, G. Auzinger, M. Bachtis, P. Baillon, A.H. Ball, D. Barney, A. Benaglia, J. Bendavid, L. Benhabib, J.F. Benitez, G.M. Berruti, P. Bloch, A. Bocci, A. Bonato, C. Botta, H. Breuker, T. Camporesi, R. Castello, G. Cerminara, S. Colafranceschi[39], M. D'Alfonso, D. d'Enterria, A. Dabrowski, V. Daponte, A. David, M. De Gruttola, F. De Guio, A. De Roeck, S. De Visscher, E. Di Marco, M. Dobson, M. Dordevic, B. Dorney, T. du Pree, M. Dünser, N. Dupont, A. Elliott-Peisert, G. Franzoni, W. Funk, D. Gigi, K. Gill, D. Giordano, M. Girone, F. Glege, R. Guida, S. Gundacker, M. Guthoff, J. Hammer,

JHEP11(2015)018

P. Harris, J. Hegeman, V. Innocente, P. Janot, H. Kirschenmann, M.J. Kortelainen, K. Kousouris, K. Krajczar, P. Lecoq, C. Lourenço, M.T. Lucchini, N. Magini, L. Malgeri, M. Mannelli, A. Martelli, L. Masetti, F. Meijers, S. Mersi, E. Meschi, F. Moortgat, S. Morovic, M. Mulders, M.V. Nemallapudi, H. Neugebauer, S. Orfanelli[40], L. Orsini, L. Pape, E. Perez, M. Peruzzi, A. Petrilli, G. Petrucciani, A. Pfeiffer, D. Piparo, A. Racz, G. Rolandi[41], M. Rovere, M. Ruan, H. Sakulin, C. Schäfer, C. Schwick, A. Sharma, P. Silva, M. Simon, P. Sphicas[42], D. Spiga, J. Steggemann, B. Stieger, M. Stoye, Y. Takahashi, D. Treille, A. Triossi, A. Tsirou, G.I. Veres[19], N. Wardle, H.K. Wöhri, A. Zagozdzinska[33], W.D. Zeuner

Paul Scherrer Institut, Villigen, Switzerland

W. Bertl, K. Deiters, W. Erdmann, R. Horisberger, Q. Ingram, H.C. Kaestli, D. Kotlinski, U. Langenegger, D. Renker, T. Rohe

Institute for Particle Physics, ETH Zurich, Zurich, Switzerland

F. Bachmair, L. Bäni, L. Bianchini, M.A. Buchmann, B. Casal, G. Dissertori, M. Dittmar, M. Donegà, P. Eller, C. Grab, C. Heidegger, D. Hits, J. Hoss, G. Kasieczka, W. Lustermann, B. Mangano, M. Marionneau, P. Martinez Ruiz del Arbol, M. Masciovecchio, D. Meister, F. Micheli, P. Musella, F. Nessi-Tedaldi, F. Pandolfi, J. Pata, F. Pauss, L. Perrozzi, M. Quittnat, M. Rossini, A. Starodumov[43], M. Takahashi, V.R. Tavolaro, K. Theofilatos, R. Wallny

Universität Zürich, Zurich, Switzerland

T.K. Aarrestad, C. Amsler[44], L. Caminada, M.F. Canelli, V. Chiochia, A. De Cosa, C. Galloni, A. Hinzmann, T. Hreus, B. Kilminster, C. Lange, J. Ngadiuba, D. Pinna, P. Robmann, F.J. Ronga, D. Salerno, Y. Yang

National Central University, Chung-Li, Taiwan

M. Cardaci, K.H. Chen, T.H. Doan, Sh. Jain, R. Khurana, M. Konyushikhin, C.M. Kuo, W. Lin, Y.J. Lu, S.S. Yu

National Taiwan University (NTU), Taipei, Taiwan

Arun Kumar, R. Bartek, P. Chang, Y.H. Chang, Y.W. Chang, Y. Chao, K.F. Chen, P.H. Chen, C. Dietz, F. Fiori, U. Grundler, W.-S. Hou, Y. Hsiung, Y.F. Liu, R.-S. Lu, M. Miñano Moya, E. Petrakou, J.f. Tsai, Y.M. Tzeng

Chulalongkorn University, Faculty of Science, Department of Physics, Bangkok, Thailand

B. Asavapibhop, K. Kovitanggoon, G. Singh, N. Srimanobhas, N. Suwonjandee

Cukurova University, Adana, Turkey

A. Adiguzel, S. Cerci[45], Z.S. Demiroglu, C. Dozen, I. Dumanoglu, S. Girgis, G. Gokbulut, Y. Guler, E. Gurpinar, I. Hos, E.E. Kangal[46], A. Kayis Topaksu, G. Onengut[47], K. Ozdemir[48], S. Ozturk[49], B. Tali[45], H. Topakli[49], M. Vergili, C. Zorbilmez

Middle East Technical University, Physics Department, Ankara, Turkey

I.V. Akin, B. Bilin, S. Bilmis, B. Isildak[50], G. Karapinar[51], M. Yalvac, M. Zeyrek

JHEP11(2015)018

Bogazici University, Istanbul, Turkey

E.A. Albayrak[52], E. Gülmez, M. Kaya[53], O. Kaya[54], T. Yetkin[55]

Istanbul Technical University, Istanbul, Turkey

K. Cankocak, S. Sen[56], F.I. Vardarlı

Institute for Scintillation Materials of National Academy of Science of Ukraine, Kharkov, Ukraine

B. Grynyov

National Scientific Center, Kharkov Institute of Physics and Technology, Kharkov, Ukraine

L. Levchuk, P. Sorokin

University of Bristol, Bristol, United Kingdom

R. Aggleton, F. Ball, L. Beck, J.J. Brooke, E. Clement, D. Cussans, H. Flacher, J. Goldstein, M. Grimes, G.P. Heath, H.F. Heath, J. Jacob, L. Kreczko, C. Lucas, Z. Meng, D.M. Newbold[57], S. Paramesvaran, A. Poll, T. Sakuma, S. Seif El Nasr-storey, S. Senkin, D. Smith, V.J. Smith

Rutherford Appleton Laboratory, Didcot, United Kingdom

K.W. Bell, A. Belyaev[58], C. Brew, R.M. Brown, D. Cieri, D.J.A. Cockerill, J.A. Coughlan, K. Harder, S. Harper, E. Olaiya, D. Petyt, C.H. Shepherd-Themistocleous, A. Thea, I.R. Tomalin, T. Williams, W.J. Womersley, S.D. Worm

Imperial College, London, United Kingdom

M. Baber, R. Bainbridge, O. Buchmuller, A. Bundock, D. Burton, S. Casasso, M. Citron, D. Colling, L. Corpe, N. Cripps, P. Dauncey, G. Davies, A. De Wit, M. Della Negra, P. Dunne, A. Elwood, W. Ferguson, J. Fulcher, D. Futyan, G. Hall, G. Iles, M. Kenzie, R. Lane, R. Lucas[57], L. Lyons, A.-M. Magnan, S. Malik, J. Nash, A. Nikitenko[43], J. Pela, M. Pesaresi, K. Petridis, D.M. Raymond, A. Richards, A. Rose, C. Seez, A. Tapper, K. Uchida, M. Vazquez Acosta[59], T. Virdee, S.C. Zenz

Brunel University, Uxbridge, United Kingdom

J.E. Cole, P.R. Hobson, A. Khan, P. Kyberd, D. Leggat, D. Leslie, I.D. Reid, P. Symonds, L. Teodorescu, M. Turner

Baylor University, Waco, USA

A. Borzou, K. Call, J. Dittmann, K. Hatakeyama, A. Kasmi, H. Liu, N. Pastika

The University of Alabama, Tuscaloosa, USA

O. Charaf, S.I. Cooper, C. Henderson, P. Rumerio

Boston University, Boston, USA

A. Avetisyan, T. Bose, C. Fantasia, D. Gastler, P. Lawson, D. Rankin, C. Richardson, J. Rohlf, J. St. John, L. Sulak, D. Zou

JHEP11(2015)018

Brown University, Providence, USA

J. Alimena, E. Berry, S. Bhattacharya, D. Cutts, N. Dhingra, A. Ferapontov, A. Garabedian, J. Hakala, U. Heintz, E. Laird, G. Landsberg, Z. Mao, M. Narain, S. Piperov, S. Sagir, T. Sinthuprasith, R. Syarif

University of California, Davis, Davis, USA

R. Breedon, G. Breto, M. Calderon De La Barca Sanchez, S. Chauhan, M. Chertok, J. Conway, R. Conway, P.T. Cox, R. Erbacher, M. Gardner, W. Ko, R. Lander, M. Mulhearn, D. Pellett, J. Pilot, F. Ricci-Tam, S. Shalhout, J. Smith, M. Squires, D. Stolp, M. Tripathi, S. Wilbur, R. Yohay

University of California, Los Angeles, USA

R. Cousins, P. Everaerts, C. Farrell, J. Hauser, M. Ignatenko, D. Saltzberg, E. Takasugi, V. Valuev, M. Weber

University of California, Riverside, Riverside, USA

K. Burt, R. Clare, J. Ellison, J.W. Gary, G. Hanson, J. Heilman, M. Ivova PANEVA, P. Jandir, E. Kennedy, F. Lacroix, O.R. Long, A. Luthra, M. Malberti, M. Olmedo Negrete, A. Shrinivas, H. Wei, S. Wimpenny, B. R. Yates

University of California, San Diego, La Jolla, USA

J.G. Branson, G.B. Cerati, S. Cittolin, R.T. D'Agnolo, A. Holzner, R. Kelley, D. Klein, J. Letts, I. Macneill, D. Olivito, S. Padhi, M. Pieri, M. Sani, V. Sharma, S. Simon, M. Tadel, A. Vartak, S. Wasserbaech[60], C. Welke, F. Würthwein, A. Yagil, G. Zevi Della Porta

University of California, Santa Barbara, Santa Barbara, USA

D. Barge, J. Bradmiller-Feld, C. Campagnari, A. Dishaw, V. Dutta, K. Flowers, M. Franco Sevilla, P. Geffert, C. George, F. Golf, L. Gouskos, J. Gran, J. Incandela, C. Justus, N. Mccoll, S.D. Mullin, J. Richman, D. Stuart, I. Suarez, W. To, C. West, J. Yoo

California Institute of Technology, Pasadena, USA

D. Anderson, A. Apresyan, A. Bornheim, J. Bunn, Y. Chen, J. Duarte, A. Mott, H.B. Newman, C. Pena, M. Pierini, M. Spiropulu, J.R. Vlimant, S. Xie, R.Y. Zhu

Carnegie Mellon University, Pittsburgh, USA

M.B. Andrews, V. Azzolini, A. Calamba, B. Carlson, T. Ferguson, M. Paulini, J. Russ, M. Sun, H. Vogel, I. Vorobiev

University of Colorado Boulder, Boulder, USA

J.P. Cumalat, W.T. Ford, A. Gaz, F. Jensen, A. Johnson, M. Krohn, T. Mulholland, U. Nauenberg, K. Stenson, S.R. Wagner

Cornell University, Ithaca, USA

J. Alexander, A. Chatterjee, J. Chaves, J. Chu, S. Dittmer, N. Eggert, N. Mirman, G. Nicolas Kaufman, J.R. Patterson, A. Rinkevicius, A. Ryd, L. Skinnari, L. Soffi, W. Sun, S.M. Tan, W.D. Teo, J. Thom, J. Thompson, J. Tucker, Y. Weng, P. Wittich

JHEP11(2015)018

Fermi National Accelerator Laboratory, Batavia, USA
S. Abdullin, M. Albrow, J. Anderson, G. Apollinari, S. Banerjee, L.A.T. Bauerdick, A. Beretvas, J. Berryhill, P.C. Bhat, G. Bolla, K. Burkett, J.N. Butler, H.W.K. Cheung, F. Chlebana, S. Cihangir, V.D. Elvira, I. Fisk, J. Freeman, E. Gottschalk, L. Gray, D. Green, S. Grünendahl, O. Gutsche, J. Hanlon, D. Hare, R.M. Harris, S. Hasegawa, J. Hirschauer, Z. Hu, S. Jindariani, M. Johnson, U. Joshi, A.W. Jung, B. Klima, B. Kreis, S. Kwan[†], S. Lammel, J. Linacre, D. Lincoln, R. Lipton, T. Liu, R. Lopes De Sá, J. Lykken, K. Maeshima, J.M. Marraffino, V.I. Martinez Outschoorn, S. Maruyama, D. Mason, P. McBride, P. Merkel, K. Mishra, S. Mrenna, S. Nahn, C. Newman-Holmes, V. O'Dell, K. Pedro, O. Prokofyev, G. Rakness, E. Sexton-Kennedy, A. Soha, W.J. Spalding, L. Spiegel, L. Taylor, S. Tkaczyk, N.V. Tran, L. Uplegger, E.W. Vaandering, C. Vernieri, M. Verzocchi, R. Vidal, H.A. Weber, A. Whitbeck, F. Yang

University of Florida, Gainesville, USA
D. Acosta, P. Avery, P. Bortignon, D. Bourilkov, A. Carnes, M. Carver, D. Curry, S. Das, G.P. Di Giovanni, R.D. Field, I.K. Furic, J. Hugon, J. Konigsberg, A. Korytov, J.F. Low, P. Ma, K. Matchev, H. Mei, P. Milenovic[61], G. Mitselmakher, D. Rank, R. Rossin, L. Shchutska, M. Snowball, D. Sperka, N. Terentyev, L. Thomas, J. Wang, S. Wang, J. Yelton

Florida International University, Miami, USA
S. Hewamanage, S. Linn, P. Markowitz, G. Martinez, J.L. Rodriguez

Florida State University, Tallahassee, USA
A. Ackert, J.R. Adams, T. Adams, A. Askew, J. Bochenek, B. Diamond, J. Haas, S. Hagopian, V. Hagopian, K.F. Johnson, A. Khatiwada, H. Prosper, M. Weinberg

Florida Institute of Technology, Melbourne, USA
M.M. Baarmand, V. Bhopatkar, M. Hohlmann, H. Kalakhety, D. Noonan, T. Roy, F. Yumiceva

University of Illinois at Chicago (UIC), Chicago, USA
M.R. Adams, L. Apanasevich, D. Berry, R.R. Betts, I. Bucinskaite, R. Cavanaugh, O. Evdokimov, L. Gauthier, C.E. Gerber, D.J. Hofman, P. Kurt, C. O'Brien, I.D. Sandoval Gonzalez, C. Silkworth, P. Turner, N. Varelas, Z. Wu, M. Zakaria

The University of Iowa, Iowa City, USA
B. Bilki[62], W. Clarida, K. Dilsiz, S. Durgut, R.P. Gandrajula, M. Haytmyradov, V. Khristenko, J.-P. Merlo, H. Mermerkaya[63], A. Mestvirishvili, A. Moeller, J. Nachtman, H. Ogul, Y. Onel, F. Ozok[52], A. Penzo, C. Snyder, P. Tan, E. Tiras, J. Wetzel, K. Yi

Johns Hopkins University, Baltimore, USA
I. Anderson, B.A. Barnett, B. Blumenfeld, D. Fehling, L. Feng, A.V. Gritsan, P. Maksimovic, C. Martin, M. Osherson, M. Swartz, M. Xiao, Y. Xin, C. You

The University of Kansas, Lawrence, USA
P. Baringer, A. Bean, G. Benelli, C. Bruner, R.P. Kenny III, D. Majumder, M. Malek, M. Murray, S. Sanders, R. Stringer, Q. Wang

JHEP11(2015)018

Kansas State University, Manhattan, USA

A. Ivanov, K. Kaadze, S. Khalil, M. Makouski, Y. Maravin, A. Mohammadi, L.K. Saini, N. Skhirtladze, S. Toda

Lawrence Livermore National Laboratory, Livermore, USA

D. Lange, F. Rebassoo, D. Wright

University of Maryland, College Park, USA

C. Anelli, A. Baden, O. Baron, A. Belloni, B. Calvert, S.C. Eno, C. Ferraioli, J.A. Gomez, N.J. Hadley, S. Jabeen, R.G. Kellogg, T. Kolberg, J. Kunkle, Y. Lu, A.C. Mignerey, Y.H. Shin, A. Skuja, M.B. Tonjes, S.C. Tonwar

Massachusetts Institute of Technology, Cambridge, USA

A. Apyan, R. Barbieri, A. Baty, K. Bierwagen, S. Brandt, W. Busza, I.A. Cali, Z. Demiragli, L. Di Matteo, G. Gomez Ceballos, M. Goncharov, D. Gulhan, Y. Iiyama, G.M. Innocenti, M. Klute, D. Kovalskyi, Y.S. Lai, Y.-J. Lee, A. Levin, P.D. Luckey, A.C. Marini, C. Mcginn, C. Mironov, X. Niu, C. Paus, D. Ralph, C. Roland, G. Roland, J. Salfeld-Nebgen, G.S.F. Stephans, K. Sumorok, M. Varma, D. Velicanu, J. Veverka, J. Wang, T.W. Wang, B. Wyslouch, M. Yang, V. Zhukova

University of Minnesota, Minneapolis, USA

B. Dahmes, A. Evans, A. Finkel, A. Gude, P. Hansen, S. Kalafut, S.C. Kao, K. Klapoetke, Y. Kubota, Z. Lesko, J. Mans, S. Nourbakhsh, N. Ruckstuhl, R. Rusack, N. Tambe, J. Turkewitz

University of Mississippi, Oxford, USA

J.G. Acosta, S. Oliveros

University of Nebraska-Lincoln, Lincoln, USA

E. Avdeeva, K. Bloom, S. Bose, D.R. Claes, A. Dominguez, C. Fangmeier, R. Gonzalez Suarez, R. Kamalieddin, J. Keller, D. Knowlton, I. Kravchenko, J. Lazo-Flores, F. Meier, J. Monroy, F. Ratnikov, J.E. Siado, G.R. Snow

State University of New York at Buffalo, Buffalo, USA

M. Alyari, J. Dolen, J. George, A. Godshalk, C. Harrington, I. Iashvili, J. Kaisen, A. Kharchilava, A. Kumar, S. Rappoccio

Northeastern University, Boston, USA

G. Alverson, E. Barberis, D. Baumgartel, M. Chasco, A. Hortiangtham, A. Massironi, D.M. Morse, D. Nash, T. Orimoto, R. Teixeira De Lima, D. Trocino, R.-J. Wang, D. Wood, J. Zhang

Northwestern University, Evanston, USA

K.A. Hahn, A. Kubik, N. Mucia, N. Odell, B. Pollack, A. Pozdnyakov, M. Schmitt, S. Stoynev, K. Sung, M. Trovato, M. Velasco

JHEP11(2015)018

University of Notre Dame, Notre Dame, USA

A. Brinkerhoff, N. Dev, M. Hildreth, C. Jessop, D.J. Karmgard, N. Kellams, K. Lannon, S. Lynch, N. Marinelli, F. Meng, C. Mueller, Y. Musienko[34], T. Pearson, M. Planer, A. Reinsvold, R. Ruchti, G. Smith, S. Taroni, N. Valls, M. Wayne, M. Wolf, A. Woodard

The Ohio State University, Columbus, USA

L. Antonelli, J. Brinson, B. Bylsma, L.S. Durkin, S. Flowers, A. Hart, C. Hill, R. Hughes, W. Ji, K. Kotov, T.Y. Ling, B. Liu, W. Luo, D. Puigh, M. Rodenburg, B.L. Winer, H.W. Wulsin

Princeton University, Princeton, USA

O. Driga, P. Elmer, J. Hardenbrook, P. Hebda, S.A. Koay, P. Lujan, D. Marlow, T. Medvedeva, M. Mooney, J. Olsen, C. Palmer, P. Piroué, X. Quan, H. Saka, D. Stickland, C. Tully, J.S. Werner, A. Zuranski

University of Puerto Rico, Mayaguez, USA

S. Malik

Purdue University, West Lafayette, USA

V.E. Barnes, D. Benedetti, D. Bortoletto, L. Gutay, M.K. Jha, M. Jones, K. Jung, D.H. Miller, N. Neumeister, B.C. Radburn-Smith, X. Shi, I. Shipsey, D. Silvers, J. Sun, A. Svyatkovskiy, F. Wang, W. Xie, L. Xu

Purdue University Calumet, Hammond, USA

N. Parashar, J. Stupak

Rice University, Houston, USA

A. Adair, B. Akgun, Z. Chen, K.M. Ecklund, F.J.M. Geurts, M. Guilbaud, W. Li, B. Michlin, M. Northup, B.P. Padley, R. Redjimi, J. Roberts, J. Rorie, Z. Tu, J. Zabel

University of Rochester, Rochester, USA

B. Betchart, A. Bodek, P. de Barbaro, R. Demina, Y. Eshaq, T. Ferbel, M. Galanti, A. Garcia-Bellido, J. Han, A. Harel, O. Hindrichs, A. Khukhunaishvili, G. Petrillo, M. Verzetti

The Rockefeller University, New York, USA

L. Demortier

Rutgers, The State University of New Jersey, Piscataway, USA

S. Arora, A. Barker, J.P. Chou, C. Contreras-Campana, E. Contreras-Campana, D. Duggan, D. Ferencek, Y. Gershtein, R. Gray, E. Halkiadakis, D. Hidas, E. Hughes, S. Kaplan, R. Kunnawalkam Elayavalli, A. Lath, K. Nash, S. Panwalkar, M. Park, S. Salur, S. Schnetzer, D. Sheffield, S. Somalwar, R. Stone, S. Thomas, P. Thomassen, M. Walker

University of Tennessee, Knoxville, USA

M. Foerster, G. Riley, K. Rose, S. Spanier, A. York

JHEP11(2015)018

Texas A&M University, College Station, USA

O. Bouhali[64], A. Castaneda Hernandez[64], M. Dalchenko, M. De Mattia, A. Delgado, S. Dildick, R. Eusebi, W. Flanagan, J. Gilmore, T. Kamon[65], V. Krutelyov, R. Mueller, I. Osipenkov, Y. Pakhotin, R. Patel, A. Perloff, A. Rose, A. Safonov, A. Tatarinov, K.A. Ulmer[2]

Texas Tech University, Lubbock, USA

N. Akchurin, C. Cowden, J. Damgov, C. Dragoiu, P.R. Dudero, J. Faulkner, S. Kunori, K. Lamichhane, S.W. Lee, T. Libeiro, S. Undleeb, I. Volobouev

Vanderbilt University, Nashville, USA

E. Appelt, A.G. Delannoy, S. Greene, A. Gurrola, R. Janjam, W. Johns, C. Maguire, Y. Mao, A. Melo, H. Ni, P. Sheldon, B. Snook, S. Tuo, J. Velkovska, Q. Xu

University of Virginia, Charlottesville, USA

M.W. Arenton, S. Boutle, B. Cox, B. Francis, J. Goodell, R. Hirosky, A. Ledovskoy, H. Li, C. Lin, C. Neu, X. Sun, Y. Wang, E. Wolfe, J. Wood, F. Xia

Wayne State University, Detroit, USA

C. Clarke, R. Harr, P.E. Karchin, C. Kottachchi Kankanamge Don, P. Lamichhane, J. Sturdy

University of Wisconsin, Madison, USA

D.A. Belknap, D. Carlsmith, M. Cepeda, A. Christian, S. Dasu, L. Dodd, S. Duric, E. Friis, B. Gomber, M. Grothe, R. Hall-Wilton, M. Herndon, A. Hervé, P. Klabbers, A. Lanaro, A. Levine, K. Long, R. Loveless, A. Mohapatra, I. Ojalvo, T. Perry, G.A. Pierro, G. Polese, T. Ruggles, T. Sarangi, A. Savin, A. Sharma, N. Smith, W.H. Smith, D. Taylor, N. Woods

JHEP11(2015)018

†: Deceased

1: Also at Vienna University of Technology, Vienna, Austria

2: Also at CERN, European Organization for Nuclear Research, Geneva, Switzerland

3: Also at State Key Laboratory of Nuclear Physics and Technology, Peking University, Beijing, China

4: Also at Institut Pluridisciplinaire Hubert Curien, Université de Strasbourg, Université de Haute Alsace Mulhouse, CNRS/IN2P3, Strasbourg, France

5: Also at National Institute of Chemical Physics and Biophysics, Tallinn, Estonia

6: Also at Skobeltsyn Institute of Nuclear Physics, Lomonosov Moscow State University, Moscow, Russia

7: Also at Universidade Estadual de Campinas, Campinas, Brazil

8: Also at Centre National de la Recherche Scientifique (CNRS) - IN2P3, Paris, France

9: Also at Laboratoire Leprince-Ringuet, Ecole Polytechnique, IN2P3-CNRS, Palaiseau, France

10: Also at Joint Institute for Nuclear Research, Dubna, Russia

11: Also at Ain Shams University, Cairo, Egypt

12: Also at Zewail City of Science and Technology, Zewail, Egypt

13: Also at British University in Egypt, Cairo, Egypt

14: Also at Université de Haute Alsace, Mulhouse, France
15: Also at Tbilisi State University, Tbilisi, Georgia
16: Also at University of Hamburg, Hamburg, Germany
17: Also at Brandenburg University of Technology, Cottbus, Germany
18: Also at Institute of Nuclear Research ATOMKI, Debrecen, Hungary
19: Also at Eötvös Loránd University, Budapest, Hungary
20: Also at University of Debrecen, Debrecen, Hungary
21: Also at Wigner Research Centre for Physics, Budapest, Hungary
22: Also at University of Visva-Bharati, Santiniketan, India
23: Now at King Abdulaziz University, Jeddah, Saudi Arabia
24: Also at University of Ruhuna, Matara, Sri Lanka
25: Also at Isfahan University of Technology, Isfahan, Iran
26: Also at University of Tehran, Department of Engineering Science, Tehran, Iran
27: Also at Plasma Physics Research Center, Science and Research Branch, Islamic Azad University, Tehran, Iran
28: Also at Università degli Studi di Siena, Siena, Italy
29: Also at Purdue University, West Lafayette, USA
30: Also at International Islamic University of Malaysia, Kuala Lumpur, Malaysia
31: Also at Malaysian Nuclear Agency, MOSTI, Kajang, Malaysia
32: Also at Consejo Nacional de Ciencia y Tecnología, Mexico city, Mexico
33: Also at Warsaw University of Technology, Institute of Electronic Systems, Warsaw, Poland
34: Also at Institute for Nuclear Research, Moscow, Russia
35: Also at St. Petersburg State Polytechnical University, St. Petersburg, Russia
36: Also at National Research Nuclear University 'Moscow Engineering Physics Institute' (MEPhI), Moscow, Russia
37: Also at California Institute of Technology, Pasadena, USA
38: Also at Faculty of Physics, University of Belgrade, Belgrade, Serbia
39: Also at Facoltà Ingegneria, Università di Roma, Roma, Italy
40: Also at National Technical University of Athens, Athens, Greece
41: Also at Scuola Normale e Sezione dell'INFN, Pisa, Italy
42: Also at University of Athens, Athens, Greece
43: Also at Institute for Theoretical and Experimental Physics, Moscow, Russia
44: Also at Albert Einstein Center for Fundamental Physics, Bern, Switzerland
45: Also at Adiyaman University, Adiyaman, Turkey
46: Also at Mersin University, Mersin, Turkey
47: Also at Cag University, Mersin, Turkey
48: Also at Piri Reis University, Istanbul, Turkey
49: Also at Gaziosmanpasa University, Tokat, Turkey
50: Also at Ozyegin University, Istanbul, Turkey
51: Also at Izmir Institute of Technology, Izmir, Turkey
52: Also at Mimar Sinan University, Istanbul, Istanbul, Turkey
53: Also at Marmara University, Istanbul, Turkey
54: Also at Kafkas University, Kars, Turkey
55: Also at Yildiz Technical University, Istanbul, Turkey
56: Also at Hacettepe University, Ankara, Turkey
57: Also at Rutherford Appleton Laboratory, Didcot, United Kingdom
58: Also at School of Physics and Astronomy, University of Southampton, Southampton, United Kingdom

JHEP11(2015)018

59: Also at Instituto de Astrofísica de Canarias, La Laguna, Spain
60: Also at Utah Valley University, Orem, USA
61: Also at University of Belgrade, Faculty of Physics and Vinca Institute of Nuclear Sciences, Belgrade, Serbia
62: Also at Argonne National Laboratory, Argonne, USA
63: Also at Erzincan University, Erzincan, Turkey
64: Also at Texas A&M University at Qatar, Doha, Qatar
65: Also at Kyungpook National University, Daegu, Korea

JHEP11(2015)018